

Preclinical Models of Rare Pediatric Sarcomas

Ewing sarcoma and Ewing-like sarcomas

Margit Bleijs

ISBN: 978-94-6416-944-7

Lay-out: Margit Bleijs

Printing: Ridderprint | www.ridderprint.nl

The work described in this thesis was performed at the Princess Maxima Center for childhood oncology, within the framework of the Cancer, Stem Cells and Developmental Biology (CSnD) graduate program of Utrecht University.

Copyright 2022 by M.W. Bleijs. All rights reserved. No parts of this book may be reproduced, stored in retrieval system, or transmitted in any form or by any means, without prior permission of the author.

Preclinical Models of Rare Pediatric Sarcomas

Ewing sarcama and Ewing-like sarcomas

Preklinische Modellen van Zeldzame Pediatrische Sarcomen

Ewing-sarcoom en Ewing-achtige sarcomen

(met een samenvatting in het Nederlands)

Proefschrift

ter verkrijging van de graad van doctor aan de Universiteit Utrecht
op gezag van de rector magnificus, prof.dr. H.R.B.M. Kummeling,
ingevolge het besluit van het college voor promoties
in het openbaar te verdedigen op

donderdag 24 februari 2022 des middags te 4.15 uur

door

Margaretha Wilhelmina Bleijs

geboren op 31 juli 1993
te Utrecht

Promotor:

Prof. dr. J.C. Clevers

Copromotoren:

Dr. M. van de Wetering

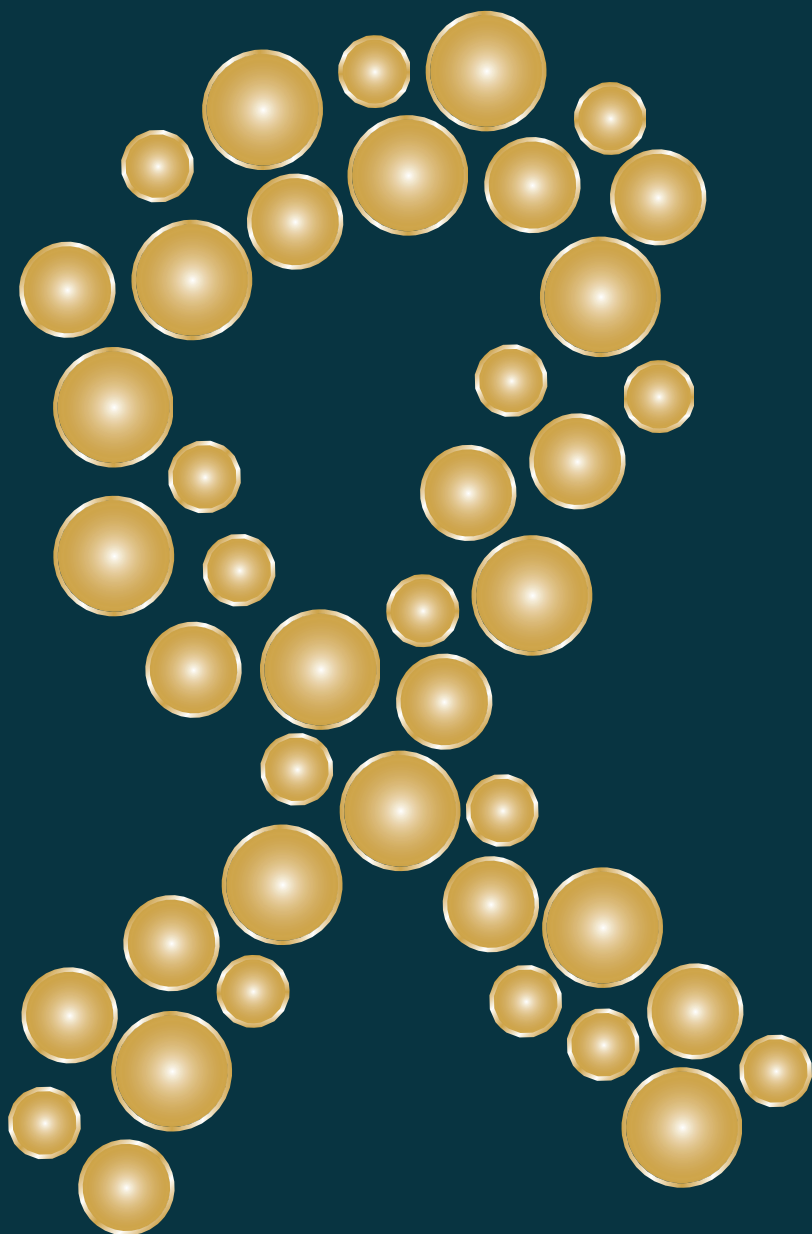
Dr. F. Meyer-Wentrup

"Nothing in life is to be feared, it is only to be understood. Now is the time to understand more, so that we may fear less."

Marie Skłodowska Curie

Table of Contents

Chapter 1	9
General introduction	
Chapter 2	19
Xenograft and organoid model systems in cancer research	
Chapter 3	43
PDO models of Ewing sarcoma allow for medium-throughput drug screening	
Chapter 4	61
The molecular mechanisms driving DSRCT expansion by the <i>EWS-WT1</i> fusion gene	
Chapter 5	87
Single cell atlas of Ewing sarcoma reveals subclonal evolution and its immune cell composition	
Chapter 6	121
General discussion	
Addendum	135
Nederlandse samenvatting	
List of publications	
Curriculum Vitea	
Acknowledgements	



Chapter 1

General Introduction

Margit Bleijs¹

1. Oncode Institute, Princess Maxima Center for Pediatric Oncology, Utrecht,
The Netherlands

Introduction

Pediatric cancers are relatively rare compared to adult cancers. Still, 650 children are diagnosed with cancer in the Netherlands each year. Three out of four children diagnosed with cancer can be cured, which represents a great improvement compared to 50 years ago when the cure rate of pediatric cancer was lower than 25% (Saletta *et al*, 2014). However, cancer is still the 2nd leading cause of death among children aged 0 to 14 years old. The past decade has witnessed a major increase in our understanding of the underlying genetics of pediatric cancers. An important difference between adult cancers and pediatric cancers is the genomic landscape. Adult cancers are often characterized by an accumulation of somatic mutations, while pediatric cancers typically have very few somatic mutations but a higher prevalence of germline alterations in cancer predisposition genes (Alejandro Sweet-Cordero & Biegel, 2019). Genetic alterations found in pediatric cancers include enhancer hijacking events and chromoplexy, which is a process of complex DNA rearrangements, leading to copy number variations and structural alterations (Alejandro Sweet-Cordero & Biegel, 2019). Chromoplexy can lead to chromosomal translocations, resulting in gene fusions. A variety of pediatric cancers are characterized by the presence of a single gene fusion. These alterations can affect a wide range of biological processes. However, the mechanisms underlying tumor progression, therapy resistance, and metastasis remain poorly understood.

Another important difference between pediatric and adult cancers is the cell-of-origin from which the cancers arise. Most common adult cancers are carcinomas which are epithelial in origin. However, cancers found in children are often solid tumors, which are thought to be neural crest derived or mesenchymal in origin. Patient-derived organoid models *in vitro* are well established for epithelial tissues and epithelial derived cancers (Bleijns *et al*, 2019). Yet, establishment of *in vitro* models of solid tumors remains limited, which underlines the need of gaining more knowledge on the origin of solid tumors and the dependency on their microenvironmental factors. Novel preclinical pediatric cancer models could greatly improve our knowledge of cancer initiation and progression.

Chromosomal translocations in pediatric sarcomas

The first discovery of a chromosomal aberration linked to a specific cancer dates back to 1960, when Nowell & Hungerford examined leukemic cells from chronic myelogenous leukemia (CML) and other leukemia patients. While cells from other leukemias did not show any chromosomal abnormalities, the cells of all CML patients presented a consistent chromosomal abnormality, which they called the Philadelphia (Ph) chromosome (Reviewed in Wong & Witte, 2004). Since the discovery of the Philadelphia chromosome, the role of genomic rearrangements and fusion genes increased exponentially. Nowadays, many chromosomal translocations are known to be linked to various types of cancers. Not only leukemias, but also many bone and soft tissue sarcomas are characterized by chromosomal translocations. Pediatric

bone and soft tissue sarcomas account for approximately 12% of all pediatric cancers and include Ewing sarcoma and Ewing-like sarcomas among others (Pappo & Dirksen, 2018). Ewing-like sarcomas are currently recognized as three main categories, including undifferentiated round cell sarcomas with *EWSR1* gene fusion with non-ETS family members, *CIC*-rearranged sarcomas, and *BCOR*-rearranged sarcomas (Sbaraglia *et al*, 2020). While these sarcomas are morphologically similar, they are genetically characterized by different chromosomal translocations, which drive distinct underlying mechanisms in cancer initiation and progression. Understanding these genetic differences and underlying mechanisms is crucial for the development of novel treatment options.

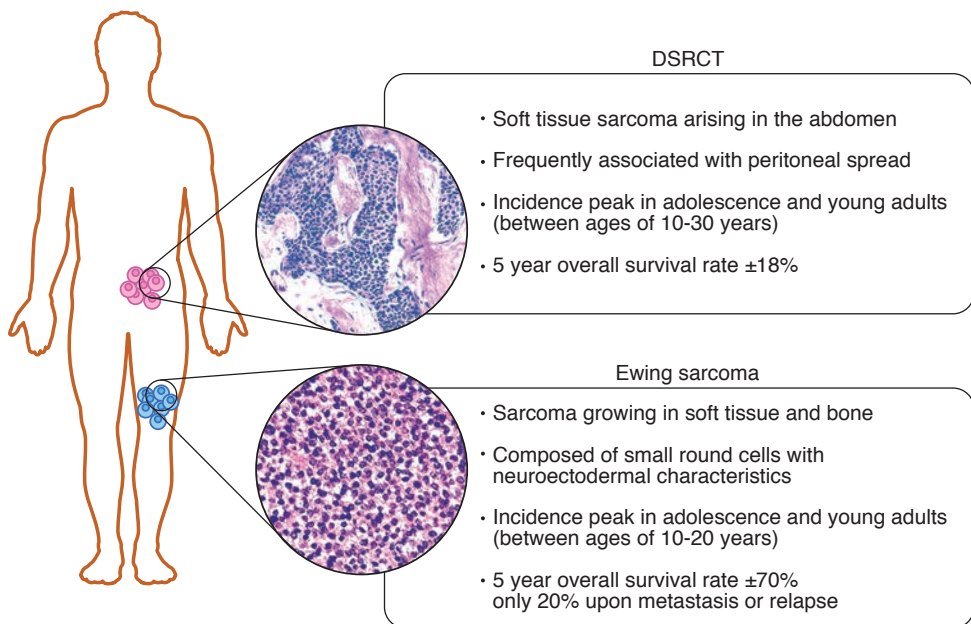


Figure 1: Animated overview presenting characteristics of DSRCTs and Ewing sarcomas.

Ewing sarcoma

Ewing sarcoma is an aggressive tumor that forms in bone or soft tissue, arising predominantly in the pelvis, femur, tibia, ribs, thoracic wall, gluteal muscle, pleural cavities and cervical muscles (Grünewald *et al*, 2018). This sarcoma is most often occurring in Caucasian adolescence and young adults with a peak incidence between the ages of 10-25 years (Ross *et al*, 2013). Treatment of Ewing sarcoma includes chemotherapy, surgery and radiation therapy, which has increased the 5-year overall survival rate to $\pm 70\%$ (Le Deley *et al*, 2014). However, when patients are diagnosed with metastatic disease, initially or at relapse, the long-term survival rate is only $\pm 20\%$ (Kovar *et al*, 2012). Ewing sarcoma is composed of small round cells with

neuroectodermal characteristics. Therefore, Ewing sarcoma is thought to be derived from early neural-crest cells (Rorie *et al*, 2004). However, other studies indicate that Ewing sarcoma is mesenchymal in origin (Tirode *et al*, 2007; Riggi *et al*, 2008). The true founder cell of Ewing sarcoma remains a matter of debate.

Genetically, Ewing sarcoma is characterized by a chromosomal translocation resulting in a gene fusion involving Ewing sarcoma region 1 (EWSR1) and an erythroblastosis virus E26 transforming sequence (ETS) family transcription factor, most frequently FLI1 (EWS-FLI1) (Ross *et al*, 2013). EWS-FLI1 can act in multiple ways as it functions as an aberrant chimeric transcription factor and it affects epigenetic control of gene expression by altering histone modifications, DNA methylation, and noncoding RNA expression (Riggi *et al*, 2021).

Despite extensive research worldwide, effective treatment is still lacking. The development of preclinical models phenocopying this sarcoma is required for studying tumor progression and acquisition of therapy resistance (Bleijs *et al*, 2019). Several preclinical models of Ewing sarcoma have been established, including patient-derived xenografts and *in vitro* cell lines (Nanni *et al*, 2019). As therapies become more biologically targeted and affect not only the tumor cells themselves, but also on the surrounding microenvironment, more effort is being made to establish 3D preclinical models that better recapitulate the original tumor and its microenvironment compared to 2D cell lines (Lamhamedi-Cherradi *et al*, 2014). Recapitulating the original tumor is key for predicting sensitivity and toxicity to anti-cancer agents.

DSRCT

Desmoplastic small round cell tumor (DSRCT) is a rare and aggressive Ewing-like soft tissue sarcoma (Hayes-jordan *et al*, 2016; Bulbul *et al*, 2017). In 1989, Gerald and Rosai were the first to characterize DSRCT as a separate entity (Gerald & Rosai, 1989). They described the histologic appearance of this sarcoma as nests of small round cells separated by desmoplastic stroma. DSRCT is usually found in the abdomen and is frequently associated with peritoneal spread. The incidence peak of this sarcoma is seen in adolescence and young adults with the age of 10-30 and is predominantly found in Caucasian male. Treatment of DSRCT includes chemotherapy, surgery and radiation therapy. Often, DSRCTs have widely spread throughout the peritoneum and are therefore inaccessible for complete removal by surgery. Accordingly, DSRCT patients have a very poor prognosis with a 5-year event-free survival rate of $\pm 18\%$ (Zhang *et al*, 2015).

Phenotypically, DSRCT exhibits features of multi-phenotypic differentiation as mesenchymal, epithelial, and neural markers are expressed within this sarcoma (Gerald & Rosai, 1989; Hayes-jordan *et al*, 2016). Similar to Ewing sarcoma, DSRCT is characterized by a chromosomal translocation involving EWSR1. However, in this sarcoma EWSR1 is fused to transcription factor Wilms tumor 1 (WT1). The chimeric EWSR1-WT1 fusion protein contains the N-terminal domain of EWSR1 and the DNA-binding region of WT1 (Karnieli *et al*, 1996). While several recent studies give

important insights on the downstream targets of the EWS-WT1 fusion gene (Kang *et al*, 2014; Gedminas *et al*, 2020; Hingorani *et al*, 2020), molecular mechanisms triggered by the gene fusion, that account for the aggressive proliferation of DSRCT, remains elusive. Additionally, preclinical models of DSRCT are limited, which hampers the research on mechanisms driving DSRCT progression and unraveling novel therapeutic strategies.

The tumor microenvironment

Tumor cells do not manifest the disease alone, but rather through interactions with non-transformed cells, which together create the tumor microenvironment (TME) (Hanahan & Coussens, 2012; Balkwill *et al*, 2012). The TME consists of tumor cells, stromal cells, including cancer-associated fibroblasts (CAFs), endothelial cells, and immune cells, and non-cellular components of extracellular matrix (ECM), such as collagen, fibronectin, and laminin (Baghban *et al*, 2020). Through complex signaling networks, tumor cells control the TME for their own benefit to promote tumorigenesis in all phases of cancer progression (Hanahan & Coussens, 2012). CAFs are mainly found at invasive tumor margins and produce tumor-promoting growth factors, such as chemokines, cytokines, and ECM components. Additionally, they can have important immunosuppressive activity (Balkwill *et al*, 2012). Endothelial cells are mainly involved in the angiogenesis process to support primary tumor growth as they form the inner layer of blood vessels. Apart from their role in angiogenesis, they can also promote tumor progression, metastasis, and drug resistance (Dudley, 2012; Baghban *et al*, 2020). The immune component of the TME is comprised of multiple different cell types. The most abundant immune cells include tumor-infiltrating lymphocytes (TILs) and tumor-associated myeloid cells (TAMs), which can both promote and inhibit cancer progression (Morales *et al*, 2020). TILs can vary with disease type and stage, CD4⁺ Th1 helper T cells and gamma-delta T cells are generally associated with a good prognosis, while FOXP3⁺ regulatory T cells and CD4⁺ Th2 helper T cells are usually associated with a poor prognosis (Balkwill *et al*, 2012). TAMs can display different activation states, described as classically (M1) or alternatively (M2) activated cells (Engblom *et al*, 2016). In growing tumors, TAMs mainly show anti-inflammatory M2-like phenotypes, which stimulate tumor progression and invasion, enhance angiogenesis, and suppress T cell functions (Engblom *et al*, 2016). In conclusion, the TME is a complex and dynamic network of intercellular communication. One of the major challenges for the establishment of preclinical models for cancer research is to capture the full complexity of tumor growth dynamics.

Scope of the thesis

Fusion-driven pediatric sarcomas are extremely rare. Therefore, research is complicated by the limited availability of tumor tissue. Patient-derived tumor *in vitro* models could fill this gap, which is of high importance for fundamental research and the discovery of effective therapies. Recent advances in patient-derived tumor

xenograft and tumor organoid model systems are reviewed in **chapter 2**. The promises and challenges as preclinical models in cancer research are discussed, including their resemblance to the original tumor, translational applications, integration of the tumor microenvironment, and drug screens and personalized medicine. In **chapter 3**, establishment of preclinical *in vitro* models of primary Ewing sarcoma are described that recapitulate their original tumor. Additionally, these Ewing sarcoma models are used for compound screens to investigate effective therapeutic options. Preclinical models for DSRCTs are very limited, only two DSRCT cell line have been reported, hampering research on mechanisms of tumor progression and discovering therapeutic options. A novel primary patient derived DSRCT *in vitro* model is described in **chapter 4**. This DSRCT *in vitro* model is used to unravel target genes of the EWS-WT1 fusion driving DSRCT, using an shRNA-mediated knock-down of *EWS-WT1*. Additionally, we discover that one of the EWS-WT1 target genes is a promising therapeutic target. **Chapter 5** describes the single cell architecture of primary Ewing sarcomas tissue. We find genetic subclonal events occurring within Ewing sarcoma patients. Additionally, we describe the immune cell composition and how the immune-suppressive nature of Ewing sarcoma can potentially be targeted by immune checkpoint inhibitors. **Chapter 6** summarizes the findings described in this thesis and discusses the challenges in preclinical research of rare pediatric sarcomas.

References

- Alejandro Sweet-Cordero E & Biegel JA (2019) The genomic landscape of pediatric cancers: Implications for diagnosis and treatment. *Science* 363: 1170–1175
- Baghban R, Roshangar L, Jahanban-Esfahlan R, Seidi K, Ebrahimi-Kalan A, Jaymand M, Kolahian S, Javaheri T & Zare P (2020) Tumor microenvironment complexity and therapeutic implications at a glance. *Cell Commun Signal* 18: 1–19
- Balkwill FR, Capasso M & Hagemann T (2012) The tumor microenvironment at a glance. *J Cell Sci* 125: 5591–5596
- Bleijis M, Wetering M, Clevers H & Drost J (2019) Xenograft and organoid model systems in cancer research. *EMBO J* 38: 1–11
- Bulbul A, Fahy BN, Xiu J, Rashad S, Mustafa A, Husain H & Hayes-jordan A (2017) Desmoplastic Small Round Blue Cell Tumor : A Review of Treatment and Potential Therapeutic Genomic Alterations. *Sarcoma* 2017:1-12
- Le Deley MC, Paulussen M, Lewis I, Brennan B, Ranft A, Whelan J, Le Teuff G, Michon J, Ladenstein R, Marec-Bérard P, et al (2014) Cyclophosphamide compared with ifosfamide in consolidation treatment of standard-risk Ewing sarcoma: Results of the randomized noninferiority Euro-EWING99-R1 trial. *J Clin Oncol* 32: 2440–2448
- Dudley AC (2012) Tumor endothelial cells. *Cold Spring Harb Perspect Med* 2: 1–18
- Engblom C, Pfirschke C & Pittet MJ (2016) The role of myeloid cells in cancer therapies. *Nat Rev Cancer* 16: 447–462
- Gedminas JM, Chasse MH, McBairty M, Beddows I, Kitchen-Goosen SM & Grohar PJ (2020) Desmoplastic small round cell tumor is dependent on the EWS-WT1 transcription factor. *Oncogenesis* 9: 1–8
- Gerald WL & Rosai J (1989) Case 2 desmoplastic small cell tumor with divergent differentiation. *Pediatr Pathol* 9: 177–183
- Grünewald TGP, Cidre-Aranaz F, Surdez D, Tomazou EM, De Álava E, Kovar H, Sorensen PH, Delattre O & Dirksen U (2018) Ewing sarcoma. *Nat Rev Dis Prim* 5:4
- Hanahan D & Coussens LM (2012) Accessories to the Crime: Functions of Cells Recruited to the Tumor Microenvironment. *Cancer Cell* 21: 309–322
- Hayes-jordan A, Laquaglia MP & Modak S (2016) Management of Desmoplastic Small Round Cell Tumor. *Semin Pediatr Surg* 25: 299–304
- Hingorani P, Dinu V, Zhang X, Lei H, Shern JF, Park J, Steel J, Rauf F, Parham D, Gastier-Foster J, et al (2020) Transcriptome analysis of desmoplastic small round cell tumors identifies actionable therapeutic targets: a report from the Children's Oncology Group. *Sci Rep* 10: 1–12
- Kang HJ, Park JH, Chen WP, Kang SI, Moroz K, Ladanyi M & Lee SB (2014) EWS-WT1 oncoprotein activates neuronal reprogramming factor ASCL1 and promotes neural differentiation. *Cancer Res* 74: 4526–4535
- Karnieli E, Werner H, Rauscher FJ, Benjamin LE & LeRoith D (1996) The IGF-I receptor gene promoter is a molecular target for the Ewing's sarcoma-Wilms' tumor 1 fusion protein. *J Biol Chem* 271: 19304–19309
- Kovar H, Alonso J, Aman P, Aryee DNT, Ban J, Burchill SA, Burdach S, De Alava E, Delattre O, Dirksen U, et al (2012) The first European interdisciplinary Ewing sarcoma research summit. *Front Oncol* 2: 1–11
- Lamhamedi-Cherradi SE, Santoro M, Ramammoorthy V, Menegaz BA, Bartholomeusz G, Iles LR, Amin HM, Livingston JA, Mikos AG & Ludwig JA (2014) 3D tissue-engineered model of Ewing's sarcoma. *Adv Drug Deliv Rev* 79: 155–171
- Morales E, Olson M, Iglesias F, Dahiya S, Luetkens T & Atanackovic D (2020) Role of immunotherapy in Ewing sarcoma. *J Immunother Cancer* 8: 1–16
- Nanni P, Landuzzi L, Manara MC, Righi A, Nicoletti G, Cristalli C, Pasello M, Parra A, Carrabotta M, Ferracin M, et al (2019) Bone sarcoma patient-derived xenografts are faithful and stable preclinical models for molecular and therapeutic investigations. *Sci Rep* 9: 1–12
- Pappo AS & Dirksen U (2018) Rhabdomyosarcoma, ewing sarcoma, and other round cell sarcomas. *J Clin Oncol* 36: 168–179
- Riggi N, Suvà ML & Stamenkovic I (2021) Ewing's Sarcoma. *N Engl J Med* 384: 154–164
- Riggi N, Suvà ML, Suvà D, Cironi L, Provero P, Tercier S, Joseph JM, Stehle JC, Baumer K, Kindler V, et al (2008) EWS-FLI-1 expression triggers a ewing's sarcoma initiation program in primary human mesenchymal stem cells. *Cancer Res* 68: 2176–2185

- Rorie CJ, Thomas VD, Chen P, Pierce HH, O'Bryan JP & Weissman BE (2004) The Ews/Fli-1 Fusion Gene Switches the Differentiation Program of Neuroblastomas to Ewing Sarcoma/Peripheral Primitive Neuroectodermal Tumors. *Cancer Res* 64: 1266–1277
- Ross KA, Smyth NA, Murawski CD & Kennedy JG (2013) The biology of ewing sarcoma. *ISRN Oncol* 2013: 759725
- Saletta F, Seng MS & Lau LMS (2014) Advances in paediatric cancer treatment. *Transl Pediatr* 3: 156–15682
- Sbaraglia M, Righi A, Gambarotti M & Dei Tos AP (2020) Ewing sarcoma and Ewing-like tumors. *Virchows Arch* 476: 109–119
- Tirode F, Laud-Duval K, Prieur A, Delorme B, Charbord P & Delattre O (2007) Mesenchymal Stem Cell Features of Ewing Tumors. *Cancer Cell* 11: 421–429
- Wong S & Witte ON (2004) The BCR-ABL story: Bench to bedside and back. *Annu Rev Immunol* 22: 247–306
- Zhang S, Zhang Y, Yu YH & Li J (2015) Results of multimodal treatment for desmoplastic small round cell tumor of the abdomen and pelvis. *Int J Clin Exp Med* 8: 9658–9666



Chapter 2

Xenograft and Organoid model systems in cancer research

Margit Bleijs¹, Marc van de Wetering¹,
Hans Clevers^{1,2}, Jarno Drost¹

Published in: *The EMBO Journal* (2019) 38: 1-11

1. Oncode Institute, Princess Maxima Center for Pediatric Oncology, Utrecht, The Netherlands
2. Oncode Institute, Hubrecht Institute, Royal Netherlands Academy of Arts and Sciences and University Medical Center, Utrecht, The Netherlands

Abstract

Patient-derived tumor xenografts and tumor organoids have become important pre-clinical model systems for cancer research. Both models maintain key features from their parental tumors, such as genetic and phenotypic heterogeneity, which allows them to be used for a wide spectrum of applications. In contrast to patient-derived xenografts, organoids can be established and expanded with high efficiency from primary patient material. On the other hand, xenografts retain tumor–stroma interactions, which are known to contribute to tumorigenesis. In this review, we discuss recent advances in patient-derived tumor xenograft and tumor organoid model systems and compare their promises and challenges as preclinical models in cancer research.

Introduction

Cancers consist of a continuously evolving heterogeneous cell mass (McGranahan & Swanton, 2017). Importantly, not all cells within a tumor contribute equally to its progression. Early studies on mouse mammary tumors revealed that cellular sub-populations from different regions of the same tumor vary in growth rate, drug response, immunogenicity and metastatic capacity (reviewed in Heppner, 1984; Tabassum & Polyak, 2015). This intra-tumor heterogeneity can arise from both genetic and non-genetic variability within tumors, such as variations in availability of resources, like differential access to oxygen and nutrients (Kreso & Dick, 2014; Tabassum & Polyak, 2015). The development of preclinical model systems phenocopying tumor heterogeneity is required for studying its contribution to tumor progression and acquisition of therapy resistance. Whereas the first patient-derived tumor xenograft (PDX) models were successfully established during the fifties (Toolan, 1953), patient-derived tumor organoid (PDO) models have been established only during the last decade (Sato *et al*, 2011) (Fig 1). Both PDX and PDO model systems are able to recapitulate the intra- and inter-tumor heterogeneity seen in human cancers (Beckhove *et al*, 2003; Guenot *et al*, 2006; Huang *et al*, 2015; van de Wetering *et al*, 2015; Bruna *et al*, 2016; George *et al*, 2017; Nanki *et al*, 2018; Sachs *et al*, 2018; Yan *et al*, 2018). Therefore, these models are promising tools to study sub-clonal dynamics within individual tumors during progression and therapy resistance (Shi *et al*, 2014). Due to the complexity of human tumors, response to clinical cancer treatments varies substantially. Additionally, mechanisms of tumor progression are poorly defined as well as drug efficacy and resistance. While a high number of anti-cancer compounds tested for clinical safety in Phase I studies progress to Phase II efficacy testing, most of these compounds fail in Phase II and III studies, which examine the power of pharmacological responses (Dimasi *et al*, 2013). Such high failure rates in clinical trials headline the need of preclinical efficacy models for improved predictions of clinical outcome. Several human preclinical models are currently used, including cancer cell lines, PDX and PDO cultures (Figs 1 and 2). These models have improved our understanding of the mechanisms of cancer progression and provided valuable tools for the development of novel cancer treatments. Additionally, these preclinical models are used to predict clinical response to anti-cancer agents. In this review, we discuss PDX and PDO model systems and compare their promises and challenges in cancer research.

PDX models

To understand cancer biology and its translation into effective treatments, human preclinical models capturing the heterogeneity of cancer are fundamental. Although with low efficiency, primary tumor tissues can be grown in 2D cultures *in vitro*, allowing tumor cells capable of adapting to these conditions to expand and form a cell line. The use of *in vitro* cancer cell lines has provided valuable insights on tumor development and mechanisms of therapeutic actions (Sos *et al*, 2009; Greshock *et al*,

2010). However, the main drawback of cancer cell lines is the lack of both phenotypic and genetic heterogeneity found in the original tumors (Sachs & Clevers, 2014; Byrne *et al*, 2017). To enhance the correlation with human cancers, surgically derived primary clinical tumor samples can be grafted into mice, known as PDX. In such models, tumor architecture and the relative proportion of cancer cells and stromal cells are maintained to a large extent, which yields better resemblance to the original tumor compared to cancer cell lines (Byrne *et al*, 2017; Fig 2). Although not all patient-derived tumors can successfully be engrafted into mice, the success rate of PDX establishment is increasing due to the establishment of immunocompromised mice (Shultz *et al*, 2005; Drake *et al*, 2012).

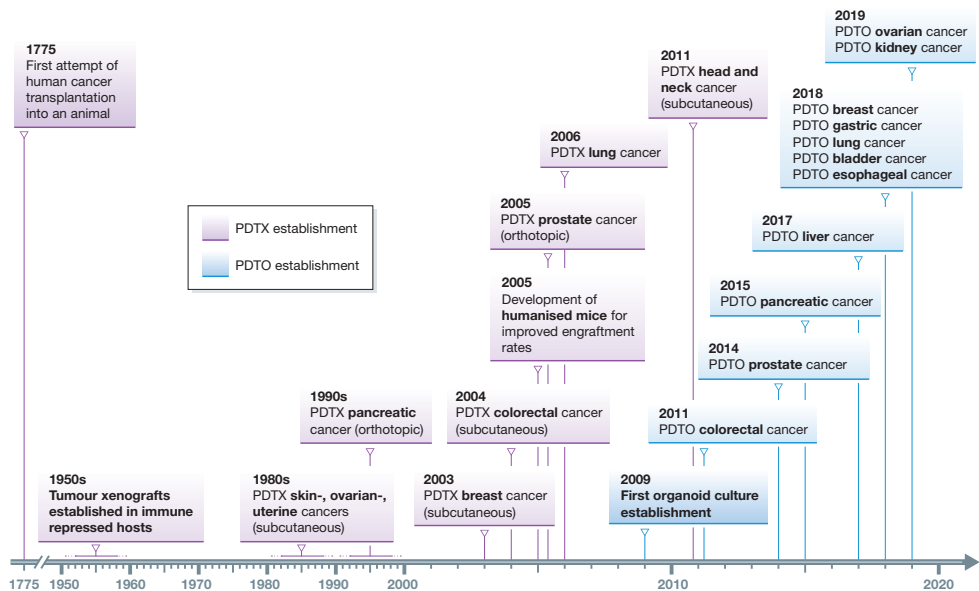


Figure 1: Timeline PDX and PDO development (Toolan, 1953; Taetle *et al*, 1987; Fu *et al*, 1992; Beckhove *et al*, 2003; Fichtner *et al*, 2004; Shultz *et al*, 2005; Wang *et al*, 2005; Cutz *et al*, 2006; Sato *et al*, 2009; Hennessey *et al*, 2011; Sato *et al*, 2011; Karthaus *et al*, 2014; Gao *et al*, 2014; Boj *et al*, 2015; Sachs *et al*, 2018; Li *et al*, 2018; Yan *et al*, 2018; Lee *et al*, 2018; Li *et al*, 2019; Schutgens *et al*, 2019; Kopper *et al*, 2019).

Although the first documented attempt to transplant a human cancer into an animal dates back to 1775, a hallmark study by Helene Toolan showed that it was possible to grow human tumor cells in x-irradiated mice and rats (Toolan, 1953). Additionally, she demonstrated that proliferation extended considerably when the x-radiated hosts were treated with the immune system suppressor cortisone (Toolan, 1953). Later, Phillips and Gazet were able to obtain a slightly higher percentage of viable patient-derived tumor grafts by treating the host mice with anti-lymphocyte serum. The number of viable grafts increased in particular when combined with thymectomy, demonstrating that a suppressed immune response enhances engraftment efficiency (Phillips & Gazet, 1970). Following these studies, several genetically modified

mouse models have been established, which are severely immune deficient, such as the NOD/SCID/IL2Rnull (NSG) mouse (Shultz *et al*, 2005). The virtual absence of an immune system in these mice allows for significantly higher engraftment rates (Shultz *et al*, 2005; Byrne *et al*, 2017). Together these studies demonstrated that loss of immune system activity improves engraftment and viability of patient-derived tumor tissue into mice. PDX models are currently established for a broad variety of cancers, including colorectal (Fichtner *et al*, 2004; Guenot *et al*, 2006), pancreatic (Fu *et al*, 1992; Kim *et al*, 2009), breast (Beckhove *et al*, 2003; Bruna *et al*, 2016), lung (Cutz *et al*, 2006), skin (Taetle *et al*, 1987), head and neck (Hennessey *et al*, 2011), prostate (Wang *et al*, 2005) and ovarian cancer (George *et al*, 2017; Fig 3). Although PDXs recapitulate tumor tissue more closely than cancer cell lines, they are usually generated from a small amount of tumor material. As a consequence, the PDX derived from it might not capture the full heterogeneity of the original tumor (Kemper *et al*, 2015). Moreover, Morgan and colleagues recently reported that from the total number of mutations detected in primary non-small-cell-lung cancer (NSCLC) tumors, only 43% were detected in the corresponding PDXs and four additional mutations arose in early passages of PDXs that were not present in the primary tumor (Morgan *et al*, 2017). These observations suggest that clonal selection and evolution may occur early on upon tumor tissue engraftment into mice. Multiple biopsies from different regions of a tumor should be engrafted to capture the complete tumor architecture *in vivo*, whereas early passages of PDXs should be used for translational applications to avoid outcomes that deviate from clinical response. Furthermore, the limited engraftment rates of PDXs remain a major challenge, which is highly variable among cancers (Rosfjord *et al*, 2014). Sub-clones of advanced tumors grow best as PDX, compared to less advanced tumors. Additionally, growth rates of engrafted tumor tissue increase over several passages of PDXs and a significant correlation was found between PDX passage number and features of higher tumor grade (Pearson *et al*, 2016). This indicates that clonal selection occurs over passages of PDXs.

The contribution of tumor stroma to tumor growth upon engraftment remains controversial in PDX models. Components of human stroma, including vasculature, immune cells and fibroblasts, are present during early passages of PDXs. The presence of these human stromal components allows for interaction studies between tumor cells and their microenvironment. However, the human stroma is subsequently replaced by murine stroma over several passages of PDXs (Julien *et al*, 2012; Peng *et al*, 2013). Gene expression studies of NSCLC PDXs confirmed depletion of human-derived tumor-associated cells with a downregulation of genes corresponding to cell adhesion and immune response pathways. This suggests that the PDX deviates from the original tumor over time (Morgan *et al*, 2017). In addition, drug metabolism and pharmacokinetics differ between mouse and human, which needs to be taken into account (Morgan *et al*, 2017).

Over the years, it has become increasingly clear that orthotopic transplantation pro-

vide a more physiological PDTX than heterotopic (e.g. subcutaneous) engraftment. It was previously demonstrated that orthotopic transplantation can lead to local invasive growth and metastases, similar to those observed in patients (Dai *et al*, 2015; Hoffman, 2015). In orthotopic PDTXs, tumor-host interactions can be investigated at the relevant location of primary and secondary tumor growth, as well as the development of metastases. In a comparison between orthotopic and subcutaneous xenografts of pancreatic ductal adenocarcinoma (PDAC), metabolic differences were

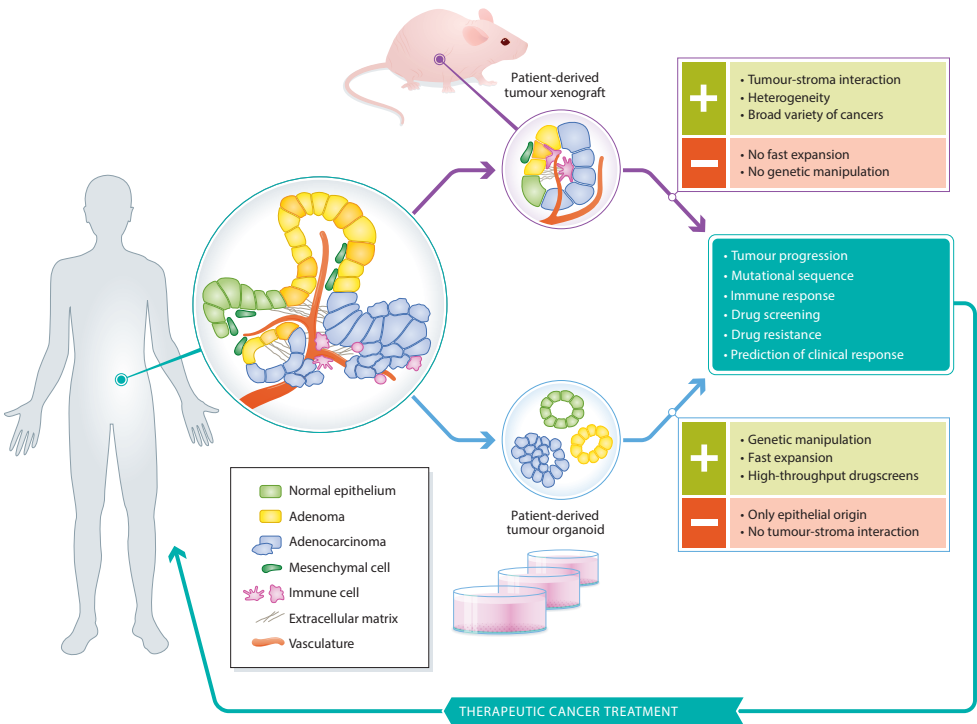


Figure 2: Schematic representation of establishing PDTX (purple) and PDO (blue) model systems to resemble human cancers. PDTX preserve tumor heterogeneity and tumor-stroma interactions. PDOs grow in a provided basement membrane extract and can be established from epithelial cancer cells as well as healthy epithelial tissue. Both models allow for several translational applications that contribute to development of therapeutic cancer treatments. Part of this figure was adapted from (Sachs & Clevers, 2014).

found. These differences could be attributed to differences in tumor microenvironment caused by the different location of engraftment (Zhan *et al*, 2017). These results highlight the complexity of cancers as well as the importance of location and environment of the transplantation site. Nonetheless, while orthotopic PDTXs more accurately mimic the primary tumors by resemblance of the native microenvironment, this method is technically challenging and labour-intensive. Therefore, most studies still use subcutaneous engraftment of tumor tissue.

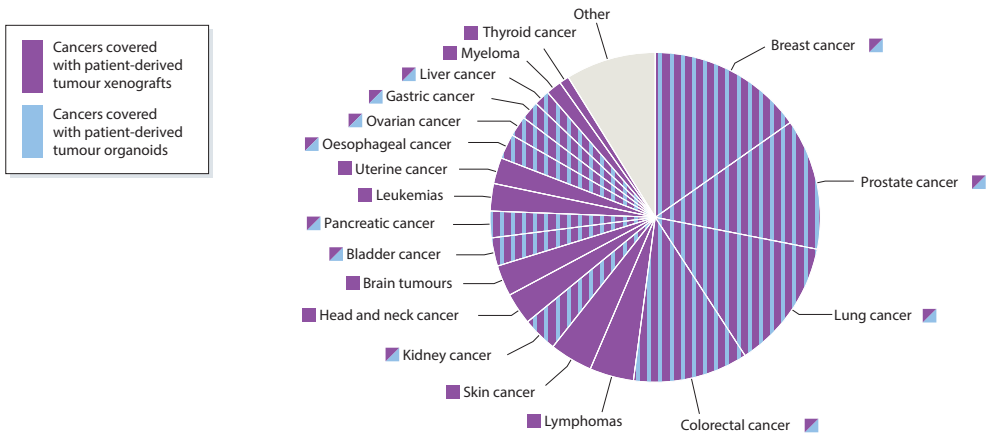


Figure 3: Different cancer types that can be grown as PDTX and PDO. In general, the engraftment efficiency of PDTXs is lower than the success rate of PDO establishment.

PDTO models

During the last decade, techniques to grow tissues *in vitro* in 3D as organotypic structures have been established. These so-called organoids can be grown from adult and embryonic stem cells and are able to self-organize into 3D structures that reflect the tissue of origin (for adult stem cell-derived organoids), or to which the differentiation was directed (embryonic stem cell-derived organoids) (for a review see Clevers, 2016). The first adult stem cell-derived organoid cultures were established from Lgr5-expressing mouse intestinal stem cells that were placed in conditions mimicking the intestinal stem cell niche (Sato *et al*, 2009). By providing R-spondin-1, epidermal growth factor (EGF) and Noggin, and embedment of the cells in an extracellular matrix-providing basement membranes extract, the Lgr5-expressing stem cells received the signalling cues necessary to self-renew, proliferate and form differentiated offspring, resembling the intestinal epithelium (Sato *et al*, 2009).

Since then, organoid cultures have been established for a variety of human tissues, including lung (Hild & Jaffe, 2016; Tan *et al*, 2017; Sachs *et al*, 2019), colon (Sato *et al*, 2011), stomach (Bartfeld *et al*, 2015), liver (Huch *et al*, 2015), pancreas (Boj *et al*, 2015), prostate (Chua *et al*, 2014; Karthaus *et al*, 2014), kidney (Jun *et al*, 2018; Schutgens *et al*, 2019) and fallopian tube (Kessler *et al*, 2015). Moreover, organoid culture protocols have been established for patient-derived tumor tissue as well. Human tumor organoids have been generated from colon (Sato *et al*, 2011; van de Wetering *et al*, 2015), pancreas (Boj *et al*, 2015; Huang *et al*, 2015), prostate (Gao *et al*, 2014; Drost *et al*, 2016), breast (Sachs *et al*, 2018), gastric (Nanki *et al*, 2018; Yan *et al*, 2018), lung (Sachs *et al*, 2019), oesophageal (Li *et al*, 2018), bladder (Lee *et al*, 2018; Mullenders *et al*, 2019), ovarian (Kopper *et al*, 2019), kidney (Schutgens *et al*, 2019) and liver (Broutier *et al*, 2017; Li *et al*, 2019) tumor tissue (Fig 3). An important fea-

ture of a number of these PDOs is that they genetically and phenotypically mirror the tumor epithelium, including its intra-tumor heterogeneity (Huang *et al*, 2015; van de Wetering *et al*, 2015; Nanki *et al*, 2018; Sachs *et al*, 2018; Yan *et al*, 2018). In a recent study, Roerink and colleagues characterized organoids derived from single cells from several colorectal cancers (CRC) and showed extensive mutational diversification as well as differences in responses to anti-cancer drugs between even closely related cells of the same tumor (Roerink *et al*, 2018). PDO models show improved resemblance to the original tumor compared to 2D cultured cancer cell lines. Thereby, organoid cultures bridge the gap between *in vitro* 2D cancer cell line cultures and *in vivo* PDTXs (Sachs & Clevers, 2014; Drost & Clevers, 2018). Importantly, they can be expanded long term and cryopreserved, allowing for the generation of living tumor organoid biobanks (Weeber *et al*, 2015; van de Wetering *et al*, 2015; Fujii *et al*, 2016; Schütte *et al*, 2017; Li *et al*, 2018; Nanki *et al*, 2018; Sachs *et al*, 2018, 2019; Seino *et al*, 2018; Tiriach *et al*, 2018; Yan *et al*, 2018). So far, the majority of established PDO cultures originate from epithelial cancers (carcinomas). Although most common adult cancers are carcinomas and epithelial in origin, a number of cancers are not, such as sarcomas, leukaemia and lymphomas. This remains a major challenge in organoid technology and is in contrast to PDTX models, which allow for the growth of a broad variety of cancers. While organoid cultures cannot mimic vasculature and tumor–stroma interactions, patient-derived tumor organoids are a promising tool for several translational applications, such as high-throughput drug screens and personalized medicine in a patient-derived manner.

Translational applications of PDTX and PDO model systems

Most preclinical anti-cancer agents entering clinical trials fail to acquire regulatory approval due to insufficient safety or inefficacy. This highlights the limitations of the predictive value of current preclinical models. However, in a study where they evaluated the therapeutic relevance of PDTXs, a panel of six human small-cell lung carcinoma (SCLC) xenografts was treated with topotecan, a topoisomerase I inhibitor, combinations of topotecan and the topoisomerase II inhibitor etoposide, or alkylating agents ifosfamide or cisplatin at maximum tolerated dose (Némati *et al*, 2010). Three out of the six PDTX models showed over 90% growth inhibition when treated with topotecan alone, similar to the therapeutic response observed in Phase II clinical trials (Ardizzoni *et al*, 1997). Growth inhibition in the PDTX models was improved when topotecan was combined with etoposide or ifosfamide. These findings demonstrate that the established xenografts are useful for preclinical assessment of new drugs and combinations of drugs (Némati *et al*, 2010; Rosfjord *et al*, 2014). Moreover, Bertotti and colleagues screened a cohort of 85 metastatic CRC (mCRC) PDTX models, treated with cetuximab, an inhibiting antibody against epidermal growth factor receptor (EGFR). They found an enrichment of tumors with *HER2* amplification in cetuximab-resistant *KRAS/NRAS/BRAF/PIK3CA* wild-type tumors (Bertotti *et al*, 2011). This proof-of-concept study revealed that the combined

inhibition of EGFR and HER2 induced long-lasting tumor regression, suggesting promising therapeutic opportunities for mCRC patients that are resistant to cetuximab (Bertotti *et al*, 2011).

Gao and colleagues generated an extensive collection of more than 1000 PDX models representing a broad range of solid cancers. In this large panel of PDX models, genetic hypotheses and biomarkers of sensitivity to cancer treatments, derived from cultured cancer cell lines, were successfully validated. Importantly, the PDX models also identified therapeutic candidates that cancer cell lines failed to capture (Gao *et al*, 2015; Byrne *et al*, 2017). The promising results of such large cohort studies increase the use of PDXs for preclinical models of testing anti-cancer drugs and to unravel biomarkers for drug sensitivity and resistance. For example, a recent study demonstrated that metformin, an anti-diabetic drug, also affects tumor growth in CRC PDX models. Administering metformin at physiological levels of 150 mg/kg per day in mice, which is equivalent to the clinical dose of 500 – 1000 mg/daily in human, is sufficient to inhibit tumor growth in CRC PDX. This implies promising therapeutic options for CRC patients (Suhaimi *et al*, 2017). Together these studies demonstrate the promises of PDXs as preclinical models to develop novel cancer treatments and predict their clinical response in patients.

Fast expansion of preclinical model systems is important to enable high-throughput drug screens. In contrast to PDXs, patient-derived organoid cultures can be more easily expanded long-term and several studies demonstrated that organoid cultures allow for the detection of gene-drug associations and enable high-throughput drug screens. Verissimo and colleagues tested KRAS pathway inhibitors and combinations of drugs on normal colon organoids and CRC PDOs and demonstrated that only organoids harboring KRAS mutations were resistant to the treatments (Verissimo *et al*, 2016). In another recent study, Vlachogiannis and colleagues reported a living biobank of PDOs from metastatic, heavily pretreated colorectal and gastroesophageal tumors, which showed a high degree of similarity to the original patient tumors. A comparison of responses to anticancer agents in PDOs and PDO-based orthotopic mouse tumor xenograft models with the responses of the patients in clinical trials, suggests that PDOs successfully recapitulate the response seen in the patient (Vlachogiannis *et al*, 2018). Additionally, Tiriác and colleagues generated a pancreatic cancer PDO library that largely maintained the mutational spectrum and transcriptional subtypes of primary pancreatic cancer. They showed that pancreatic cancer PDOs exhibited heterogeneous responses to standard-of-care chemotherapeutics and that these therapeutic profiles correspond to patient outcomes. These data suggest that combined molecular and therapeutic profiling of PDOs may predict treatment response and enable prospective therapeutic selection (Tiriác *et al*, 2018). Moreover, Schütte and colleagues collected a large biobank of 106 CRCs, 35 PDOs and 59 PDXs to identify novel biomarkers by linking molecular profiles with drug sensitivity patterns. Although the genetic landscape of the original tumors was largely maintained, they also found some dif-

ferences between PDXs and PDOs, as PDXs appeared closer to the molecular distinct CRC groups than PDOs. Additionally, PDOs showed elevated expression levels of genes involved in xenobiotic and fatty acid processes, which may affect drug sensitivity (Schütte *et al*, 2017).

Organoid cultures additionally allow for genetic engineering to study effects of oncogenic mutations in detail. Li and colleagues introduced oncogenic mutations into primary organoids from mouse colon, stomach and pancreas. This study shows that pancreatic and gastric organoids presented dysplasia as a result of the activating *Kras*^{G12D} mutation, loss of *Tp53* or both and formed adenocarcinoma upon *in vivo* transplantation. In contrast, primary colon organoids required combinatorial *Apc*, *Tp53*, *Kras*^{G12D} and *Smad4* mutations for the formation of adenocarcinoma *in vivo*. Opposed to colon organoids, small intestine organoids showed more rapid dysplasia even with only the combination of mutated *Apc* and *Kras* or mutated *Apc* and *Tp53*. (Li *et al*, 2014). Subsequently, two studies translated this to the human situation by CRISPR/Cas9-mediated genome editing of common CRC driver mutations in healthy human small intestinal and colonic organoids (Drost *et al*, 2015; Matano *et al*, 2015). These studies demonstrated that organoids harbouring an activating mutation in *KRAS*, in combination with inactivating mutations in *APC*, *TP53* and *SMAD4*, are able to grow independent of the intestinal stem cell niche factors EGF, Wnt, R-spondin, and Noggin. Additionally, Drost *et al* showed that loss of *APC* and *TP53* are key drivers of chromosome instability and aneuploidy (Drost *et al*, 2015). Not only adult stem cell-derived organoids can be used to study cancer initiation and progression, but also embryonic stem cell-derived organoids can be valuable tools in cancer research. Huang *et al* directed the differentiation of human embryonic stem cells towards pancreatic progenitor cells that formed ductal and acinar structures. Expression of mutant *KRAS* or *TP53* in progenitor organoids induced mutation-specific phenotypes. For instance, mutated *TP53*, but not mutated *KRAS*, induced cytosolic SOX9 localization, which was associated with mortality of patients (Huang *et al*, 2015). In another recent study, Drost *et al* used CRISPR-modified human stem cell organoids to study DNA repair defects in cancer (Drost *et al*, 2017). This showed that accumulation of mutations in organoids deficient in the mismatch repair gene *MLH1* accurately models the mutation profiles observed in mismatch repair-deficient CRC. Application of this approach to the cancer predisposition gene *NTHL1* demonstrated that a high contribution of a mutational footprint (signature 30), observed in a breast cancer cohort, within a tumor can be indicative of germline mutations in *NTHL1* (Drost *et al*, 2017). These studies demonstrate the immense opportunities organoid technology gives to study the effects of specific genetic alterations during cancer initiation and progression.

Integrating the tumor environment in PDX and PDO

The location in which a tumor resides, the tumor niche or microenvironment, plays an important role in cancer development. Stromal cells not only modulate the behav-

our of tumor cells directly but are also able to influence the immune system (Tauriello *et al*, 2018). This is effectively shown in a study by Batlle and colleagues, using a mouse model in which the main four CRC driver mutations can be specifically modified in intestinal stem cells. Quadruple-mutant mice developed metastatic tumors in the small and large intestine that showed hallmarks of human CRC, including T-cell exclusion and TGF β -activated stroma. They showed that inhibition of TGF β induced a cytotoxic T-cell response against tumor cells that prevented metastasis, highlighting the importance of the tumor microenvironment (Tauriello *et al*, 2018).

Immune cells recognize antigens present on cell membranes and distinguish between cancer cells and non-cancer cells (Schumacher & Schreiber, 2015). As a consequence of tumor-specific mutations, cancer cells start expressing neoantigens on their membranes, which can be recognized by T lymphocytes. The recognition of such neoantigens is an important factor in the efficacy of clinical immunotherapies. Additionally, the neoantigen load may form a biomarker for cancer cells (Schumacher & Schreiber, 2015). However, the lack of an immune competent environment in both immune-deficient mice and organoid cultures limits the utility of these models to explore the interaction between a tumor cell and the immune system. To overcome this limitation in PDX models, humanized mouse models have been developed (Info box humanized mouse models). For this, selected immune components were introduced to establish a competent human immune system (HIS) in mice. Humanized mice maintain various lineages of human blood cells throughout the lifetime of the recipient animal. Ideally, the hematopoietic stem cells (HSCs) come from the same patient from whom the PDX will be established, in order to avoid immune reactions caused by human leukocyte antigen mismatch. This is challenging, because bone marrow biopsies are a burden for weakened patients. Additionally, growth factor-stimulated bone marrow mobilization for collecting HSCs from peripheral blood might support tumor progression (Voloshin *et al*, 2011). The low yields of CD34-positive HSCs obtainable from cancer patients, strongly limits the number of humanized mice. Nonetheless, humanized mice allow studying features of the human anti-tumor immune response in a mouse model system (Shultz *et al*, 2012; Byrne *et al*, 2017). In such a study, newborn NSG mice were co-engrafted with human HSCs and human breast cancer cells. In these mice, tumor growth was accompanied by specific T cell maturation as well as tumor cell-specific activation of T cells. Additionally, an accumulation of NK cells was observed at the tumor site (Wege *et al*, 2011). Transplantation of primary lung tumors into humanized mice revealed the existence of tumor-infiltrating effector memory T cells that were activated upon human IL-12 administration (Simpson-Abelson *et al*, 2008). The ability to study tumor progression combined with its engrafted immune system provides new approaches for cancer immunotherapy, resistance of tumor cells to anti-cancer therapies, and the involvement of the immune system in response to chemotherapy.

In tumor organoid cultures, the lack of an immune competent environment can be overcome by co-culture with immune cells. Nozaki and colleagues devel-

oped a novel co-culture system of mouse intra-epithelial lymphocytes and intestinal epithelial cells. In this co-culture, the intra-epithelial lymphocytes were expanded with intestinal organoids in the presence of IL-2, IL-7, and IL15 (Nozaki *et al*, 2016).

Info box humanized mouse models

Humanized mice are immunodeficient mice engrafted with human hematopoietic stem cells which give rise to a variety of human blood cell lineages throughout the life of the animal. The human immune system (HIS) mouse model can be generated by transplantation of CD34-positive human hematopoietic stem cells (HSCs) or precursor cells. These cells can be isolated from bone marrow, peripheral blood, or umbilical cord blood. CD34-positive HSC transplantation can be performed alone or in combination with transplantation of human immune tissues, such as thymic tissue (Drake *et al*, 2012). Humanized mouse models are powerful tools for studying cancer, haematopoiesis, and inflammatory and infectious disease.

Recently, Zumwalde and colleagues succeeded in characterizing the intra-epithelial lymphocyte compartment of healthy human breast tissue as well as identifying a subset of T lymphocytes that can be pharmacologically targeted to enhance their response to breast cancer cells (Zumwalde *et al*, 2016). Specifically, V δ 2⁺ $\gamma\delta$ T cells were constantly present in the preparation of mammary ductal epithelial organoids. In response to zoledronic acid, an aminobisphosphonate drug, these T lymphocytes started to proliferate. Additionally, V δ 2⁺ T cells from breast ductal organoids produced IFN γ , an anti-tumor cytokine, and efficiently killed bisphosphonate-pulsed breast cancer cells. Together these results demonstrate the potential for V δ 2⁺ $\gamma\delta$ T lymphocytes to respond to FDA-approved bisphosphonate drugs as a novel immunotherapeutic approach to inhibit cancer growth (Zumwalde *et al*, 2016). In another recent study, Dijkstra and colleagues established and validated a platform to induce and analyse tumor-specific T-cell responses to epithelial cancers, including mismatch repair-deficient CRC and NSCLC, in a personalized manner. Enrichment of tumor-reactive T cells from peripheral blood of patients was successfully established by co-cultures of peripheral blood lymphocytes with autologous tumor organoids. Moreover, they demonstrated that these tumor-reactive T cells efficiently recognize and kill autologous tumor organoids, while leaving the healthy organoids or tissue unharmed (Dijkstra *et al*, 2018). In addition, Neal *et al* developed an air-liquid interface PDTO culture system that recapitulates complex tumor architecture including stromal and immune compartments (Neal *et al*, 2018). They demonstrated that the T cell receptors are highly conserved between the PDTO culture and the parental tumor. Crucially, they showed that the PDTO cultures functionally recapitulate the PD-1/PD-L1 dependent immune checkpoint (Neal *et al*, 2018).

In addition to the immune system, cancer associated fibroblasts (CAFs) play an important role in the tumor environment. As such, Öhlund and colleagues showed that a co-culture of murine pancreatic stellate cells (PSCs) and PDAC tu-

mor organoids recapitulate properties of PDAC desmoplasia. They demonstrate that PSCs differentiate into two distinct subtypes of CAFs with elevated expression of α SMA and secretion of IL-6 and additional inflammatory mediators, respectively (Öhlund *et al*, 2017). In accordance with this, Seino and colleagues established a co-culture of PDAC organoids and CAFs and showed that the CAFs provide a WNT niche for PDAC (Seino *et al*, 2018), highlighting the importance of CAFs in the tumor microenvironment. In an effort to model diabetic vasculopathy *in vitro*, a recent study reported the development of human blood vessel organoids from pluripotent stem cells that self-assemble into capillary networks, containing endothelial cells and pericytes, surrounded by a basement membrane. Upon transplantation of these organoids into mice, a perfused vascular tree is formed, including arteries, arterioles and venules (Wimmer *et al*, 2019). These human blood vessel organoids may open new doors for PDTO co-cultures. Culturing PDTOs in the presence of the vascular system, in addition to co-cultures with CAFs and immune cells, can recapitulate more components of the tumor microenvironment *in vitro*.

In conclusion, the lack of an immune competent environment in both PDX and PDTO model systems can be overcome by using humanized mouse models or generating co-cultures with immune cells, respectively. Additionally, to mimic the tumor stroma in the organoid model system, PDTOs can be co-cultured with CAFs.

Drug screens and personalized medicine using PDX and PDTO models

The discovery of molecular biomarkers for drug sensitivity is of high importance for the treatment of cancer patients. As illustrated by the EGFR tyrosine kinase inhibitor gefitinib in NSCLC, some drugs can give exceptional responses in small subsets of patients. However, when these patients are not properly identified within larger cohorts, it results in an overall negative clinical trial outcome (Thatcher *et al*, 2005). PDX models can be used as screening platforms for predicting clinical outcome of the response rate to drugs, identifying biomarkers for drug sensitivity and studying drug resistance. For example, a prospective study in PDAC showed that the combination of the anti-microtubule agent nab-paclitaxel and the anti-metabolite gemcitabine is effective in PDX models of PDAC, which correlated with the clinical efficacy of this combination. Moreover, this combination of chemotherapeutics has been demonstrated to provide a survival benefit for advanced PDAC patients in a randomized phase III study (Von Hoff *et al*, 2013; Hidalgo *et al*, 2015). Additionally, PDX models are not only able to provide potential clinical indications, but they may also facilitate the identification of potential drug efficacy biomarkers. In CRC for example, several studies have shown that *KRAS* mutant PDX models do not respond to cetuximab. The wild-type status of *KRAS* is now a well-documented clinical biomarker for this targeted therapy (Hidalgo *et al*, 2015). Furthermore, melanoma PDX models were involved in the identification of a mechanism of resistance to targeted drugs, such as the BRAF^{V600E} inhibitor vemurafenib. Additionally, a novel drug administration strategy that is clinically applicable was proposed to

overcome resistance (Das Thakur *et al*, 2013). Although PDTX models are useful for low-throughput drug screens and predicting clinical outcome, they do not allow for high-throughput drug screens.

In contrast to PDTX models, PDOs can be established and expanded more efficiently, which allows them to be used in medium- to high-throughput drug screens. The use of PDOs as a preclinical model for finding biomarkers and performing genotype-drug associations is just starting to be explored. A few studies already show promising results. For example, drug testing on a panel of organoids derived from 20 chemo-naïve CRC patients confirmed known drug sensitivity-genotype correlations. This proof of principle highlighted the potential of screening organoid biobanks to detect novel genotype-phenotype correlations (van de Wetering *et al*, 2015). In a recent study, Pauli and colleagues collected 145 specimens, representing 18 different tumor types derived from patients with metastatic solid tumors. PDO cultures were established from 56 of these specimens (38.6%), which were obtained from biopsies or surgical resection and stored in a living biobank (Pauli *et al*, 2017). PDOs of four patients were used to perform drug screens, targeting mutated pathways that were identified using whole exome sequencing (WES). PDTX models were subsequently used for the validation of the compounds that affected PDO growth. They found that two patients, suffering from uterine carcinosarcoma and endometrial adenocarcinoma, respectively, carried similar driver mutations in *PIK3CA* and *PTEN*. Yet, the drug response profiles clearly distinguished the two patients. For the uterine carcinosarcoma case they identified the combination of the PIK3 inhibitor buparlisib (Armstrong *et al*, 2017) with the hypoxia signalling suppressor vorinostat (Zhang *et al*, 2017) as one of the top drug combinations. By contrast, for the endometrial adenocarcinoma case, a combination of buparlisib with the PARP and HDAC inhibitor olaparib (Yuan *et al*, 2017) was found as optimal treatment in both PDO and PDTX models. The latter is of high relevance, as no targeted therapies are approved for endometrial cancer yet (Pauli *et al*, 2017). The combination of WES, PDO and PDTX models makes it possible to compare the efficacy of specific drugs on individual tumors thereby providing recommendations for patient care in a personalized manner. Moreover, it enables assessing how individual tumors evolve in response to therapies as well as determining next therapeutic steps for cases where standard clinical options have already been exhausted. Additionally, the combination of these techniques allows creating a database that relates drug sensitivity to tumor genetics. This enables to nominate potential therapeutic strategies even when only genomic data are available (Pauli *et al*, 2017). In conclusion, combining different techniques and model systems for cancer research can improve the prediction of clinical response to anti-cancer treatments in a personalized manner.

Outlook and challenges

The main challenge in preclinical cancer research remains the establishment of models that recapitulate the patient situation as close as possible, retaining intratumor

heterogeneity and the tumor environment. So far, not all cancer types can be grown in mice or as tumor organoids. For the establishment of more PDO models, it is of high relevance to find the optimal *in vitro* growth conditions that enable tumor cells to grow, while keeping as much cellular heterogeneity as possible. Selection pressure occurs in both PDX and PDO model systems (Pauli *et al*, 2017; Morgan *et al*, 2017). Therefore, combining the strengths of both preclinical model systems will be powerful for investigating therapeutic responses. For example, PDTOs can be used for high-throughput drug screenings and selecting effective drugs or drug combinations. Subsequently, the efficacy of these selected drugs should be validated in PDX models (Pauli *et al*, 2017). Together, these preclinical models can reflect the response to anti-cancer therapies and give indications for patient-tailored treatment.

Conclusions

In this review, we discussed the role of PDX and PDO model systems in cancer research and therapy development (Table 1). While PDXs have already been established for a broad variety of cancers (Fig. 3), the fast-evolving improvements in PDO culture systems hold great promise. Transplanting primary tumor tissue directly into mice allows for the partial resemblance of the tumor micro-environment, including stromal components, such as CAFs and vasculature. Although PDO cultures do - so far - not maintain the stromal components of human tumors, they represent genetic and phenotypic heterogeneity found in human cancers. Additionally, organoid cultures can be expanded relatively fast, cryopreserved, and genetically modified. These features allow for generating living tumor organoid biobanks and providing a platform for high-throughput drug screens. Although both models lack an immune competent environment, this limitation can be overcome by transplantation of HSCs and co-culture with T lymphocytes for PDX and PDO models, respectively.

In addition to PDX and PDO, several other pre-clinical models have been developed over the years. Induced pluripotent stem cells (iPSCs) can be differentiated towards several lineages and can be used to model normal development *in vitro*. iPSCs were successfully used for exocrine differentiation of pancreatic progenitors and for modelling PDAC tumor organoids (Huang *et al*, 2015) as well as for differentiation to colonic organoids for the modelling of CRC (Crespo *et al*, 2018). However, two main challenges in the establishment of iPSC-derived cancer models are the efficiency of malignant cell reprogramming and the capability to differentiate the iPSCs into the cell lineage of interest (Papapetrou, 2016). Additionally, during the establishment of iPSC-derived cancer models, selective outgrowth of tumor subclones may occur when a subset of cells harbours specific mutations resulting in a loss of heterogeneity. This is in stark contrast to PDO model systems that largely recapitulate the genetic heterogeneity of the parental tumor (van de Wetering *et al*, 2015; Huang *et al*, 2015; Sachs *et al*, 2018; Yan *et al*, 2018; Nanki *et al*, 2018). Another recent study described a technology termed conditional reprogramming, which allows ef-

ficient establishment of patient tissue-derived 2D cancer cell cultures in the presence of RHO kinase inhibitor and a fibroblast feeder layer (Liu *et al*, 2012). It is of high importance to combine multiple cancer models to get the best possible prediction of tumor sensitivity to and toxicity of anti-cancer treatments, which will ultimately result in more efficient translation from bench to bedside.

Conflict of interest

The authors declare that they have no conflict of interest

Acknowledgements

This review was prepared with support from the Dutch Cancer Society (KWF)/Alpe d'HuZes Bas Mulder Award to J.D. (KWF/Alpe d'HuZes, grant #10218), and On-code Institute to H.C. and J.D.

References

- Ardizzoni BA, Hansen H, Dombernowsky P, Gamucci T, Kaplan S & Postmus P (1997) Topotecan , a New Active Drug in the Second-Line Treatment of Small-Cell Lung Cancer : A Phase II Study in Patients With Refractory and Sensitive Disease. *J Clin Oncol* 15: 2090–2096
- Armstrong AJ, Halabi S, Healy P, Alumkal JJ, Winters C, Kephart J, Bitting RL, Hobbs C, Soleau CF, Beer TM, Slottke R, Mundy K, Yu EY & George DJ (2017) Phase II trial of the PI3 kinase inhibitor buparlisib (BKM-120) with or without enzalutamide in men with metastatic castration resistant prostate cancer. *Eur. J. Cancer* 81: 228–236
- Bartfeld S, Bayram T, Wetering M Van De, Huch M, Begthel H, Kujala P, Vries R, Peters PJ & Clevers H (2015) *In Vitro* Expansion of Human Gastric Epithelial Stem Cells and Their Responses to Bacterial Infection. *Gastroenterology* 148: 126–136
- Beckhove P, Schütz F, Diel IJ, Solomayer EF, Bastert G, Foerster J, Feuerer M, Bai L, Sinn HP, Umansky V & Schirmacher V (2003) Efficient engraftment of human primary breast cancer transplants in nonconditioned NOD/SCID mice. *Int. J. Cancer* 105: 444–453
- Bertotti A, Migliardi G, Galimi F, Sassi F, Torti D, Isella C, Corà D, di Nicolantonio F, Buscarino M, Petti C, Ribero D, Russolillo N, Muratore A, Massucco P, Pisacane A, Molinaro L, Valtorta E, Sartore-Bianchi A, Risio M, Capussotti L, et al (2011) A molecularly annotated platform of patient- derived xenografts ('xenopatiens') identifies HER2 as an effective therapeutic target in cetuximab-resistant colorectal cancer. *Cancer Discov.* 1: 508–523
- Boj SF, Hwang C II, Baker LA, Chio IIC, Engle DD, Corbo V, Jager M, Ponz-Sarvisé M, Tiriác H, Spector MS, Gracani A, Oni T, Yu KH, Van Boxtel R, Huch M, Rivera KD, Wilson JP, Feigin ME, Öhlund D, Handly-Santana A, et al (2015) Organoid models of human and mouse ductal pancreatic cancer. *Cell* 160: 324–338
- Broutier L, Mastrogianni G, Verstegen MMA, Francies HE, Gavarró LM, Bradshaw CR, Allen GE, Arnes-benito R, Sidorova O, Gaspersz MP, Georgakopoulos N, Koo B, Dietmann S, Davies SE, Praseedom RK, Lieshout R, Ijzermans JNM, Wigmore SJ, Saeb-parsy K, Garnett MJ, et al (2017) Human primary liver cancer – derived organoid cultures for disease modeling and drug screening. *Nat. Med.* 23: 1424–1435
- Bruna A, Rueda OM & Caldas C (2016) Modeling breast cancer intertumor and intratumor heterogeneity using xenografts. *Cold Spring Harb. Symp. Quant. Biol.* 81: 227–230
- Byrne AT, Alf  rez DG, Amant F, Annibali D, Arribas J, Biankin A V, Bruna A, Budinsk   E, Caldas C, Chang DK, Clarke RB, Clevers H, Coukos G, Dangles-Marie V, Gail Eckhardt S, Gonzalez-Suarez E, Hermans E, Hidalgo M, Jarzabek MA, De Jong S, et al (2017) Interrogating open issues in cancer precision medicine with patient-derived xenografts. *Nat. Rev. Cancer* 17: 254–268
- Chua CW, Shibata M, Lei M, Toivanen R, Barlow LJ, Bergren SK, Badani KK, Mckiernan JM, Benson MC, Hibshoosh H & Shen MM (2014) Single luminal epithelial progenitors can generate prostate organoids in culture. *Nat. Cell Biol.* 16: 951–961
- Clevers H (2016) Modeling Development and Disease with Organoids. *Cell* 165: 1586–1597
- Crespo M, Vilar E, Tsai S, Chang K, Amin S, Srinivasan T, Zhang T, Pipalia NH, Chen HJ, Witherspoon M, Gordillo M, Xiang JZ, Maxfield FR, Lipkin S, Evans T & Chen S (2018) Colonic organoids derived from human induced pluripotent stem cells for modeling colorectal cancer and drug testing. *Nat. Med.* 23: 878–884
- Cutz J, Guan J, Bayani J, Xue H, Sutcliffe M, English J, Flint J, Leriche J, Yee J, Squire J, Gout PW, Lam S & Wang Y (2006) Cancer Therapy : Preclinical Establishment in Severe Combined Immunodeficiency Mice of Subrenal Capsule Xenografts and Transplantable Tumor Lines from a Variety of Primary Human Lung Cancers : Potential Models for Studying Tumor Progression-related Changes. *Clin. cancer res.* 12: 4043–4055
- Dai L, Lu C, Yu X, Dai L-J & Zhou JX (2015) Construction of orthotopic xenograft mouse models for human pancreatic cancer. *Exp. Ther. Med.* 10: 1033–1038
- Dijkstra KK, Cattaneo CM, Weeber F, Chalabi M, van de Haar J, Fanchi LF, Slagter M, van der Velden DL, Kaing S, Kelderman S, van Rooij N, van Leerdam ME, Depla A, Smit EF, Hartemink KJ, de Groot R, Wolkers MC, Sachs N, Snaebjornsson P, Monkhorst K, et al (2018) Generation of Tumor-Reactive T Cells by Co-culture of Peripheral Blood Lymphocytes and Tumor Organoids. *Cell* 174: 1586-1598.e12
- Dimasi JA, Reichert JM, Feldman L & Malins A (2013) Clinical approval success rates for investigational cancer drugs. *Clin. Pharmacol. Ther.* 94: 329–335
- Drake AC, Chen Q & Chen J (2012) Engineering humanized mice for improved hematopoietic reconsti-

- tution. *Cell. Mol. Immunol.* 9: 215–224
- Drost J, Boxtel R Van, Blokzijl F, Mizutani T, Sasaki N, Sasselli V, de Ligt J, Behjati S, Grolleman JE, van Wezel T, Nik-Zainal S, Kuiper RP, Cuppen E & Clevers H (2017) Use of CRISPR-modified human stem cell organoids to study the origin of mutational signatures in cancer. *Science* 91: 399–404
- Drost J & Clevers H (2018) Organoids in cancer research. *Nat. Rev. Cancer* 18: 407–418
- Drost J, Jaarsveld RH Van, Ponsioen B, Zimmerlin C, Boxtel R Van, Buijs A, Overmeer M, Offerhaus GJ, Begthel H, Korving J, Wetering M Van De, Sachs N, Schwank G, Logtenberg M, Cuppen E, Snippert HJ, Medema JP, Kops GJPL & Clevers H (2015) Sequential cancer mutations in cultured human intestinal stem cells. *Nature* 521: 43–47
- Drost J, Karthaus WR, Gao D, Driehuis E, Sawyers CL, Chen Y & Clevers H (2016) Organoid culture systems for prostate epithelial and cancer tissue. *Nat. Protoc.* 11: 347–358
- Fichtner I, Slisow W, Gill J, Becker M, Elbe B, Hillebrand T & Bibby M (2004) Anticancer drug response and expression of molecular markers in early-passage xenotransplanted colon carcinomas. *Eur. J. Cancer* 40: 298–307
- Fu X, Guadagni F & Hoffman RM (1992) A metastatic nude-mouse model of human pancreatic cancer constructed orthotopically with histologically intact patient specimens. *Proc. Natl. Acad. Sci.* 89: 5645–5649
- Fujii M, Shimokawa M, Date S, Takano A, Matano M, Nanki K, Ohta Y, Toshimitsu K, Nakazato Y, Kawasaki K, Uraoka K, Watanabe T, Kanai T & Sato T (2016) A Colorectal Tumor Organoid Library Demonstrates Progressive Loss of Niche Factor Requirements during Tumorigenesis. *Cell Stem Cell* 18: 827–838
- Gao D, Vela I, Sboner A, Iaquinta PJ, Karthaus WR, Gopalan A, Dowling C, Wanjala JN, Undvall EA, Arora VK, Wongvipat J, Kossai M, Ramazanoglu S, Barboza LP, Di W, Cao Z, Zhang QF, Sirota I, Ran L, Macdonald TY, et al (2014) Organoid cultures derived from patients with advanced prostate cancer. *Cell* 159: 176–187
- Gao H, Korn JM, Ferretti S, Monahan JE, Wang Y, Singh M, Zhang C, Schnell C, Yang G, Zhang Y, Balbin OA, Barbe S, Cai H, Casey F, Chatterjee S, Chiang DY, Chuai S, Cogan SM, Collins SD, Dammasa E, et al (2015) High-throughput screening using patient-derived tumor xenografts to predict clinical trial drug response. *Nat. Med.* 21: 1318–1325
- George E, Kim H, Krepler C, Wenz B, Makvandi M, Tanyi JL, Brown E, Zhang R, Brafford P, Jean S, Mach RH, Lu Y, Mills GB, Herlyn M, Morgan M, Zhang X, Soslow R, Drapkin R, Johnson N, Zheng Y, et al (2017) A patient-derived-xenograft platform to study BRCA-deficient ovarian cancers. *JCI Insight* 2: e89760
- Greshock J, Bachman KE, Degenhardt YY, Jing J, Wen YH, Eastman S, McNeil E, Moy C, Wegrzyn R, Auger K, Hardwicke MA & Wooster R (2010) Molecular target class is predictive of *in vitro* response profile. *Cancer Res.* 70: 3677–3686
- Guenot D, Guérin E, Aguilon-Romain S, Pencreach E, Schneider A, Neuville A, Chenard MP, Duluc I, Du Manoir S, Brigand C, Oudet P, Kedingier M & Gaub MP (2006) Primary tumor genetic alterations and intra-tumoral heterogeneity are maintained in xenografts of human colon cancers showing chromosome instability. *J. Pathol.* 208: 643–652
- Hennessey PT, Ochs ME, Mydlarz WW, Hsueh W, Cope L, Yu W & Califano JA (2011) Promoter methylation in head and neck squamous cell carcinoma cell lines is significantly different than methylation in primary tumors and xenografts. *PLoS One* 6: e20584
- Heppner GH (1984) Tumor Heterogeneity. *Cancer Res.* 44: 2259–2265
- Hidalgo M, Amant F, Biankin A V, Budinská E, Byrne AT, Caldas C, Clarke RB, Jong S De, Jonkers J & Mari G (2015) Patient Derived Xenograft Models : An Emerging Platform for Translational Cancer Research. *Cancer Discov.* 4: 998–1013
- Hild M & Jaffe AB (2016) Production of 3-D Airway Organoids From Primary Human Airway Basal Cells and Their Use in High-Throughput Screening. *Curr. Protoc. Stem Cell Biol.* 37: IE.9.1 – IE.9.15
- Von Hoff DD, Ervin T, Arena FP, Chiorean EG, Infante J, Moore M, Seay T, Tjulandin SA, Ma WW, Saleh MN, Harris M, Reni M, Dowden S, Laheru D, Bahary N, Ramanathan RK, Tabernero J, Hidalgo M, Goldstein D, Van Cutsem E, et al (2013) Increased Survival in Pancreatic Cancer with nab-Paclitaxel plus Gemcitabine. *N. Engl. J. Med.* 369: 1691–1703
- Hoffman RM (2015) Patient-derived orthotopic xenografts: Better mimic of metastasis than subcutaneous xenografts. *Nat. Rev. Cancer* 15: 451–452
- Huang L, Holtzinger A, Jagan I, Begora M, Lohse I, Ngai N, Nostro C, Wang R, Muthuswamy LB, Crawford HC, Arrowsmith C, Kalloger SE, Renouf DJ, Connor AA, Cleary S, Schaeffer DF, Roehrl M,

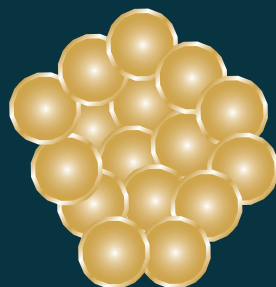
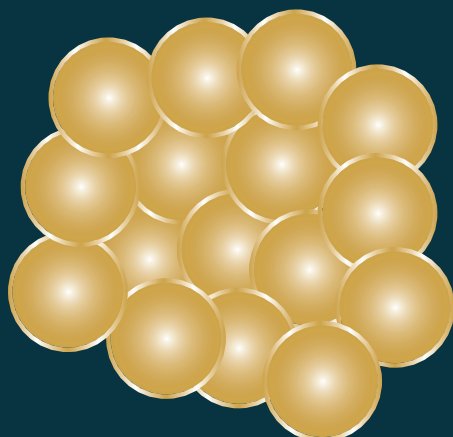
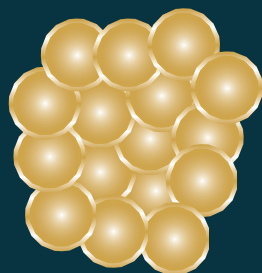
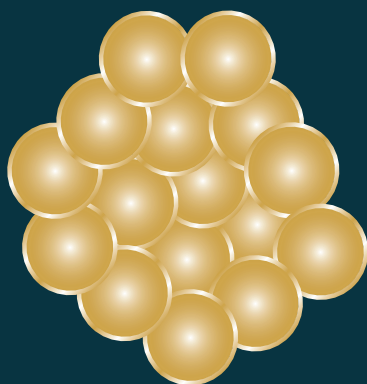
- Tsao MS, Gallinger S, Keller G, et al (2015) Ductal pancreatic cancer modeling and drug screening using human pluripotent stem cell- and patient-derived tumor organoids. *Nat. Med.* 21: 1364–1371
- Huch M, Gehart H, Boxtel R Van, Hamer K, Blokzijl F, Verstegen MMA, Ellis E, Wenum M Van, Fuchs SA, Lig J De, Wetering M Van De, Sasaki N, Boers SJ, Kemperman H, Jonge J De, Ijzermans JNM, Nieuwenhuis EES, Hoekstra R, Strom S, Vries RRG, et al (2015) Long-Term Culture of Genome-Stable Bipotent Stem Cells from Adult Human Liver. *Cell* 160: 299–312
- Julien S, Merino-trigo A, Lacroix L, Pocard M, Go  re D, Mariani P, Landron S, Bigot L, Nemati F, Dartigues P, Weiswald L, Lantuas D, Morgand L, Pham E, Gonin P, Dangles-marie V, Job B, Th H De, Soliman H, Nunes M, et al (2012) Characterization of a Large Panel of Patient-Derived Tumor Xenografts Representing the Clinical Heterogeneity of Human Colorectal Cancer. *Clin Cancer Res* 18: 5314–5329
- Jun D, Kim SY, Na JC, Ho H, Id L, Kim J, Yoon YE, Hong SJ, Kyu W & Id H (2018) Tubular organotypic culture model of human kidney. *PLoS One* 13: e0206447
- Kartha WR, Iaquina PJ, Drost J, Gracanin A, Van Boxel R, Wongvipat J, Dowling CM, Gao D, Begthel H, Sachs N, Vries RGJ, Cuppen E, Chen Y, Sawyers CL & Clevers HC (2014) Identification of multipotent luminal progenitor cells in human prostate organoid cultures. *Cell* 159: 163–175
- Kemper K, Krijgsman O, Cornelissen-Steijger P, Shahrabi A, Weeber F, Song J-Y, Kuilman T, Vis DJ, Wessels LF, Voest EE, Schumacher TN, Blank CU, Adams DJ, Haanen JB & Peeper DS (2015) Intra- and inter-tumor heterogeneity in a vemurafenib-resistant melanoma patient and derived xenografts. *EMBO Mol. Med.* 7: 1104–1118
- Kessler M, Hoffmann K, Brinkmann V, Thieck O, Jackisch S, Toelle B, Berger H, Mollenkopf HJ, Mangler M, Sehouli J, Fotopoulou C & Meyer TF (2015) The Notch and Wnt pathways regulate stemness and differentiation in human fallopian tube organoids. *Nat. Commun.* 6: 8989
- Kim MP, Evans DB, Wang H, Abbruzzese JL, Fleming JB & Gallick GE (2009) Generation of orthotopic and heterotopic human pancreatic cancer xenografts in immunodeficient mice. *Nat. Protoc.* 4: 1670–1680
- Kopper O, Witte CJ De, L  hmussaar K, Valle-inclan JE, Hami N, Kester L, Balgobind AV, Korving J, Proost N, Begthel H, Wijk LM Van, Revilla SA, Theeuwse R, Ven M Van De, Roosmalen MJ Van, Ponsioen B, Ho VWH, Neel BG, Bosse T, Gaarenstroom KN, et al (2019) An organoid platform for ovarian cancer captures intra- and interpatient heterogeneity. *Nat. Med.* 25: 838 – 849
- Kreso A & Dick JE (2014) Review Evolution of the Cancer Stem Cell Model. *Stem Cell* 14: 275–291
- Lee SH, Hu W, Matulay JT, Al-ahmadie H, Solit DB, Shen MM, Lee SH, Hu W, Matulay JT, Silva M V, Owczarek TB, Kim K, Chua CW, Barlow LJ, Kandath C, Williams AB, Bergen SK, Pietzak EJ, Anderson CB, Benson MC, et al (2018) Tumor Evolution and Drug Response in Patient-Derived Organoid Models of Bladder Cancer. *Cell* 173: 515–528
- Li L, Bader JS, Selaru FM, Li L, Knutsdottir H, Hui K, Weiss MJ, He J, Philosophie B, Ewald AJ, Mezey E, Bader JS & Selaru FM (2019) Human primary liver cancer organoids reveal intratumor and interpatient drug response heterogeneity. *JCI Insight* 4: 121490
- Li X, Francies HE, Secrier M, Perner J, Miremadi A, Galeano-dalmau N, Barendt WJ, Letchford L, Leyden GM, Goffin EK, Barthorpe A, Lightfoot H, Chen E, Gilbert J, Noorani A, Devonshire G, Bower L, Grantham A, MacRae S, Grehan N, et al (2018) Organoid cultures recapitulate esophageal adenocarcinoma heterogeneity providing a model for clonality studies and precision therapeutics. *Nat. Commun.* 9: 2983
- Li X, Nadauld L, Ootani A, Corney DC, Pai RK, Gevaert O, Cantrell MA, Rack PG, Neal JT, Chan CWM, Yeung T, Gong X, Yuan J, Wilhelmy J, Robine S, Attardi LD, Plevritis SK, Hung KE, Chen CZ, Ji HP, et al (2014) Oncogenic transformation of diverse gastrointestinal tissues in primary organoid culture. *Nat. Med.* 20: 769–777
- Liu X, Ory V, Chapman S, Yuan H, Albanese C, Kallakury B, Timofeeva OA, Nealon C, Dakic A, Simic V, Haddad BR, Rhim JS, Dritschilo A, Riegel A, McBride A & Schlegel R (2012) ROCK Inhibitor and Feeder Cells Induce the Conditional Reprogramming of Epithelial Cells. *AJPA* 180: 599–607
- Matano M, Date S, Shimokawa M, Takano A, Fujii M, Ohta Y, Watanabe T, Kanai T & Sato T (2015) Modeling colorectal cancer using CRISPR-Cas9-mediated engineering of human intestinal organoids. *Nat. Med.* 21: 256–262
- McGranahan N & Swanton C (2017) Clonal Heterogeneity and Tumor Evolution: Past, Present, and the Future. *Cell* 168: 613–628
- Morgan KM, Riedlinger GM, Rosenfeld J, Ganesan S & Pine SR (2017) Patient-Derived Xenograft Models of Non-Small Cell Lung Cancer and Their Potential Utility in Personalized Medicine. *Front.*

Oncol. 7: 2

- Mullenders J, Jongh E De, Brousalı A, Roosen M, Blom JPA, Begthel H, Korving J, Jonges T, Kranenburg O, Meijer R & Clevers HC (2019) Mouse and human urothelial cancer organoids : A tool for bladder cancer research. *PNAS* 116: 4567–4574
- Nanki K, Toshimitsu K, Takano A, Fujii M, Shimokawa M, Ohta Y, Matano M, Seino T, Nishikori S, Ishikawa K, Kawasaki K, Togasaki K, Takahashi S, Sukawa Y, Ishida H, Sugimoto S, Kawakubo H, Kim J, Kitagawa Y, Sekine S, et al (2018) Divergent Routes toward Wnt and R-spondin Niche Independency during Human Gastric Carcinogenesis. *Cell* 174: 856–869.e17
- Neal JT, Li X, Zhu J, Giangarra V, Grzeskowiak CL, Ju J, Liu IH, Chiou SH, Salahudeen AA, Smith AR, Deutsch BC, Liao L, Zemek AJ, Zhao F, Karlsson K, Schultz LM, Metzner TJ, Nadauld LD, Tseng YY, Alkhairy S, et al (2018) Organoid Modeling of the Tumor Immune Microenvironment. *Cell* 175: 1972–1988.e16
- Némati F, Daniel C, Arvelo F, Legrier ME, Froget B, Livartowski A, Assayag F, Bourgeois Y, Poupon MF & Decaudin D (2010) Clinical relevance of human cancer xenografts as a tool for preclinical assessment: Example of *in-vivo* evaluation of topotecan-based chemotherapy in a panel of human small-cell lung cancer xenografts. *Anticancer. Drugs* 21: 25–32
- Nozaki K, Mochizuki W, Matsumoto Y, Matsumoto T, Fukuda M, Mizutani T, Watanabe M & Nakamura T (2016) Co-culture with intestinal epithelial organoids allows efficient expansion and motility analysis of intraepithelial lymphocytes. *J. Gastroenterol.* 51: 206–213
- Öhlund D, Santana AH, Biffi G, Elyada E, Almeida AS, Sarvis MP, Corbo V, Oni TE, Hearn SA, Lee EJ, In I, Chio C, Hwang C II, Tiriac H, Baker LA, Engle DD, Feig C, Kultti A, Egeblad M, Fearon DT, et al (2017) Distinct populations of inflammatory fibroblasts and myofibroblasts in pancreatic cancer. *JEM* 214: 579–596
- Papapetrou EP (2016) perspective Patient-derived induced pluripotent stem cells in cancer research and precision oncology. *Nat. Med.* 22: 1392–1401
- Pauli C, Hopkins BD, Prandi D, Shaw R, Fedrizzi T, Sboner A, Sailer V, Augello M, Puca L, Rosati R, McNary TJ, Churakova Y, Cheung C, Triscott J, Pisapia D, Rao R, Mosquera JM, Robinson B, Faltas BM, Emerling BE, et al (2017) Personalized *in vitro* and *in vivo* cancer models to guide precision medicine. *Cancer Discov.* 7: 462–477
- Pearson AT, Finkel KA, Warner KA, Nör F, Tice D, Martins MD, Jackson TL & Nör JE (2016) Patient-derived xenograft (PDX) tumors increase growth rate with time. *Oncotarget* 7: 7993–8005
- Peng S, Creighton CJ, Zhang Y, Sen B, Mazumdar T, Myers JN, Lai SY, Woolfson A, Lorenzi M V, Bell D, Williams MD & Johnson FM (2013) Tumor grafts derived from patients with head and neck squamous carcinoma authentically maintain the molecular and histologic characteristics of human cancers. *J. Transl. Med.* 11: 198
- Phillips B & Gazet JC (1970) Transplantation of primary explants of human tumor to mice treated with antilymphocyte serum. *Br. J. Cancer* 24: 92–95
- Roerink SF, Sasaki N, Lee-Six H, Young MD, Alexandrov LB, Behjati S, Mitchell TJ, Grossmann S, Lightfoot H, Egan DA, Pronk A, Smakman N, Van Gorp J, Anderson E, Gamble SJ, Alder C, Van De Wetering M, Campbell PJ, Stratton MR & Clevers H (2018) Intra-tumor diversification in colorectal cancer at the single-cell level. *Nature* 556: 437–462
- Rosfjord E, Lucas J, Li G & Gerber HP (2014) Advances in patient-derived tumor xenografts: From target identification to predicting clinical response rates in oncology. *Biochem. Pharmacol.* 91: 135–143
- Sachs N & Clevers H (2014) ScienceDirect Organoid cultures for the analysis of cancer phenotypes. *Curr. Opin. Genet. Dev.* 24: 68–73
- Sachs N, de Lig J, Kopper O, Gogola E, Bounova G, Weeber F, Balgobind AV, Wind K, Gracanin A, Begthel H, Korving J, Van Bostel R, Alves Duarte A, Lelieveld D, Van Hoeck A, Ernst RF, Blokzijl E, Nijman IJ, Hoogstraat M, van de Ven M, et al (2018) Resource A Living Biobank of Breast Cancer Organoids Resource A Living Biobank of Breast Cancer Organoids Captures Disease Heterogeneity. *Cell* 172: 373–386
- Sachs N, Pappaspyropoulos A, Ommen DDZ, Heo I, Klay D, Weeber F, Huelsz-prince G, Iakobachvili N, Gimano D, Lig J De, Hoeck A Van, Proost N, Viveen MC, Lyubimova A, Teeven L, Derakhshan S, Korving J, Begthel H, Dekkers JF, Ramos E, et al (2019) Long-term expanding human airway organoids for disease modeling. *EMBO J.* 38: e100300
- Sato T, Stange DE, Ferrante M, Vries RGJ, Van Es JH, Van Den Brink S, Van Houdt WJ, Pronk A, Van Gorp J, Siersema PD & Clevers H (2011) Long-term expansion of epithelial organoids from human colon, adenoma, adenocarcinoma, and Barrett's epithelium. *Gastroenterology* 141: 1762–1772

- Sato T, Vries RG, Snippert HJ, Wetering M Van De, Barker N, Stange DE, Es JH Van, Abo A, Kujala P, Peters PJ & Clevers H (2009) Single Lgr5 stem cells build crypt – villus structures *in vitro* without a mesenchymal niche. *Nature* 459: 262–265
- Schumacher TN & Schreiber RD (2015) Neoantigens in cancer immunotherapy. *Sci. Rev.* 348: 69–74
- Schutgens F, Rookmaaker MB, Margaritis T, Rios A, Ammerlaan C, Jansen J, Gijzen L, Vormann M, Vonk A, Viveen M, Yengej FY, Derakhshan S, Groot KMDW, Artegiani B, Boxtel R Van, Cuppen E, Hendrickx APA, Heuvel-eibrink MM Van Den, Heitzer E, Lanz H, et al (2019) Tubuloids derived from human adult kidney and urine for personalized disease modeling. *Nat. Biotechnol.* 37: 303–313
- Schütte M, Risch T, Abdavi-Azar N, Boehnke K, Schumacher D, Keil M, Yildirim R, Jandrasits C, Borodina T, Amstislavskiy V, Worth CL, Schweiger C, Liebs S, Lange M, Warnatz HJ, Butcher LM, Barrett JE, Sultan M, Wierling C, Golob-Schwarzl N, et al (2017) Molecular dissection of colorectal cancer in pre-clinical models identifies biomarkers predicting sensitivity to EGFR inhibitors. *Nat. Commun.* 8: 14262
- Seino T, Kawasaki S, Shimokawa M, Tamagawa H, Toshimitsu K & Fujii M (2018) Human Pancreatic Tumor Organoids Reveal Loss of Stem Cell Niche Factor Dependence during Disease Human Pancreatic Tumor Organoids Reveal Loss of Stem Cell Niche Factor Dependence during Disease Progression. *Stem Cell* 22: 454–467
- Shi H, Hugo W, Kong X, Hong A, Koya RC, Moriceau G, Chodon T, Guo R, Johnson DB, Dahlman KB, Kelley MC, Kefford RF, Chmielowski B, Glaspy JA, Sosman JA, Van Baren N, Long G V., Ribas A & Lo RS (2014) Acquired resistance and clonal evolution in melanoma during BRAF inhibitor therapy. *Cancer Discov.* 4: 80–93
- Shultz LD, Brehm MA, Victor Garcia-Martinez J & Greiner DL (2012) Humanized mice for immune system investigation: Progress, promise and challenges. *Nat. Rev. Immunol.* 12: 786–798
- Shultz LD, Lyons BL, Burzenski LM, Gott B, Chen X, Chaleff S, Koth M, Gillies SD, King M, Mangada J, Greiner DL & Handgretinger R (2005) Human Lymphoid and Myeloid Cell Development in NOD/LtSz-scid IL2R null Mice Engrafted with Mobilized Human Hemopoietic Stem Cells. *J. Immunol.* 174: 6477–6489
- Simpson-Abelson MR, Sonnenberg GF, Takita H, Yokota SJ, Conway TF, Kelleher RJ, Shultz LD, Barcos M & Bankert RB (2008) Long-Term Engraftment and Expansion of Tumor-Derived Memory T Cells Following the Implantation of Non-Disrupted Pieces of Human Lung Tumor into NOD-scid IL2R null Mice. *J. Immunol.* 180: 7009–7018
- Sos ML, Michel K, Zander T, Weiss J, Frommolt P, Peifer M, Li D, Ullrich R, Koker M, Fischer F, Shimamura T, Rauh D, Mermel C, Fischer S, Stückerath I, Heynck S, Beroukhim R, Lin W, Winckler W, Shah K, et al (2009) Predicting drug susceptibility of non - small cell lung cancers based on genetic lesions. *J. Clin. Invest.* 119: 1727–1740
- Suhaimi N-AM, Phyo WM, Yap HY, Choy SHY, Wei X, Choudhury Y, Tan WJ, Tan LAPY, Foo RSY, Tan SHS, Tiang Z, Wong CF, Koh PK & Tan M-H (2017) Metformin Inhibits Cellular Proliferation and Bioenergetics in Colorectal Cancer Patient-Derived Xenografts. *Mol. Cancer Ther.* 16: 2035–2044
- Tabassum DP & Polyak K (2015) Tumorigenesis: It takes a village. *Nat. Rev. Cancer* 15: 473–483
- Taetle R, Jones OW, Honeysett JM, Abramson I, Bradshaw C & Reid S (1987) Use of nude mouse xenografts as preclinical screens: Characterization of xenograft-derived melanoma cell lines. *Cancer* 60: 1836–1841
- Tan Q, Choi KM, Sicard D & Tschumperlin DJ (2017) Human airway organoid engineering as a step toward lung regeneration and disease modeling. *Biomaterials* 113: 118–132
- Tauriello DVF, Palomo-Ponce S, Stork D, Berenguer-Llargo A, Badia-Ramentol J, Iglesias M, Sevillano M, Ibiza S, Cañellas A, Hernando-Momblona X, Byrom D, Matarin JA, Calon A, Rivas EI, Nebreda AR, Riera A, Attolini CSO & Batlle E (2018) TGF β drives immune evasion in genetically reconstituted colon cancer metastasis. *Nature* 554: 538–543
- Das Thakur M, Salangsang F, Landman AS, Sellers WR, Pryer NK, Levesque MP, Dummer R, McMahon M & Stuart DD (2013) Modelling vemurafenib resistance in melanoma reveals a strategy to forestall drug resistance. *Nature* 494: 251–255
- Thatcher N, Chang A, Parikh P, Rodrigues Pereira J, Ciuleanu T, von Pawel J, Thongprasert S, Tan EH, Pemberton K, Archer V & Carroll K (2005) Gefitinib plus best supportive care in previously treated patients with refractory advanced non-small-cell lung cancer: results from a randomised, placebo-controlled, multicentre study (Iressa Survival Evaluation in Lung Cancer). *Lancet* 366: 1527–1537
- Tiriach H, Belleau P, Engle DD, Plenker D, Deschênes A, Somerville TDD, Froeling FEM, Burkhart RA, Denroche RE, Jang G, Miyabayashi K, Young CM, Patel H, Ma M, Lacombe JF, Palmaira RLD, Javed

- AA, Huynh JC, Johnson M, Arora K, et al (2018) Organoid Profiling Identifies Common Responders to Chemotherapy in Pancreatic Cancer. *Cancer Discov.* 8: 1112–1129
- Toolan HW (1953) Growth of Human Tumors in Cortisone-treated Laboratory Animals: The Possibility of Obtaining Permanently Transplantable Human Tumors. *Cancer Res.* 13: 389–394
- Verissimo CS, Overmeer M, Ponsioen B, Drost J, Mertens S, Verlaan-klink I, Gerwen B Van, Ven M Van Der, Wetering M Van De, Egan DA, Clevers H, Bos JL & Snippert HJ (2016) Targeting mutant RAS in patient-derived colorectal cancer organoids by combinatorial drug screening. *Elife* 5: e18489
- Vlachogiannis G, Hedayat S, Vatsiou A, Jamin Y, Fernández-mateos J, Khan K, Lampis A, Eason K, Huntingford I, Burke R, Rata M, Koh D, Tunariu N, Collins D, Hulkki-wilson S, Ragulan C, Spiteri I, Moorcraft SY, Chau I, Rao S, et al (2018) Patient-derived organoids model treatment response of metastatic gastrointestinal cancers. *Science* 926: 920–926
- Voloshin T, Gingis-Velitski S, Bril R, Benayoun L, Munster M, Milsom C, Man S, Kerbel RS & Shaked Y (2011) G-CSF supplementation with chemotherapy can promote revascularization and subsequent tumor regrowth: Prevention by a CXCR4 antagonist. *Blood* 118: 3426–3435
- Wang Y, Revelo MP, Sudilovsky D, Cao M, Chen WG, Goetz L, Xue H, Sadar M, Shappell SB, Cunha GR & Hayward SW (2005) Development and characterization of efficient xenograft models for benign and malignant human prostate tissue. *Prostate* 64: 149–159
- Weeber F, van de Wetering M, Hoogstraat M, Dijkstra KK, Krijgsman O, Kuilman T, Gadellaa-van Hooijdonk CGM, van der Velden DL, Peeper DS, Cuppen EPJG, Vries RG, Clevers H & Voest EE (2015) Preserved genetic diversity in organoids cultured from biopsies of human colorectal cancer metastases. *Proc. Natl. Acad. Sci.* 112: 13308–13311
- Wege AK, Ernst W, Eckl J, Frankenberger B, Vollmann-Zwerenz A, Männel DN, Ortmann O, Kroemer A & Brockhoff G (2011) Humanized tumor mice—A new model to study and manipulate the immune response in advanced cancer therapy. *Int. J. Cancer* 129: 2194–2206
- van de Wetering M, Francies HE, Francis JM, Bounova G, Iorio E, Pronk A, Van Houdt W, Van Gorp J, Taylor-Weiner A, Kester L, McLaren-Douglas A, Blokker J, Jaksani S, Bartfeld S, Volckman R, Van Sluis P, Li VSW, Seepo S, Sekhar Pedamallu C, Cibulskis K, et al (2015) Prospective derivation of a living organoid biobank of colorectal cancer patients. *Cell* 161: 933–945
- Wimmer RA, Leopoldi A, Aichinger M, Wick N, Hantusch B, Novatchkova M, Taubenschmid J, Hämmerle M, Esk C, Bagley JA, Lindenhofer D, Chen G, Boehm M, Agu CA, Yang F, Fu B, Zuber J, Knoblich JA, Kerjaschki D & Penninger JM (2019) Human blood vessel organoids as a model of diabetic vasculopathy. *Nature* 565: 505–510
- Yan HHN, Siu HC, Law S, Ho SL, Yue SSK, Tsui WY, Chan D, Chan AS, Ma S, Lam KO, Bartfeld S, Man AHY, Lee BCH, Chan ASY, Wong JWH, Cheng PSW, Chan AKW, Zhang J, Shi J, Fan X, et al (2018) A Comprehensive Human Gastric Cancer Organoid Biobank Captures Tumor Subtype Heterogeneity and Enables Therapeutic Screening. *Cell Stem Cell* 23: 882–897
- Yuan Z, Chen S, Sun Q, Wang N, Li D, Miao S, Gao C, Chen Y, Tan C & Jiang Y (2017) Olaparib hydroxamic acid derivatives as dual PARP and HDAC inhibitors for cancer therapy. *Bioorganic Med. Chem.* 25: 4100–4109
- Zhan B, Wen S, Lu J, Shen G, Lin X, Feng J, Huang H, Zhan B, Wen S, Lu J, Shen G, Lin X, Feng J & Huang H (2017) Identification and causes of metabonomic difference between orthotopic and subcutaneous xenograft of pancreatic cancer. *Oncotarget* 8: 61264–61281 Available at: <http://www.oncotarget.com/fulltext/18057>
- Zhang C, Yang C, Feldman MJ, Wang H, Pang Y, Maggio DM, Zhu D, Nesvick CL, Dmitriev P, Bullova P, Chittiboina P, Brady RO, Pacak K & Zhuang Z (2017) Vorinostat suppresses hypoxia signaling by modulating nuclear translocation of hypoxia inducible factor 1 alpha. *Oncotarget* 8: 56110–56125
- Zumwalde NA, Haag JD, Sharma D, Mirrieles JA, Wilke LG, Gould MN & Gumperz JE (2016) Analysis of immune cells from human mammary ductal epithelial organoids reveals Vδ2+T cells that efficiently target breast carcinoma cells in the presence of bisphosphonate. *Cancer Prev. Res.* 9: 305–316



Chapter 3

PDTO models of Ewing sarcoma allow for medium-throughput drug screening

Margit Bleijs^{1,*}, Femke Ringnalda^{1,*}, Laura Hiemcke-Jiwa²,
Kimberley Ober², Selma Eising², Hans Clevers^{1,3}

1. Oncode Institute, Prinses Máxima Center for Pediatric Oncology, Utrecht,
The Netherlands

2. Prinses Máxima Center for Pediatric Oncology, Utrecht, The Netherlands

3. Oncode Institute, Hubrecht Institute, Royal Netherlands Academy of Arts
and Sciences (KNAW) and University Medical Centre Utrecht, the Netherlands

* These authors contributed equally to this work

Abstract

Ewing sarcoma (ES) is an aggressive tumor found in bone and soft tissues of adolescents and young adults. The establishment of preclinical models that recapitulate essential features of the originating tumor is of high relevance for the development of treatment strategies. Here, we establish four Patient-derived Tumor Organoid (PDTO) models from three different ES patients that recapitulate both phenotypic and genetic features of the original tumor. ES PDTO models allow for *in vitro* compound screens, which reveal drug sensitivity to several cytotoxic compounds and targeted compounds, including HDAC inhibitors. Together, this study provides proof of principle for ES PDTO model establishment and for predicting drug responses in ES patients in a personalized manner.

Introduction

Ewing sarcoma (ES) is an aggressive tumor arising in soft tissue and bone. This sarcoma commonly occurs in adolescents and young adults with a peak incidence between 10-25 years of age (Ross *et al.*, 2013). ES is predominantly located in the pelvis, femur, tibia, ribs, thoracic wall, gluteal muscle, pleural cavities and cervical muscles (Grünewald *et al.*, 2018). Genetically, ES is characterized by a chromosomal translocation resulting in the expression of a *EWSR1-ETS* fusion gene, most frequently *EWSR1-FLI1* (Ross *et al.*, 2013). Expression of this fusion gene affects the control of gene expression in various ways: through changes in DNA methylation, histone modifications and noncoding RNA expression, all presumably due to its activity as an aberrant chimeric transcription factor (Riggi *et al.*, 2021). Treatment of ES includes chemotherapy, surgery and local radiation therapy, which has increased the 5-year overall survival rate to $\pm 70\%$ (Le Deley *et al.*, 2014). However, when patients are diagnosed with metastatic or relapsed disease, the long-term survival rate decreases to only $\pm 20\%$ (Kovar *et al.*, 2012). The poor prognosis upon metastatic and relapsed disease underlines the need to investigate mechanisms of tumor progression and therapy resistance.

Preclinical models phenocopying primary tumor material are required to study mechanisms driving tumor progression and drug resistance (Bleijs *et al.*, 2019). Several preclinical models of ES have been established, including patient-derived tumor xenografts (PDTX) and *in vitro* cell lines, which have led to several novel therapeutic options (Nanni *et al.*, 2019). For example, Nanni and colleagues found that a combination of anti-CD99 diabody C7 and Irinotecan inhibits tumor growth in ES PDTX models (Nanni *et al.*, 2019). Another recent study identified a synergistic effect of the thioredoxin reductase inhibitor Auranofin and HSP90 inhibitor Ganetespib in preclinical ES models, both in PDTX models and cell lines (Pessetto *et al.*, 2017). While PDTX models can better predict therapy response in a physiologically relevant environment, cell lines are easier to expand and therefore more suitable for medium- to high-throughput drug screens. Patient-derived tumor organoid (PDTO) models that resemble the architecture of the original tumor may bridge the gap between cell lines and PDTX models (Bleijs *et al.*, 2019; Sachs & Clevers, 2014). PDTO models additionally allow for genetic engineering to study oncogenic mutations and tumor cell heterogeneity (Drost *et al.*, 2017; Keskin *et al.*, 2021). Recently, patient-derived 3D ES cultures were used to introduce a microRNA-145 based live-cell reporter assay to identify two Ewing cell populations with different tumorigenic properties when transplanted into mice (Keskin *et al.*, 2021). Here, we establish four ES PDTO models from three different patients, that both genetically and phenotypically recapitulate the original tumor. These PDTO models enabled us to perform medium-throughput drug screens to uncover effective therapeutic compounds for the treatment of ES.

Results

Establishment of ES PDO models

Preclinical *in vitro* models are of high value to study drug sensitivity and resistance. For the establishment of preclinical ES PDO models, primary material from freshly resected tumors was obtained with informed consent (Fig. 1, Table 1). ES PDO models were established from four different samples derived from three different patients. The locations of the primary tumor tissues varied among these patients. The Ewing samples ES-010 and ES-046 were derived from the distal femur of the same patient, with an 18-month gap between the two biopsies (Table 1). ES-041 was derived from the flank of the patient and ES-055 was derived from a lymph node metastasis (Table 1). The PDO *in vitro* cultures were established and maintained in basal medium (AddMEM/F12+) supplemented with EGF, FGF2, IGF1, and 0.5% BME. To ensure long-term expansion of the Ewing PDOs, the cultures were passaged for at least five times before they were characterized and compared to the original tumor.

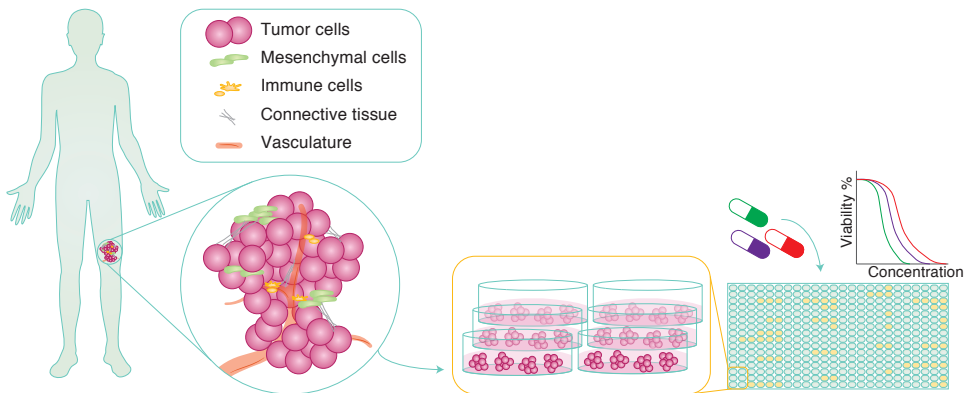


Figure 1: Animation depicting PDO models of Ewing sarcoma enable medium-throughput drug screens to predict therapeutic response.

Phenotypic characterization ES PDO models

To identify how well ES PDO models recapitulate the tumor they derived from, the PDO models were characterized based on their phenotypes and the presence of the *EWS-FLI1* fusion gene. The ES PDO models appeared as dense spheres of small round cells, which is typically also seen in ES tumors (Fig. 2). To compare the phenotypic appearance of the PDO models with their original tumor tissue, PDOs were paraffin-embedded and stained with Hematoxylin and Eosin (H&E) and the diagnostic marker CD99 (Fig. 2). The H&E stains on the PDO models presented small

blue round cells, similar to the H&E stains on the original tumor tissues. Additionally, PDTOs were positive for the diagnostic membrane marker CD99, recapitulating the ES cells at the primary tumor site (Fig. 2).

Patient	Gender	Location	Fusion gene	Breakpoint 1	Breakpoint 2
ES-010	male	femur	EWS-FLI1	chr22:29291599	chr11:128772782
ES-041	male	flank	EWS-FLI1	chr22:29287134	chr11:128781958
ES-046	male	femur	EWS-FLI1	chr22:29291599	chr11:128772782
ES-055	male	lymp node	EWS-FLI1	chr22:29287134	chr11:128805366

Table 1: Details of the ES primary tumor samples, including their gender, location, fusion gene, and fusion breakpoints.

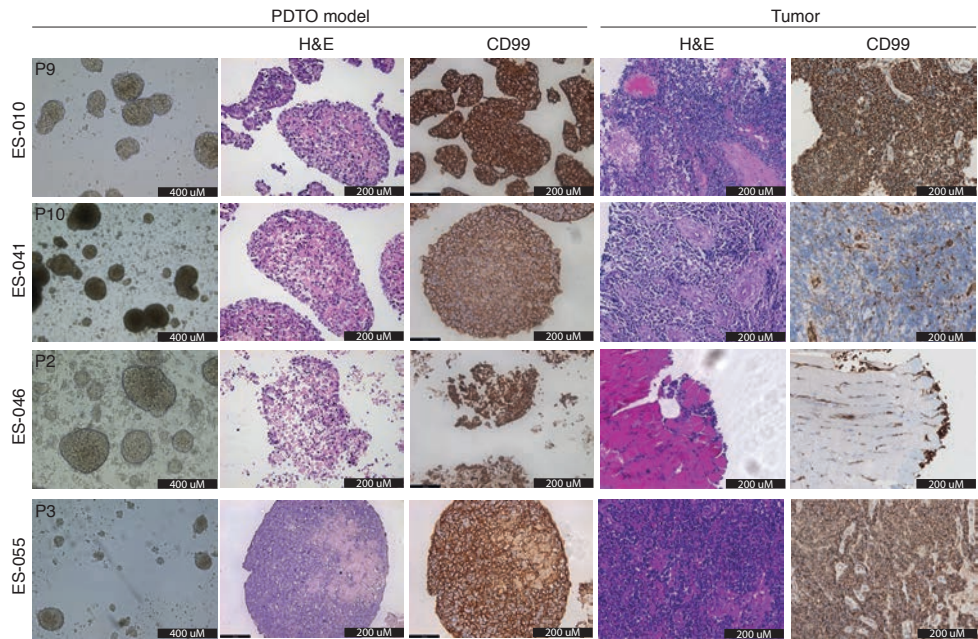


Figure 2: Pictures depicting the 4 PDTO models established from primary Ewing sarcoma tissue and their original tumor. stained for H&E and CD99. Scale bars: 400uM (pictures of *in vitro* cultures) and 200 uM (pictures of stainings).

Genetically, ES cells are characterized by a genomic translocation, resulting in a fusion between *EWSR1* and an *ETS*-family transcription factor, most frequently *FLI1* (Ross *et al.*, 2013). RNA sequencing and STAR-Fusion analysis identified the *EWS-FLI1* fusion in all three patients (Table 1). However, the breakpoint between those two genes varied between different ES patients. ES-010 and ES-046 (derived from the same patient) harbored an *EWS-FLI1* fusion with a breakpoint between *EWSR1* exon 8 and *FLI1* exon 5, while ES-041 harbored a fusion with a breakpoint between

EWSR1 exon 7 and *FLI1* exon 6. In ES-055, the *EWS-FLI1* fusion breakpoint was located between *EWSR1* exon 7 and *FLI1* exon 7 (Fig. 3A). To confirm the presence of the *EWS-FLI1* fusion gene in the ES PDTO models, a real-time PCR was performed on the specific fusion breakpoint found in the original tumor tissue. Indeed, all four PDTO models revealed expression of the *EWS-FLI1* fusion gene corresponding to the tumor tissue they derived from (Fig. 3B). Interestingly, the relative expression levels of *EWS-FLI1* varied between the different PDTO models (Fig. 3B). PDTO models ES-010 and ES-046, derived from the same patient, showed much lower relative expression levels of *EWS-FLI1*, compared to the other two PDTO models (Fig. 3B), suggesting that different patients can have different *EWS-FLI1* activity. Additionally, the genes *CD99*, *JAK1*, *CAV1*, and *FN1* were found to be expressed in our ES PDTO models, while expression was absent in the negative control neuroblastoma cell line SH-SY5Y (Fig. 3C). These genes were previously shown to be highly expressed in ES, and *CAV1* was identified as a potential direct target of *EWS-FLI1* (Aynaud et al., 2020), confirming their ES phenotype.

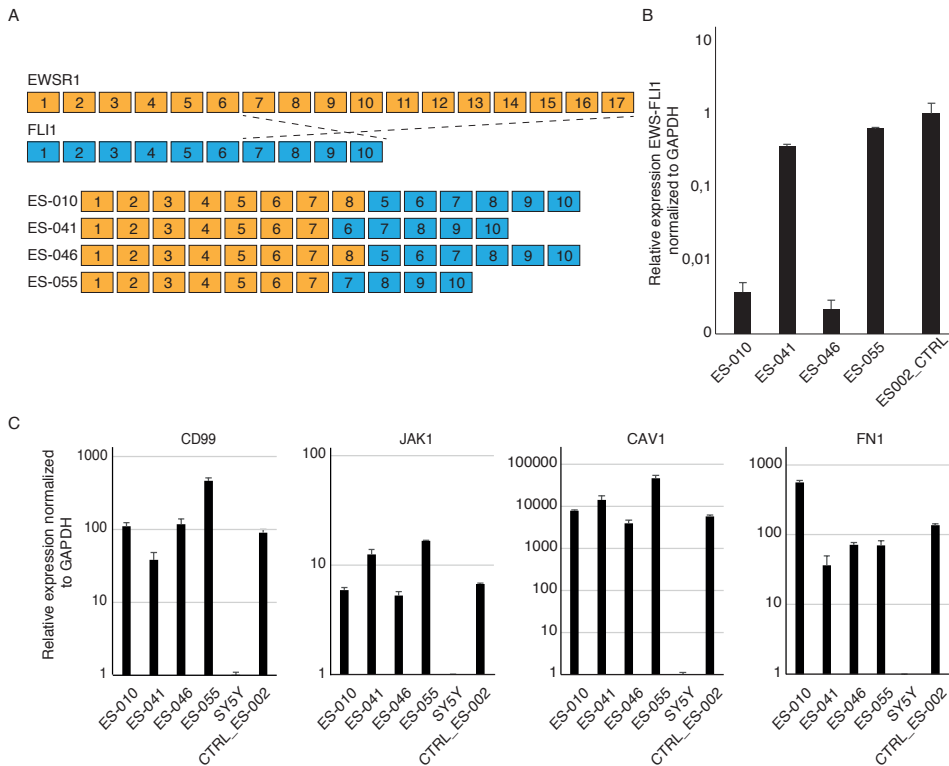


Figure 3: Fusion and EWS-specific gene expression in the PDTO models. A) Animated overview of different *EWS-FLI1* fusion breakpoints per patient. B) Bar plot depicting relative expression levels of *EWS-FLI1* as determined by qPCR per patient, normalized to *GAPDH*. Y-axis in log-scale. C) Bar plots depicting relative expression of genes expressed in ES, including *CD99*, *JAK1*, *CAV1*, and *FN1*, per patient as determined by qPCR. Normalized to *GAPDH*. Y-axis in log-scale.

Genetic characterization of ES PDTO models

ES tumors harbor relatively few single-nucleotide variants, indels, structural variants, and copy-number variation. Generally, most common somatic mutations are detected in *STAG2*, *CDKN2A*, and *TP53*, aside from whole chromosome arm copy-number variations (CNVs) (Tirode *et al.*, 2014). Whole genome sequencing (WGS) or whole exome sequencing (WXS) analysis was performed on primary ES tumor tissue. This revealed that ES-041 and ES-046 both harbored a gain of chromosome 8 (Fig. 4), which is frequently found in ES (Tirode *et al.*, 2014). ES-010 harbored a partial gain of chromosome 1, which was also present in the biopsy taken later from the same patient (ES-046). Additional amplification of chromosomes 5, 8, 16, 17, 18, and 21 were found in ES-046, indicating that genetic evolution occurred over time in this patient, which were likely therapy-induced genetic aberrations (Cheng *et al.*, 2019). To identify to what extent the PDTO models genetically mirror their original tumor, we also performed WGS on the ES PDTO models. As expected, a few additional genetic aberrations were found in the PDTO models (Fig. 4), which can occur upon *in vitro* propagation (Kuijk *et al.*, 2020). Overall, we found very similar patterns of CNVs, indicating that the PDTO models also genetically recapitulated the tumor tissue from which they were derived. As these ES PDTO models both phenotypically and genetically largely resembled their original primary tumor, this allowed for medium-throughput screening to study sensitivity to chemotherapeutic compounds.

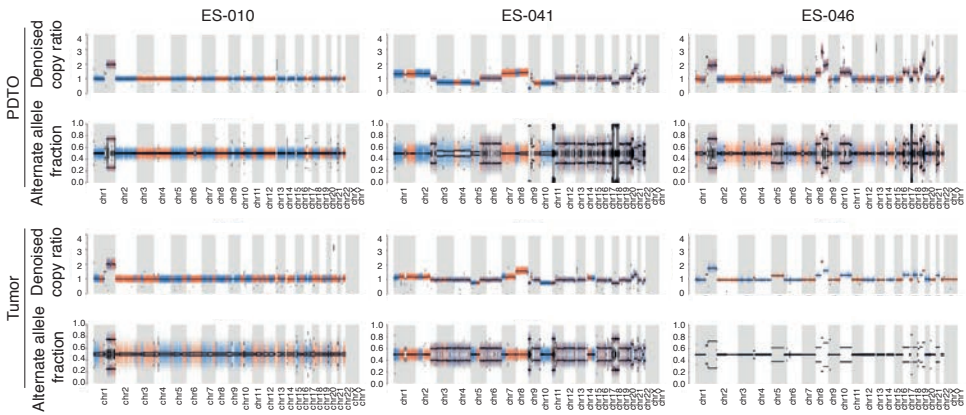


Figure 4: WGS/WXS of the PDTO models and primary ES tissue. Plots depicting copy number variation in the PDTO models ES-010, ES-041 and ES-046 compared to their originating tumor. Bottom plots depict the alternate allele fraction, and the upper plots depict the denoised copy ratios.

Medium-throughput compounds screens reveal drug sensitivity of ES PDTOs

The ES PDTO models ES-010, ES-041, and ES-046 were expanded for compound screens to investigate drug sensitivity. The compound screen included a panel of 201 single compounds. Several compounds showed an effective response in the ES

PDTO models. Overall, the different ES PDTO models showed very comparable responses to the compound panel, indicating that drug sensitivity is similar between ES patients. When the area under the curve (AUC) Z-scores of ES PDTOs were compared to the AUC Z-scores of several rhabdomyosarcoma (RMS) PDTO models, we observed some differences in drug sensitivity. The compounds that showed a higher sensitivity in the ES PDTO models included mostly cytotoxic compounds, such as Irinotecan, Camptothecin, Paclitaxel, Vinblastine, and Methotrexate (Fig. 5A-B). For several of these compounds, including Irinotecan, Camptothecin, Paclitaxel and Methotrexate, the IC₅₀ of the ES cells appeared at lower concentrations than the relevant plasma concentrations (Fig. 5B), indicating that these compounds are potentially effective in ES patients.

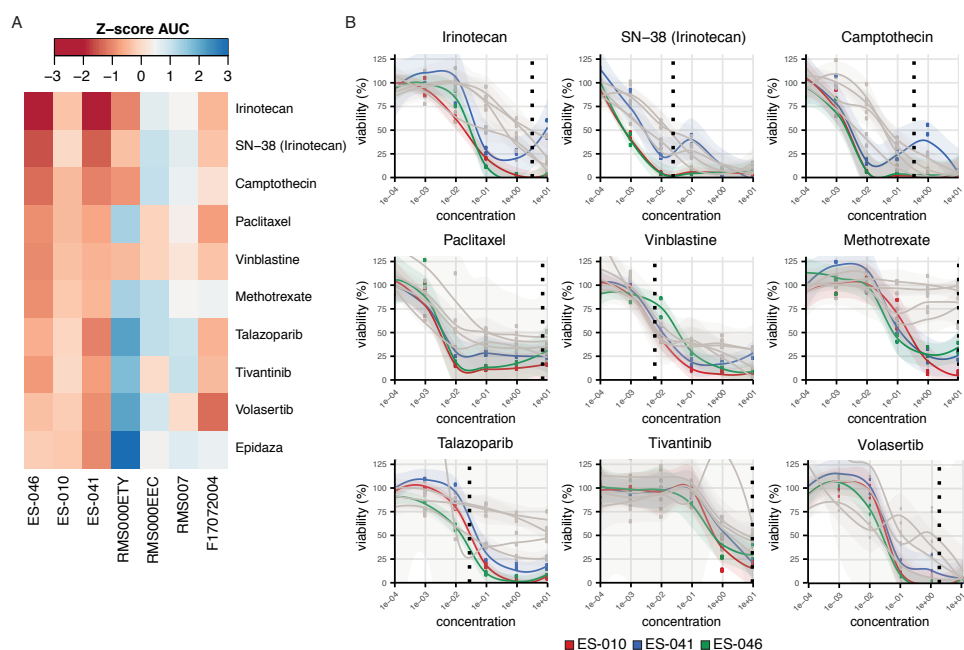


Figure 5: Compound screen sensitivity to cytotoxic compounds for ES vs RMS PDTOs. A) Heatmap depicting AUC z-scores of the ES PDTOs ES-046, ES-010, and ES-041 and RMS PDTOs RMS000ETY, RMS000EEC, RMS007, and F17072004. B) Graphs depicting cell viability of ES-010 (red), ES-041 (blue), ES-046 (green), and RMS models (gray) after exposure to the compounds for 5 days. Vertical dashed line represents relevant plasma concentrations.

Additionally, various targeting compounds showed an effective response with IC₅₀ concentrations lower or around the relevant plasma concentrations. These included MET inhibitor Tivantinib, PLK1 inhibitor Volasertib, and PARP inhibitor Talazoparib (Fig. 5B). Interestingly, for nearly all histone deacetylase (HDAC) inhibitors included in the compound screen, we observed an effective response in ES PDTO models. Several of these HDAC inhibitors showed IC₅₀ concentrations below or

around the relevant plasma concentrations, including Belinostat, Romidespin, Fimepinostat, and Panobinostat (Fig. 6A-B), indicating that modulation of HDAC activity greatly influences ES cell survival.

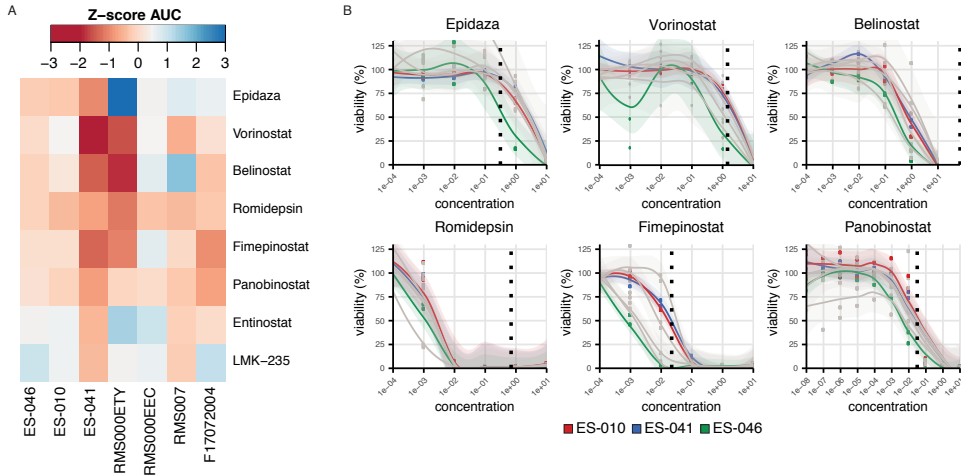


Figure 6: Compound screen sensitivity to HDAC inhibiting compounds for ES vs RMS PDOs. A) Heatmap depicting AUC z-scores of the ES PDOs ES-046, ES-010, and ES-041 and RMS PDOs RMS000ETY, RMS000EEC, RMS007, and F17072004. B) Graphs depicting cell viability of ES-010 (red), ES-041 (blue), ES-046 (green), and RMS models (grey) after exposure to the compounds for 5 days. Vertical dashed line represents relevant plasma concentrations.

Discussion

ES is an aggressive bone and soft tissue sarcoma with a dismal prognosis and a lack of effective treatment for advanced disease. The consistent establishment of preclinical models from the original tumor is crucial for the development of novel therapies (Bleijns *et al.*, 2019). While PDTX models are useful to study treatment response in a physiologically relevant manner, cell lines can be rapidly expanded and used for medium-throughput drug screens. PDO models that phenotypically and genetically resemble the original tumor can bridge the gap between PDTX models and established cell lines (Bleijns *et al.*, 2019; Sachs & Clevers, 2014). We established four PDO models from three different ES patients that recapitulate both phenotypic and genetic features of the tumor they derived from. Three of these models were expanded for medium-throughput compound screens, which reveal drug sensitivity to several cytotoxic compounds and several targeting compounds, including various HDAC inhibitors.

All four ES PDO models express the *EWS-FLI1* fusion gene, confirming their Ewing cell identity. However, the expression levels of the fusion gene vary among different patients. Previously, *EWS-FLI1* expression levels were shown to be associated with cell proliferation and migration (Franzetti *et al.*, 2017). Franzetti

and colleagues show that ES cells that express high levels of *EWS-FLI1* are characterized by highly active cell proliferation, while ES cells expressing low levels of *EWS-FLI1* have a strong tendency to migrate and metastasize (Franzetti *et al.*, 2017). Patient variation of *EWS-FLI1* expression might predict ES behavior and its ability to metastasize. However, the PDTO models from ES lymph node metastasis ES-055 express higher levels of the *EWS-FLI1* fusion gene compared to ES-010 and ES-046, which were derived from the primary location in the femur. Additionally, the fusion breakpoint differs between the three ES patients, which might affect fusion gene expression. We also cannot exclude technical discrepancies as different real-time PCR primers were used to cover the different *EWS-FLI1* fusion breakpoints.

A major challenge in preclinical cancer research remains the establishment of models that recapitulate the original tumor as close as possible. For the establishment of PDTO models, it is key to find the optimal growth conditions *in vitro* for tumor cells to expand, while maintaining the cellular heterogeneity. However, selective pressure in cultured tumor cells is inevitable (Bleijs *et al.*, 2019; Pauli *et al.*, 2017). Faster cycling cells have a growth advantage *in vitro*, however, this could affect the response to cytotoxic compounds that target cell cycle mechanisms, like DNA replication. Additionally, a previous study shows that *in vitro* culturing of human pluripotent stem cells results in increased mutation rates, which leaves a mutational footprint related to oxidative stress (Kuijk *et al.*, 2020). This effect caused by *in vitro* culturing of cells could also occur in PDTO models.

A previous study has demonstrated that HDAC3 is a transcriptional target of the *EWS-FLI1* fusion protein and that HDAC inhibitor Entinostat inhibits ES cell growth by suppressing the *EWS-FLI1*/HDAC3/HSP90 signaling axis (Ma *et al.*, 2019). Additionally, Souza and colleagues showed that inhibition of HDAC activity in ES cell lines results in reprogramming of ES cells towards a more differentiated state and affects cell expansion and survival (Souza *et al.*, 2018). In line with these studies, the established ES PDTO models in our study show sensitivity to several HDAC inhibitors, including Belinostat, Romidespin, Fimepinostat, and Panobinostat. This illustrates that HDAC activity is key in ES progression and survival. HDAC inhibitor Vorinostat is currently being explored in a clinical phase I trial for multiple solid tumors, including ES (ClinicalTrials.gov Identifier: NCT04308330).

Taken together, we provide a protocol which allows for the derivation and long-term expansion of organoid lines from Ewing Sarcoma patients in a personalized fashion. These PDTO models hold promise for the development of personalized treatment strategies for Ewing Sarcoma.

Methods

Patient derived ES specimen

Surgically resected tissue was obtained from ES patients at the Princess Maxima Center with informed consent. Tumor material was washed with Advanced Dulbecco's Modified Eagle's Medium F12 (AdDMEM-F12) (Thermo Fisher Scientific, #12634010) supplemented with 1% pen/strep (Thermo Fisher Scientific, #15140122), 1% Glutamax (Thermo Fisher Scientific, #35050038), 1% Hepes (Thermo Fisher Scientific, #15630056) and minced into tumor pieces. Red blood cell lysis buffer (Sigma-Aldrich, #11814389001) was applied for 5 min to lyse the red blood cells. The tumor pieces were washed with AdDMEM-F12 and a part of the tumor pieces were frozen into AdDMEM-F12, supplemented with 50% Fetal Calf Serum (FCS) (Gibco) and 10% Dimethyl Sulfoxide (DMSO) (Sigma-aldrich, # D8418). The rest of the tumor pieces were minced using scalpels and mechanically disrupted by pipetting up and down before plating into suspension cell culture plates.

Cell culture

The patient-derived ES organoids were maintained in EWS medium, containing Advanced Dulbecco's Modified Eagle's Medium F12 (AdDMEM-F12) (Thermo Fisher Scientific, #12634010) supplemented with 1% pen/strep (Thermo Fisher Scientific, #15140122), 1% Glutamax (Thermo Fisher Scientific, #35050038), 1% N2 (Gibco, #17502048), 1% Hepes (Thermo Fisher Scientific, #15630056), 2% B27 (Gibco, #12587010), 0.25% NAC (Sigma Aldrich, #A9165), 50 ng/mL FGF2 (Peprotech, #100-18B), 50 ng/mL EGF (Peprotech, #AF-100-15), 10 ng/mL IGF1 (Peprotech, #100-11), and 0.5% BME (Gibco, #31350-010). Cells were incubated at 37°C with 5% CO₂ and passaged by mechanical disruption by pipetting up and down.

DNA and RNA isolation

DNA and RNA were isolated from snap frozen cell pellets after passaging the PDTO cultures for >5 times. DNA was isolated using DNeasy Blood and Tissue Kit (Qiagen, #69504) according manufacturer's protocol. RNA was isolated using Direct-zol RNA MicroPrep (Zymo Research, #R2060) according manufacturer's protocol. RNA was used for cDNA synthesis and qPCR of the EWS-FLI1 fusion using iQ SYBR Green (Bio-Rad, #1708882). The following primers were used for the detection of *EWS-FLI1* fusion mRNA: *EWSR1* exon 7 FW "AACACCTATGGGCAACCGAG", *EWSR1* exon 8 FW "AGGAGAGAACCGGAGCATGA", *FLI1* exon 5 REV "CCCTGAGGTAAGT-GAGGTGTG", *FLI1* exon 6 REV "TGAGGATTGGTGGGTGTGG", and *FLI1* exon 8 REV "GTTGAGGCCAGAATTCATGTTA".

WGS

150 ng of total DNA was used for library preparation using the KAPA HyperPlus kit (Roche), according to the manufacturer's instructions. Libraries from tumor and normal tissue were pooled in a 3:1 ratio, with a total of 7 tumor/normal pairs per S4 sequencing kit. Libraries were sequenced using 2x150 cycles on a NovaSeq 6000 (Illumina). The WGS sequencing data was processed as per the GATK 4.0 workflow for variant calling, using a wdl and cromwell based workflow. Reads were aligned to GRCh38 using Burrows-Wheeler Aligner software package (BWA-0.7.13) (Li & Durbin, 2009), and QC was performed using FastQC (version 0.11.5) and picard-Tools (version 2.20.1). Somatic variants were identified using Mutect2 from GATK v4.1 and annotated using Vep (version v92). Similarly, CNA's were identified using GATK v4.1.

Medium-throughput compound screen

Two days prior to the addition of compounds, ES PDOs were seeded in 384-well plates. A panel of 201 drugs was added to the 384-well plates in different concentrations using the Beckman Coulter Biomek i7 Hybrid liquid handling workstation. After 5 days of exposure to the compounds, cell viability was measured with CellTiter-Glo Assay (Promega) using the Spectramax i3x luminescence microplate reader. Values were normalized to DMSO.

References

- Aynaud, M., Mirabeau, O., Gruel, N., Barillot, E., Delattre, O., & Zinovyev, A. (2020). Transcriptional Programs Define Intratumoral Heterogeneity of Ewing Sarcoma at Single-Cell Resolution. *Cell Rep.* 30: 6: 1767–1779.
- Bleijis, M., Wetering, M., Clevers, H., & Drost, J. (2019). Xenograft and organoid model systems in cancer research. *The EMBO Journal*, 38(15), 1–11.
- Cheng, L., Pandya, P. H., Liu, E., Chandra, P., Wang, L., Murray, M. E., Carter, J., Ferguson, M., Saadatza-deh, M. R., Bijangi-Visheshsaraei, K., Marshall, M., Li, L., Pollok, K. E., & Renbarger, J. L. (2019). Integration of genomic copy number variations and chemotherapy-response biomarkers in pediatric sarcoma. *BMC Medical Genomics*, 12: S1 23.
- de Bono, J., Ramanathan, R. K., Mina, L., Chugh, R., Glaspy, J., Rafii, S., Kaye, S., Sachdev, J., Heymach, J., Smith, D. C., Henshaw, J. W., Herriott, A., Patterson, M., Curtin, N. J., Byers, L. A., & Wainberg, Z. A. (2017). Phase I, Dose-Escalation, Two-Part Trial of the PARP Inhibitor Talazoparib in Patients with Advanced Germline BRCA1/2 Mutations and Selected Sporadic Cancers. *Cancer Discovery*, 7(6), 620–629.
- Drost, J., Boxtel, R. Van, Blokzijl, F., Mizutani, T., Sasaki, N., Sasselli, V., de Ligt, J., Behjati, S., Grolleman, J. E., van Wezel, T., Nik-Zainal, S., Kuiper, R. P., Cuppen, E., & Clevers, H. (2017). Use of CRISPR-modified human stem cell organoids to study the origin of mutational signatures in cancer. *Science*, 91: 399–404.
- Franzetti, G. A., Laud-Duval, K., Van Der Ent, W., Brisac, A., Irondelle, M., Aubert, S., Dirksen, U., Bouvier, C., De Pinieux, G., Snaar-Jagalska, E., Chavrier, P., & Delattre, O. (2017). Cell-to-cell heterogeneity of EWSR1-FLI1 activity determines proliferation/migration choices in Ewing sarcoma cells. *Oncogene*, 36(25), 3505–3514.
- Fukutomi, A., Hatake, K., Matsui, K., Sakajiri, S., Hirashima, T., Tani, H., Kobayashi, K., & Yamamoto, N. (2012). A phase I study of oral panobinostat (LBH589) in Japanese patients with advanced solid tumors. *Investigational New Drugs*, 30(3), 1096–1106.
- Grünewald, T. G. P., Cidre-Aranaz, F., Surdez, D., Tomazou, E. M., De Álava, E., Kovar, H., Sorensen, P. H., Delattre, O., & Dirksen, U. (2018). Ewing sarcoma. *Nature Reviews Disease Primers*, 4(5).
- Huizinga, M. T., Vermorken, J. B., Rosing, H., Huinink, W. W. T. B., Mandjes, I., Pinedo, H. M., & Beijnen, J. H. (1995). Pharmacokinetics of paclitaxel and three major metabolites in patients with advanced breast carcinoma refractory to anthracycline therapy treated with a 3-hour paclitaxel infusion: A European Cancer Centre (ECC) trial. *Annals of Oncology*, 6(7), 699–704.
- Keskin, T., Rucci, B., Cornaz-Buros, S., Martin, P., Fusco, C., Broje, L., Cisarova, K., Perez, E. M., Letovanec, I., La Rosa, S., Cherix, S., Diezi, M., Renella, R., Provero, P., Suvà, M. L., Stamenkovic, I., & Riggi, N. (2021). A live single-cell reporter assay links intratumor heterogeneity to metastatic proclivity in Ewing sarcoma. *Science Advances*, 7(27), eabf9394.
- Kobayashi, Y., Yamauchi, T., Kiyoi, H., Sakura, T., Hata, T., Ando, K., Watabe, A., Harada, A., Taube, T., Miyazaki, Y., & Naoe, T. (2015). Phase I trial of volasertib, a Polo-like kinase inhibitor, in Japanese patients with acute myeloid leukemia. *Cancer Science*, 106(11), 1590–1595.
- Kovar, H., Alonso, J., Aman, P., Aryee, DNT, Ban, J., Burchill, S., Burdach, S., De Alava, E., Delattre, O., Dirksen, U., et al (2012) The first European interdisciplinary Ewing sarcoma research summit. *Front Oncol* 2: 1–11
- Kuijk, E., Jager, M., van der Roest, B., Locati, M. D., Van Hoeck, A., Korzelius, J., Janssen, R., Besselink, N., Boymans, S., van Boxtel, R., & Cuppen, E. (2020). The mutational impact of culturing human pluripotent and adult stem cells. *Nature Communications*, 11(1).
- Le Deley, M. C., Paulussen, M., Lewis, I., Brennan, B., Ranft, A., Whelan, J., Le Teuff, G., Michon, J., Ladenstein, R., Marec-Bérard, P., Van Den Berg, H., Hjorth, L., Wheatley, K., Judson, I., Juergens, H., Craft, A., Oberlin, O., & Dirksen, U. (2014). Cyclophosphamide compared with ifosfamide in consolidation treatment of standard-risk Ewing sarcoma: Results of the randomized noninferiority Euro-EWING99-R1 trial. *Journal of Clinical Oncology*, 32(23), 2440–2448.
- Links, M., Watson, S., Lethlean, K., Aherne, W., Kirsten, F., Clarke, S., Law, M., Friedlander, M., Galettis, P., & McKeage, M. J. (1999). Vinblastine pharmacokinetics in patients with non-small cell lung cancer given cisplatin. *Cancer Investigation*, 17(7), 479–485.
- Liston, D. R., & Davis, M. (2017). Clinically relevant concentrations of anticancer drugs: A guide for nonclinical studies. *Clinical Cancer Research*, 23(14), 3489–3498.
- Ma, Y., Baltezor, M., Rajewski, L., Crow, J., Samuel, G., Staggs, V. S., Chastain, K. M., Toretzky, J. A.,

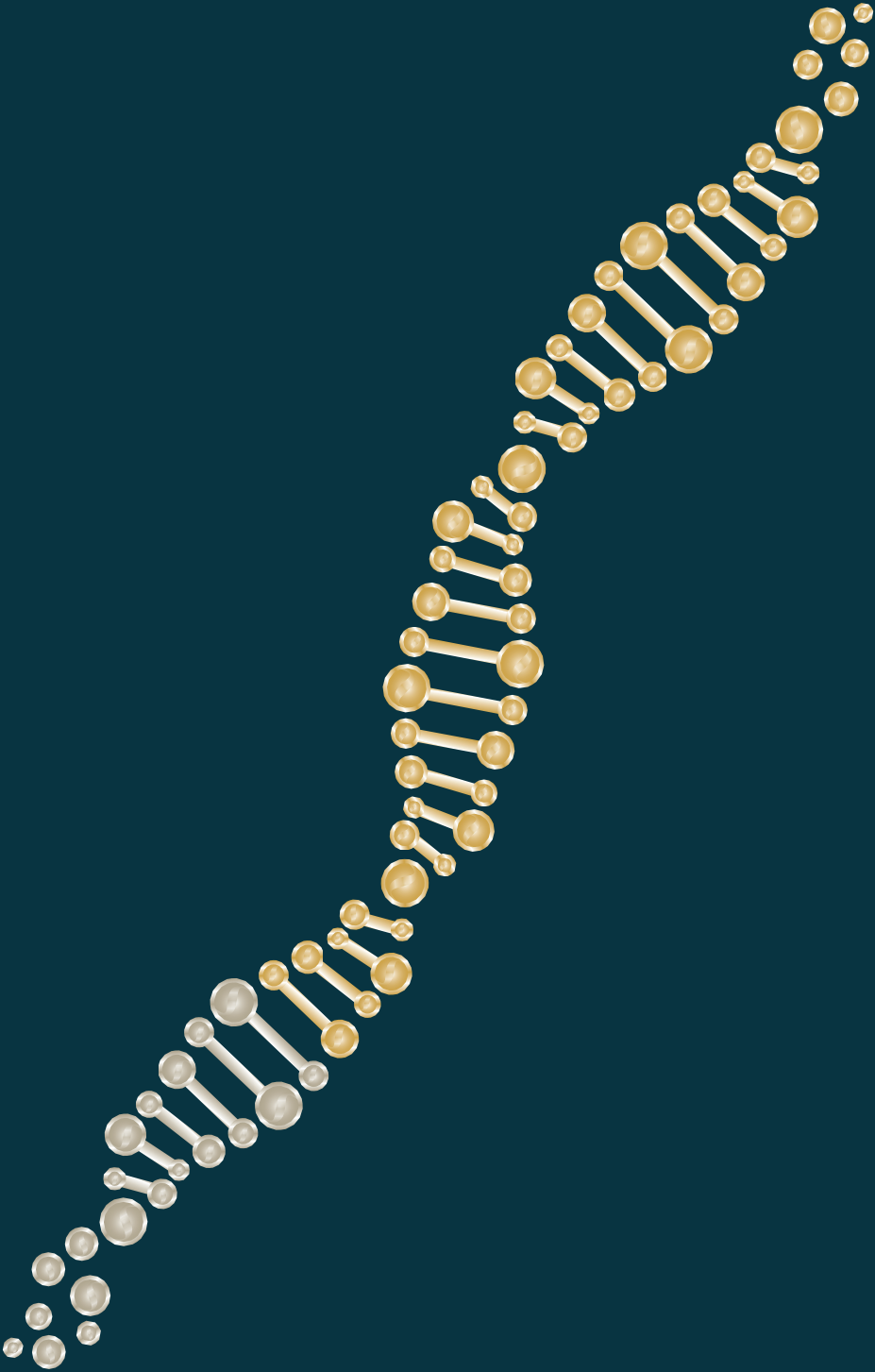
- Weir, S. J., & Godwin, A. K. (2019). Targeted inhibition of histone deacetylase leads to suppression of Ewing sarcoma tumor growth through an unappreciated EWS-FLI1/HDAC3/HSP90 signaling axis. *Journal of Molecular Medicine*, 97(7), 957–972.
- Mross, K., Richly, H., Schleucher, N., Korfee, S., Tewes, M., Scheulen, M. E., Seeber, S., Beinert, T., Schweigert, M., Sauer, N., Unger, C., Behringer, D., Brendel, E., Haase, C. G., Voliotis, D., & Strumberg, D. (2004). A phase I clinical and pharmacokinetic study of the camptothecin glycoconjugate, BAY 38-3441, as a daily infusion in patients with advanced solid tumors. *Annals of Oncology*, 15(8), 1284–1294.
- Nanni, P., Landuzzi, L., Manara, M. C., Righi, A., Nicoletti, G., Cristalli, C., Pasello, M., Parra, A., Carabotta, M., Ferracin, M., Palladini, A., Ianzano, M. L., Giusti, V., Ruzzi, F., Magnani, M., Donati, D. M., Picci, P., Lollini, P. L., & Scotlandi, K. (2019). Bone sarcoma patient-derived xenografts are faithful and stable preclinical models for molecular and therapeutic investigations. *Scientific Reports*, 9(1), 1–12.
- Pan, D. S., Yang, Q. J., Fu, X., Shan, S., Zhu, J. Z., Zhang, K., Li, Z. Bin, Ning, Z. Q., & Lu, X. P. (2014). Discovery of an orally active subtype-selective HDAC inhibitor, chidamide, as an epigenetic modulator for cancer treatment. *MedChemComm*, 5(12), 1789–1796.
- Pauli, C., Hopkins, B. D., Prandi, D., Shaw, R., Fedrizzi, T., Sboner, A., Sailer, V., Augello, M., Puca, L., Rosati, R., McNary, T. J., Churakova, Y., Cheung, C., Triscott, J., Pisapia, D., Rao, R., Mosquera, J. M., Robinson, B., Faltas, B. M., ... Rubin, M. A. (2017). Personalized in vitro and in vivo cancer models to guide precision medicine. *Cancer Discovery*, 7(5), 462–477.
- Pesetto, Z. Y., Chen, B., Alturkmani, H., Hyter, S., Flynn, C. A., Baltezor, M., Ma, Y., Rosenthal, H. G., Neville, K. A., Weir, S. J., Butte, A. J., & Godwin, A. K. (2017). In silico and in vitro drug screening identifies new therapeutic approaches for Ewing sarcoma. *Oncotarget*, 8(3), 4079–4095.
- Pignon, T., Lacarelle, B., Duffaud, F., Guillet, P., Catalin, J., Durand, A., Monjanel, S., & Favre, R. (1994). Pharmacokinetics of high-dose methotrexate in adult osteogenic sarcoma. *Cancer Chemotherapy and Pharmacology*, 33(5), 420–424.
- Ramalingam, S. S., Kummar, S., Sarantopoulos, J., Shibata, S., LoRusso, P., Yerk, M., Holleran, J., Lin, Y., Beumer, J. H., Harvey, R. D., Ivy, S. P., Belani, C. P., & Egorin, M. J. (2010). Phase I study of vorinostat in patients with advanced solid tumors and hepatic dysfunction: A National Cancer Institute Organ Dysfunction Working Group study. *Journal of Clinical Oncology*, 28(29), 4507–4512.
- Riggi, N., Suvà, M. L., & Stamenkovic, I. (2021). Ewing's Sarcoma. *New England Journal of Medicine*, 384(2), 154–164.
- Ross, K. A., Smyth, N. A., Murawski, C. D., & Kennedy, J. G. (2013). The biology of ewing sarcoma. *ISRN Oncology*, 2013(1), 759725.
- Sachs, N., & Clevers, H. (2014). Organoid cultures for the analysis of cancer phenotypes. *Current Opinion in Genetics and Development*, 24(1), 68–73.
- Santoro, A., Simonelli, M., Rodriguez-Lope, C., Zucali, P., Camacho, L. H., Granito, A., Senzer, N., Rimassa, L., Abbadessa, G., Schwartz, B., Lamar, M., Savage, R. E., & Bruix, J. (2013). A Phase-1b study of tivantinib (ARQ 197) in adult patients with hepatocellular carcinoma and cirrhosis. *British Journal of Cancer*, 108(1), 21–24.
- Satoh, T., Yasui, H., Muro, K., Komatsu, Y., Sameshima, S., Yamaguchi, K., & Sugihara, K. (2013). Pharmacokinetic assessment of irinotecan, SN-38, and SN-38-glucuronide: A substudy of the FIRIS study. *Anticancer Research*, 33(9), 3845–3854.
- Souza, B. K., da Costa Lopez, P. L., Menegotto, P. R., Vieira, I. A., Kersting, N., Abujamra, A. L., Brunetto, A. T., Brunetto, A. L., Greganin, L., de Farias, C. B., Thiele, C. J., & Roesler, R. (2018). Targeting Histone Deacetylase Activity to Arrest Cell Growth and Promote Neural Differentiation in Ewing Sarcoma. *Molecular Neurobiology*, 55(9), 7242–7258.
- Takebe, N., Beumer, J. H., Kummur, S., Kiesel, B. F., Dowlati, A., O'Sullivan Coyne, G., Piekarz, R., Rubinstein, L., Fogli, L. K., Vaishampayan, U., Goel, S., O'Bryant, C. L., El-Rayes, B. F., Chung, V., Lenz, J., Kim, R., Belani, C. P., Tusciano, J. M., Schelman, W., ... Chen, A. P. (2019). A phase I pharmacokinetic study of belinostat in patients with advanced cancers and varying degrees of liver dysfunction. *British Journal of Clinical Pharmacology*, 85(11), 2499–2511.
- Tirode, F., Surdez, D., Ma, X., Parker, M., Le Deley, M. C., Bahrami, A., Zhang, Z., Lapouble, E., Grossetete-Lalami, S., Rusch, M., Reynaud, S., Rio-Frio, T., Hedlund, E., Wu, G., Chen, X., Pierron, G., Oberlin, O., Zaidi, S., Lemmon, G., ... Delattre, O. (2014). Genomic landscape of ewing sarcoma defines an aggressive subtype with co-association of STAG2 and TP53 mutations. *Cancer Discovery*, 4(11), 1342–1353.

Younes, A., Berdeja, J. G., Patel, M. R., Flinn, I., Gerecitano, J. F., Neelapu, S. S., Kelly, K. R., Copeland, A. R., Akins, A., Clancy, M. S., Gong, L., Wang, J., Ma, A., Viner, J. L., & Oki, Y. (2016). Safety, tolerability, and preliminary activity of CUDC-907, a first-in-class, oral, dual inhibitor of HDAC and PI3K, in patients with relapsed or refractory lymphoma or multiple myeloma: An open-label, dose-escalation, phase 1 trial. *The Lancet Oncology*, 17(5), 622–631.

Supplemental information

Compound	Plasma concentration (uM)	Reference
Irinotecan	3,1	(Sato <i>et al.</i> , 2013)
SN-38	0,05	(Sato <i>et al.</i> , 2013)
Camptothecin	0,3	(Mross <i>et al.</i> , 2004)
Paclitaxel	6,9	(Huizing <i>et al.</i> , 1995)
Vinblastine	0,01	(Links <i>et al.</i> , 1999)
Methotrexate	1016	(Pignon <i>et al.</i> , 1994)
Talazoparib	0,03	(de Bono <i>et al.</i> , 2017)
Tivantinib	9,5	(Santoro <i>et al.</i> , 2013)
Volasertib	1,7	(Kobayashi <i>et al.</i> , 2015)
Epidaza	0,3	(Pan <i>et al.</i> , 2014)
Vorinostat	1,4	(Ramalingam <i>et al.</i> , 2010)
Belinostat	68,8	(Takebe <i>et al.</i> , 2019)
Romidespin	0,7	(Liston & Davis, 2017)
Fimepinostat	0,02	(Younes <i>et al.</i> , 2016)
Panobinostat	0,03	(Fukutomi <i>et al.</i> , 2012)

Supplemental table 1: Plasma concentrations of effective compounds.



Chapter 4

The molecular mechanisms driving DSRCT
expansion by the EWS-WT1 fusion gene

Margit Bleijs¹, Corine Pleijte², Sem Engels²,
Femke Ringnalda¹, Friederike Meyer-Wentrup²,
Marc van de Wetering¹, Hans Clevers^{1,3}

1. Oncode Institute, Prinses Máxima Center for Pediatric Oncology, Utrecht, The Netherlands
2. Prinses Máxima Center for Pediatric Oncology, Utrecht, The Netherlands
3. Oncode Institute, Hubrecht Institute, Royal Netherlands Academy of Arts and Sciences (KNAW) and University Medical Centre Utrecht, the Netherlands

Abstract

Desmoplastic small round cell tumor (DSRCT) is a rare and aggressive soft tissue sarcoma with a lack of effective treatment options and a poor prognosis. DSRCT is characterized by a chromosomal translocation, resulting in the *EWS-WT1* gene fusion. Molecular mechanisms driving DSRCT are poorly understood, and a paucity of preclinical models hamper DSRCT research. Here, we establish a novel primary patient-derived DSRCT *in vitro* model, recapitulating the original tumor. We find that *EWS-WT1* expression affects cell shape and cell survival, and we identify downstream target genes of the *EWS-WT1* fusion. Additionally, this preclinical *in vitro* model allows for medium-throughput drug screening. We discover sensitivity to several drugs, including compounds targeting RTKs. MERTK, which has been described as a therapeutic target for several malignancies, correlates with *EWS-WT1* expression. Inhibition of MERTK with the small molecule inhibitor UNC2025 results in reduced proliferation of DSRCT cells *in vitro*, suggesting MERTK as a therapeutic target in DSRCT. This study underscores the usefulness of preclinical *in vitro* models to study molecular mechanisms and potential therapeutic options.

Introduction

Desmoplastic small round cell tumor (DSRCT) is a highly aggressive and rare soft tissue sarcoma (Hayes-jordan *et al*, 2016; Bulbul *et al*, 2017). This sarcoma was first characterized as a separate entity by Gerald and Rosai in 1989, who described the histologic appearance of DSRCT as nests of small round blue cells separated by desmoplastic stroma (Gerald & Rosai, 1989). DSRCT exhibits features of multi-phenotypic differentiation since mesenchymal, epithelial, and neural markers are expressed within this sarcoma (Gerald & Rosai, 1989; Hayes-jordan *et al*, 2016). Genetically, DSRCT is characterized by a chromosomal translocation, resulting in a gene fusion involving Ewing sarcoma region 1 (*EWSR1*) and Wilms tumor 1 (*WT1*). The chimeric protein contains the N-terminal domain of *EWSR1* fused to the DNA-binding domain of *WT1*, including zinc fingers 2-4 (Karnieli *et al*, 1996). The N-terminal domain of *EWSR1* is thought to act as a transcriptional activator, while the zinc finger domains of *WT1* bind DNA of regulatory elements in its target genes (Gerald & Haber, 2005). Previously it has been shown that two different isoforms of *EWS-WT1* are expressed, distinguished by the presence or absence of a three amino acid KTS domain, which induce distinct transcriptional profiles (Karnieli *et al*, 1996; Kim *et al*, 1998; Kang *et al*, 2014).

Recently, several downstream targets of *EWS-WT1* were identified. Kang and colleagues showed that *EWS-WT1* directly binds to the promoter of neural reprogramming factor *ASCL1*, activating neural gene expression (Kang *et al*, 2014). Gedminas and colleagues identified *EWS-WT1* target genes using an siRNA knock-down model of the fusion in the patient-derived JN-DSRCT-1 cell line and the patient-derived xenograft (PDX)-derived BER cell line (Gedminas *et al*, 2020; Nishio *et al*, 2002; Markides *et al*, 2013). They discover several downstream target pathways commonly deregulated in fusion-positive sarcomas; and observe overlap between *EWS-WT1*- and *EWS-FLI1*- (the fusion gene driving Ewing sarcoma) gene signatures. Hingorani and colleagues performed bulk RNA sequencing of patient-derived DSRCT specimens and identified CD200 and CD276 as potentially targetable immune checkpoint molecules whose expression is independent of *EWS-WT1* expression. Additionally, they performed *WT1* ChIP-sequencing and established an shRNA knock-down model of *EWS-WT1* in the JN-DSRCT-1 cell line and identified *IGF2* and *FGFR4* as potential therapeutic targets in DSRCT patients (Hingorani *et al*, 2020). While these studies give important insights on the downstream targets of the *EWS-WT1* fusion gene, molecular mechanisms triggered by the gene fusion, that account for the aggressive proliferation of DSRCT, have remain elusive.

Preclinical models, such as cell lines, organoids and patient-derived xenografts (PDXs), are key for investigating tumor progression and molecular mechanisms (Bleijds *et al*, 2019). While several PDX models have been established from DSRCT specimens by transplantation into the flank of the mouse (Markides *et al*, 2013), only two *in vitro* models of DSRCT have been published: one primary pa-

tient-derived cell line and one PDX-derived cell line (Nishio *et al*, 2002; Gedminas *et al*, 2020; Markides *et al*, 2013). The paucity of preclinical DSRCT models hampers the research on mechanisms driving DSRCT and the discovery of therapeutic options. Here, we establish a novel primary patient derived DSRCT model *in vitro*, which recapitulates morphological and transcriptomic features of the originating tumor. We use a shRNA knock-down model to identify molecular mechanisms triggered by the EWS-WT1 fusion and observe novel target genes driving this sarcoma. Additionally, this preclinical *in vitro* model allows for medium-throughput drug screening to discover drug sensitivity in DSRCT cells. Finally, we discover promising therapeutic targets, including an EWS-WT1 driven receptor tyrosine kinase (RTK).

Results

Establishment and characterization of a DSRCT *in vitro* preclinical model

Surgically resected tissue was obtained from a DSRCT patient and was successfully cultured *in vitro* under various conditions, including in 3D basement membrane extract type 2 (BME) droplets, as a 2D layer in 0.1% BME, and in suspension without BME (Fig. 1A). The expanding cultures were maintained for over two years in basal medium (AddMEM/F12+) supplemented with EGF, FGF2, IGF1, RKI, and BMP4. While these growth factors were essential for initial growth of DSRCT cells, the established OV-054 DSRCT cultures were able to be maintained without the additional growth factors EGF, FGF2, IGF1, RKI, and BMP4 for several weeks. The addition of the growth factors independently did not affect DSRCT cell expansion *in vitro* (Supp. Fig. 1), suggesting that these OV-054 DSRCT cells are able to adapt fast and are able to propagate independently of their microenvironment. H&E staining on OV-054 DSRCT cultures revealed nests of small round cells with large nuclei (Fig. 1A), which is typically seen in DSRCT tissue (Gerald & Rosai, 1989). To investigate transcriptomic similarity of DSRCT cells under different *in vitro* conditions, single cell RNA sequencing (scRNAseq) was performed. scRNAseq analysis of 2D and 3D OV-054 DSRCT cultures revealed a homogeneous, tight cluster of DSRCT cells (Fig. 1B-C). The slight difference between clustering of 2D versus 3D cultured cells was likely due to sequencing depth variation (Fig. 1D). Approximately 0-2 reads per million (RPM) of *WT1* were picked up per cell in the scRNAseq analysis (Fig. 1G), indicating low *EWS-WT1* expression. Importantly, expression of *EWS-WT1* was similar between the 2D and 3D cultures (Fig. 1E,G).

The DSRCT patient described in this study was enrolled in the INFORM (individualized therapy for relapsed malignancies in childhood) pilot study (Tilburg *et al*, 2021). The INFORM registry applied comprehensive molecular profiling to provide information on actionable gene variants, which may be used for subsequent therapeutic approaches. Microarray data of the original tumor of this DSRCT patient was obtained from the INFORM study and used to create two gene-sets from the

gene expression list: high-genes (Z-score >1) and low-genes (Z-score <-1). Average read counts of the two gene-sets were collected from the scRNAseq data of the 2D and 3D cultured DSRCT cells and a similar trend was found between expression of the gene-sets in the *in vitro* cultures compared to the original tumor (Fig. 1F). This indicated that both the 2D and 3D cultured DSRCT cells closely resemble features of the original tumor. To check whether wild-type *WT1* is expressed in OV-054 DSRCT cells, the *EWS-WT1* fusion breakpoint from cDNA as well as several regions of *WT1* were amplified. In our *in vitro* OV-054 DSRCT model, only the 3'-most exons of *WT1* were expressed (Fig. 1H-I), while expression of *WT1* exon 4-7 was absent. This indicated that exons 9-10 from *WT1* were derived from the *EWS-WT1* fusion cDNA and that wild-type *WT1* was not expressed in these cells (Fig. 1H-I). As a control, cDNA of a *WT1*-expressing malignant rhabdoid tumor of the kidney (MRTK) model was taken along, which indeed showed expression of all regions of the *WT1* gene (Fig. 1H).

ShRNAs targeting the *EWS-WT* breakpoint create an effective knock-down of the fusion mRNA

The OV-054 DSRCT *in vitro* model enabled us to study the molecular mechanisms driving DSRCT by generating a knock-down model of the *EWS-WT1* fusion mRNA. To this end, we sequenced the breakpoint of *EWS-WT1* cDNA in order to identify the exact location of the gene-fusion and found that *EWSR1* exon 7 was fused to *WT1* exon 8. This enabled us to design short hairpin RNAs (shRNAs) targeting the exact *EWS-WT1* breakpoint (shRNA 3, 5) or exon 8-10 of *WT1* (shRNA 2, 4, 6). With these, we created a DOX-inducible knock-down of the *EWS-WT1* fusion mRNA (Fig. 2A). As a control, a non-targeting (NT) DOX-inducible scrambled shRNA sequence was taken along. An effective knock-down of the *EWS-WT1* fusion was observed with shRNA 2, 3, and 5 after 24 hours of DOX induction (Fig. 2B). When cells were harvested 8, 16, 24, 32, and 40 hours after DOX induction, a gradual decrease of *EWS-WT1* transcripts was observed (Fig. 2C), where shRNA 3 resulted in the most efficient knock-down. To identify genes that are affected upon *EWS-WT1* knock-down, RNA sequencing was performed. RNA sequencing reads were mapped to a reference transcriptome in which *EWSR1* and *WT1* were split into a 3' end and a 5' end to be able to distinguish between the *EWS-WT1* fusion transcripts and wild-type *EWSR1* and *WT1* transcripts. 5'*WT1* was not expressed (Fig. 2D), again confirming that wild-type *WT1* was not expressed in these DSRCT cells. 5'*EWSR1* and 3'*WT1* showed a gradual decrease upon DOX induction (Fig. 2D), indicative of efficient knock-down of the *EWS-WT1* fusion transcripts. A slight decrease was seen in 3'*EWSR1* transcripts (Fig. 2D), suggesting that shRNA 3 could also target wild-type *EWSR1*. However, the RPKM did not drop below the 3'*EWSR1* levels in the NT shRNA control, indicating that this effect was minimal. Sequencing reads were picked-up from both +KTS and -KTS isoforms, which were decreased to a similar extent after induction of shRNA 3 (Fig. 2E). Hence, knock-down of the *EWS-WT1* fusion with shRNA 3 did

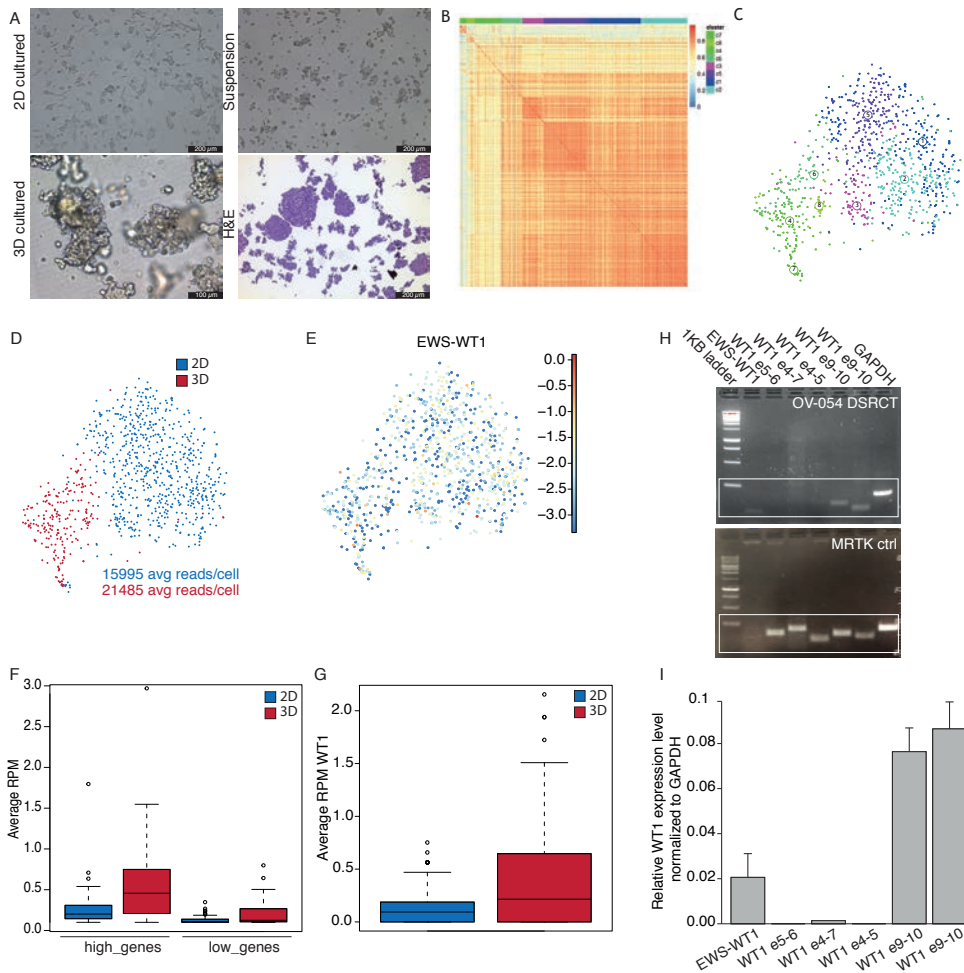


Figure 1: Establishment of a patient derived DSRCT model *in vitro*. A) Pictures of OV-054 DSRCT cells in different growth conditions: 2D on 0.1% BME, 3D in BME droplets and in suspension without BME. H&E staining is performed on cells in suspension. Scale bar: 100 μm (3D) and 200 μm (2D, suspension, and H&E). B) Heatmap depicting cell clustering based on differentially expressed genes. C) tSNE plot depicting clusters of OV-054 DSRCT cells. D) tSNE plot depicting clustering of 2D (blue) and 3D (red) cultured OV-054 DSRCT cells. E) tSNE plot depicting *EWS-WT1* expression in 2D and 3D OV-054 DSRCT cells. F) Box plot depicting the average RPM in 2D (blue) and 3D (red) cultured DSRCT cells for highly expressed and lowly expressed gene-sets. G) Box plot depicting the average *WT1* RPM in 2D (blue) and 3D (red) cultured OV-054 DSRCT cells. H) Picture depicting gel electrophoresis of PCR amplicons of the *EWS-WT1* fusion breakpoint and different regions of *WT1* from cDNA of OV-054 DSRCT cells and MRTK control cells. I) Bar plot depicting relative expression of *EWS-WT1* and different regions of *WT1* by qPCR, normalized to *GAPDH*.

not result in an isoform bias. Together, these data showed that induction of shRNA 3 (targeting the *EWS-WT1* breakpoint in DSRCT cells) resulted in an efficient knock-down of the fusion gene. Wild-type *EWSR1* and *WT1* were not affected, and no bias was observed for the +KTS or -KTS isoform. This *EWS-WT1* knock-down model was used to further investigate genes affected by levels of *EWS-WT1* expression.

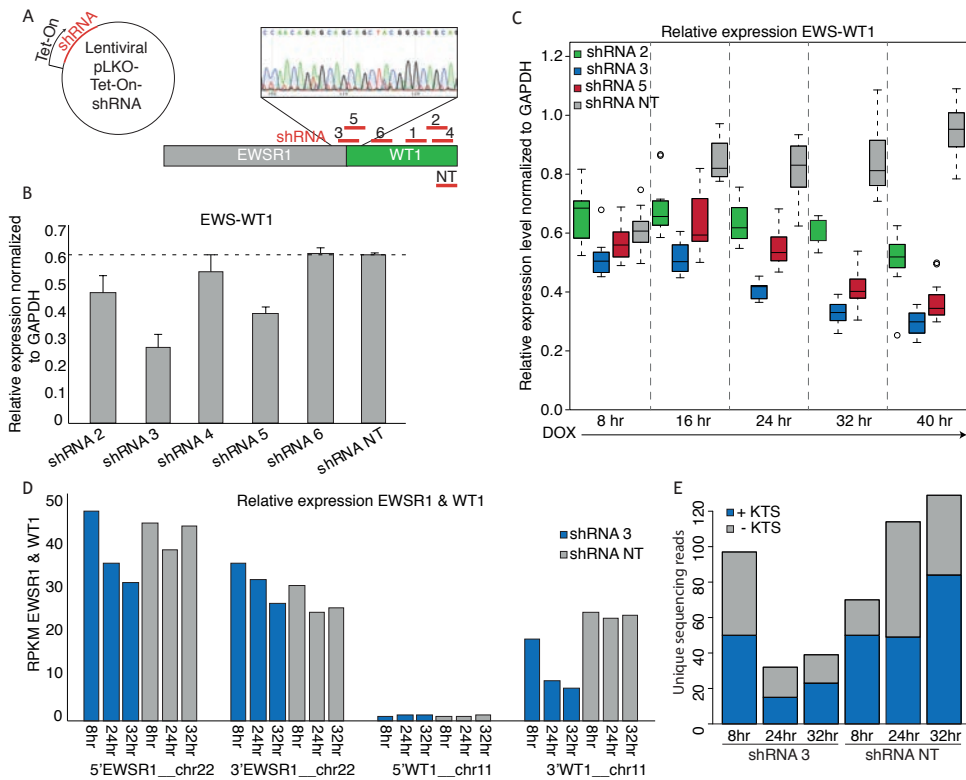


Figure 2: shRNA-mediated *EWS-WT1* knock-down in the DSRCT *in vitro* model. A) Animation depicting the design of shRNAs targeting the breakpoint of *EWS-WT1*, 3'*WT1* and a non-targeting (NT) shRNA. shRNAs were cloned into a lentiviral Tet-On backbone. B) Bar plot depicting relative *EWS-WT1* expression levels 24 hours post DOX-induction of shRNAs normalized to *GAPDH* as determined by qPCR. C) Box plot depicting relative *EWS-WT1* expression levels at 8, 16, 24, 32, and 40 hours post DOX-induction of shRNA 2, 3, 5, and NT normalized to *GAPDH* as determined by qPCR. D) Bar plot depicting RPKM counts of 5'*EWSR1*, 3'*EWSR1*, 5'*WT1*, and 3'*WT1* at 8, 24, and 32 hours post DOX-induction of shRNA 3 and NT as determined by mRNA paired-end sequencing. E) Bar plot depicting number of +KTS (blue) and -KTS (gray) isoform reads as determined by mRNA paired-end sequencing.

EWS-WT1 expression affects cell shape, cell propagation and the transcriptome

To investigate the phenotypic effects of EWS-WT1 in OV-054 DSRCT cells, time-lapse imaging was performed. Knock-down of the *EWS-WT1* fusion mRNA, monitored between 24hr and 40hr after DOX induction, resulted in a decrease of cell-cell adhesion and an increase of cell-matrix adhesion (Fig. 3A, Supp. Fig. 2, Supp. Fig. 3A-B). Additionally, after 4 days of DOX-induction of shRNA 3 OV-054 DSRCT cells appeared more stretched, creating additional cell-matrix adhesion. As controls, non-induced cells and cells with DOX-induction of the NT shRNA control remained in clusters of inter-adhesive cells (Fig. 3B). Knock-down of *EWS-WT1* led to an arrest in cell expansion (Fig. 3C), while the cells became enlarged and flattened compared

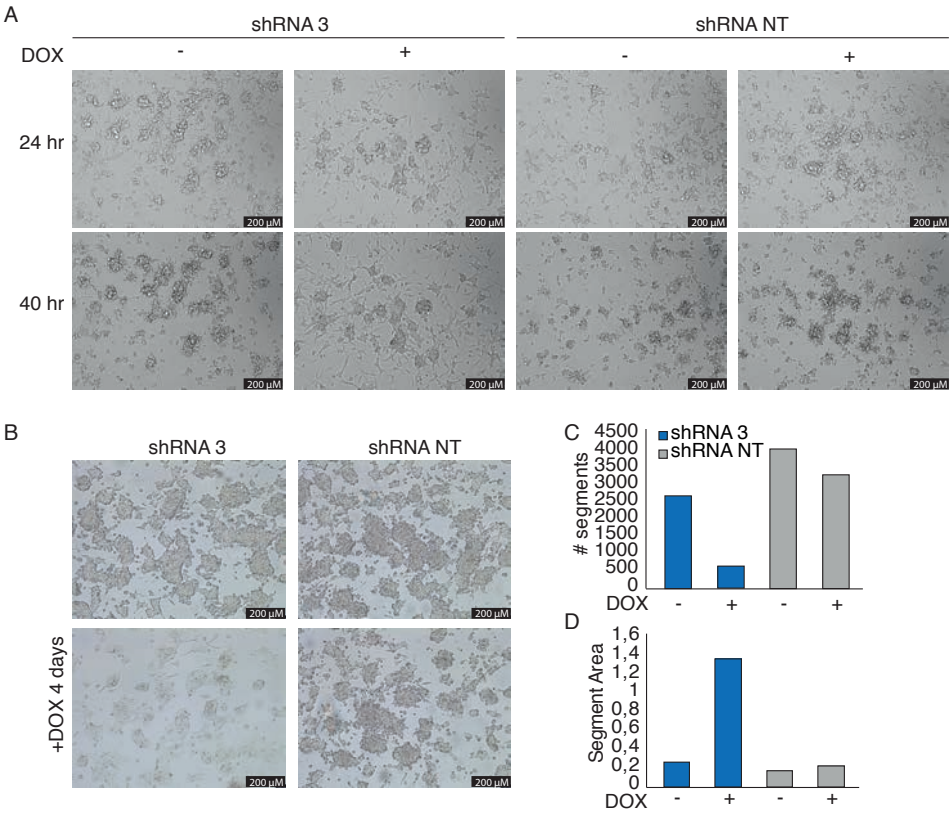


Figure 3: EWS-WT1 affects OV-054 DSRCT cell shape and propagation. A) Time-lapse images of OV-054 DSRCT cells upon *EWS-WT1* knock-down 24 and 40 hours post DOX-induction. Scale bar: 200 μ m. B) Representative pictures taken 4 days post DOX-induction of shRNA 3 and shRNA NT in DSRCT cells. Scale bar: 200 μ m. C) Bar plot depicting number of segments representing OV-054 DSRCT cells 4 days post DOX-induction of shRNA 3 and shRNA NT using particle analysis in ImageJ. D) Bar plot depicting segment area representing OV-054 DSRCT cells found 4 days post DOX-induction of shRNA 3 and shRNA NT using particle analysis in ImageJ.

to the control (Fig. 3D), showing that decreased expression of *EWS-WT1* quickly affects shape and expansion of DSRCT cells. A similar effect was previously shown by an siRNA-mediated knock-down of the *EWS-WT1* mRNA in JN-DSRCT-1 cells (Gedminas *et al.*, 2020).

To investigate the effect of *EWS-WT1* expression on the transcriptome, RNA sequencing was performed 8, 24, and 32 hours after induction of shRNA 2, 3, and NT. To control for off-target effects, both shRNA 2 and shRNA 3 were used, which target *WT1* exon 10 and the *EWS-WT1* breakpoint, respectively. For both shRNA 2 and shRNA 3, the genes were selected that were at least 25% up- or downregulated compared to the NT shRNA control. A cut-off was set at 5 RPKM to extract truly expressed genes. Genes that were affected by both shRNA 2- and shRNA 3-mediated knock-down of the *EWS-WT1* fusion were called as true target genes of *EWS-WT1* (Fig. 4A). After 32 hours of DOX-induction, we identified 75 genes that were down-regulated upon *EWS-WT1* knock-down and 174 genes that were upregulated upon

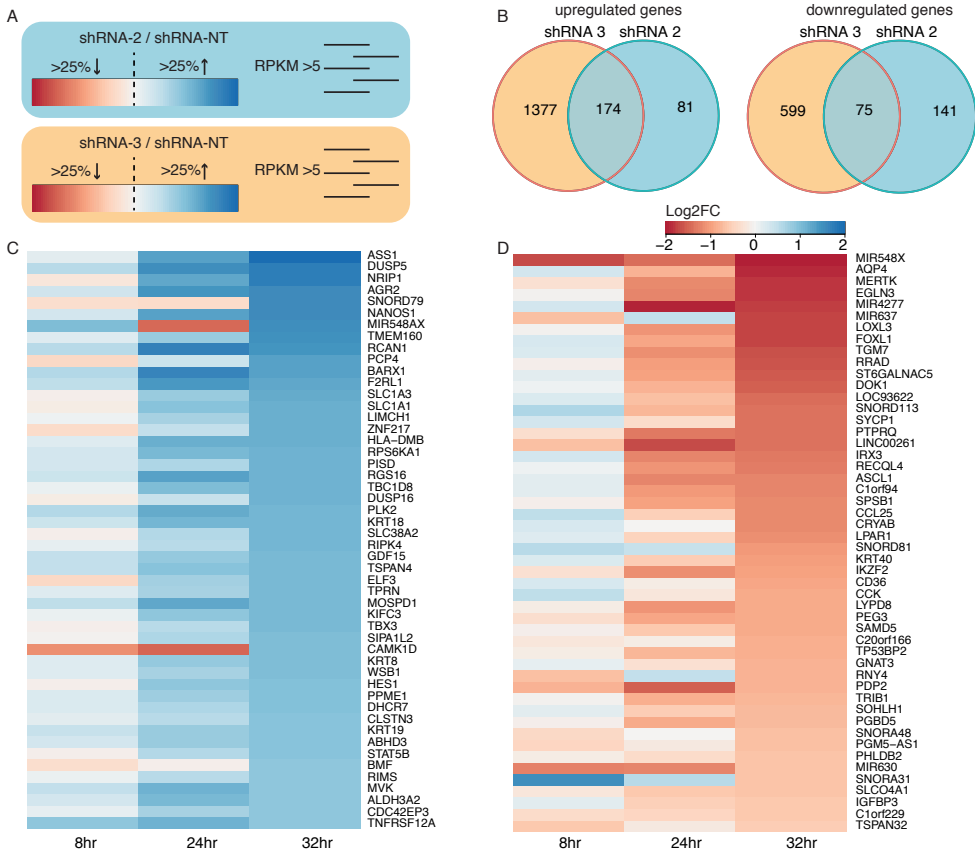


Figure 4: Target genes of EWS-WT1. A) Animation of the approach to find EWS-WT1 target genes: select genes that are at least 25% upregulated or downregulated and have an RPKM value >5 with both shRNA 2- and shRNA 3-mediated knock-down. B) Venn diagram depicting upregulated and downregulated genes upon knock-down of *EWS-WT1* with shRNA 2 and shRNA 3. C) Heatmap depicting the 50 highest upregulated genes upon *EWS-WT1* knock-down, colors represent log2FC compared to shRNA NT. D) Heatmap depicting 50 most downregulated genes upon *EWS-WT1* knock-down, colors represent log2FC compared to shRNA NT.

EWS-WT1 knock-down (Fig. 4B). The expression levels of the 50 most upregulated genes and most downregulated genes upon *EWS-WT1* knock-down are shown in heatmaps (Fig. 4C&D). The phenotypic effects that we observed were accompanied by an increased expression of several cell migration and cell adhesion genes (Supp. Fig. 3C). While phenotypically the DSRCT cells appeared more mesenchymal upon knock-down of the *EWS-WT1* fusion, no evidence was found for epithelial to mesenchymal transition (EMT) (Supp. Fig. 3D). Together, these data showed that cell migration and cell adhesion genes are upregulated upon knock-down of *EWS-WT1* resulting in phenotypic changes, including a decreased cell expansion and an increase in cell surface area. Subsequently, OV-054 DSRCT cells with decreased *EWS-WT1* levels create more cell-matrix interactions (Supp. Fig. 3A-B).

The genes that were affected upon knock-down of *EWS-WT1* were next compared to a recent study in which a siRNA mediated knock-down of the *EWS-WT1* fusion gene was performed in the JN-DSRCT-1 and BER cell lines (Gedminas et al, 2020). From the 174 upregulated genes upon *EWS-WT1* knock-down in our OV-054 DSRCT cells, 6% (11/174) showed an overlap with both the JN-DSRCT-1 and BER lines: *CST1*, *FILIP1L*, *CHST1*, *ALCAM*, *EPHA4*, *KRT8*, *ELF3*, *KRT18*, *SLC1A1*, *PCP4*, and *ASS1* (Fig. 5A). We found that 9% (7/75) of the downregulated genes upon *EWS-WT1* knock-down in our OV-054 DSRCT cells were shared with the other two *in vitro* models: *LOXL3*, *FOXL1*, *RRAD*, *ST6GALNAC5*, *CCL25*, *IGF-*

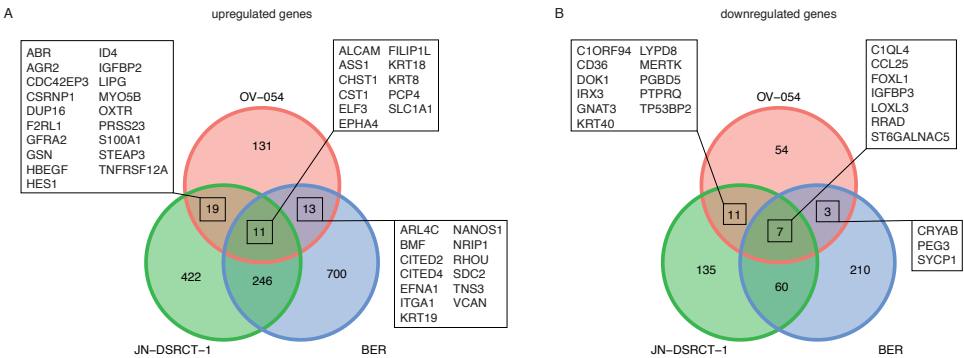


Figure 5: Comparison of EWS-WT1 target genes in OV-054, JN-DSRCT-1, and BER cell lines (Gedminas et al, 2020). A) Venn diagram depicting overlapping upregulated genes upon knock-down of *EWS-WT1*. B) Venn diagram depicting overlapping downregulated genes upon knock-down of *EWS-WT1*.

BP3, *C1QL4* (Fig. 5B). ShRNA3 resulted in a more efficient knock-down of *EWS-WT1* compared to shRNA 2-mediated knock-down. When only the genes affected upon shRNA 3-mediated knock-down were compared with the JN-DSRCT-1 and BER cell lines we indeed discovered additional genes to overlap between the three *in vitro* models (Supp. Fig. 4). The overlap of the transcriptomic effects upon knock-down of *EWS-WT1* in three independent DSRCT cell lines confirmed that these genes are direct or indirect targets of the *EWS-WT1* fusion and potentially play an important role in tumor development and progression.

Drug screen on OV-054 cells reveals effective compounds targeting RTKs and downstream pathways

The established preclinical OV-054 DSRCT *in vitro* model enabled us to perform a medium-throughput drug screen for DSRCT. The screen involved a panel of 201 different compounds. Several of these compounds affected DSRCT cell viability. The area under the curve (AUC) Z-scores of OV-054 DSRCT cells were compared to the Z-scores of two Ewing sarcoma *in vitro* models, ES-041 and ES-046, to unravel compounds that showed a higher sensitivity in DSRCT cells (Fig. 6A). From these drugs, the compounds were selected that presented with an IC₅₀ value, which was below or around the relevant plasma concentrations (Fig. 6B). Several of the compounds that showed an effective response were targeting apoptosis regulators (such as XIAP and BCL2L), including AZD5582, Birinapant, and Navitoclax (Fig. 6B), suggesting that regulation of apoptosis is relevant in DSRCT cells. Interestingly, many other compounds that showed an effective response, including Regorafenib, Lapatinib, Entrectinib, Linsitinib, Crizotinib, Dovitinib, Sorafenib, Vandetanib, and Brigatinib (Fig. 6B), target RTKs. Additionally, compounds targeting downstream targets of RTK signaling pathways (Fig. 6B), such as the PI3K-AKT signaling pathway and the mTOR signaling pathway, showed effective cell killing, including AT7519 and AZD8055. Together, the drug screening data suggested that regulation of apoptosis and RTK-driven signaling pathways are important for DSRCT tumor cell survival.

MERTK, regulated by EWS-WT1, is a potential therapeutic target

Since RTKs and downstream pathways or RTKs appeared to be important for DSRCT tumor progression, we looked for RTKs that are regulated by *EWS-WT1* expression. *MERTK* is one of the most downregulated genes upon knock-down of *EWS-WT1* in OV-054 DSRCT cells (Fig. 4C) and in the JN-DSRCT-1 cell line (Fig. 5B), suggesting that high expression of *MERTK* (Fig. 7A) is regulated by the *EWS-WT1* fusion. Interestingly, *MERTK* has been described as a therapeutic target in several cancers, including melanoma, leukemia, glioblastoma, and gastric cancer (Schlegel *et al*, 2013; DeRyckere *et al*, 2017; Graham *et al*, 2014). To investigate the function of *MERTK* in DSRCT cells, different concentrations of a *MERTK*/FLT3 small molecule inhibitor UNC2025 were added to the culture medium and live cells were counted after 4 and 7 days. Inhibition of *MERTK* resulted in reduced cell expansion of

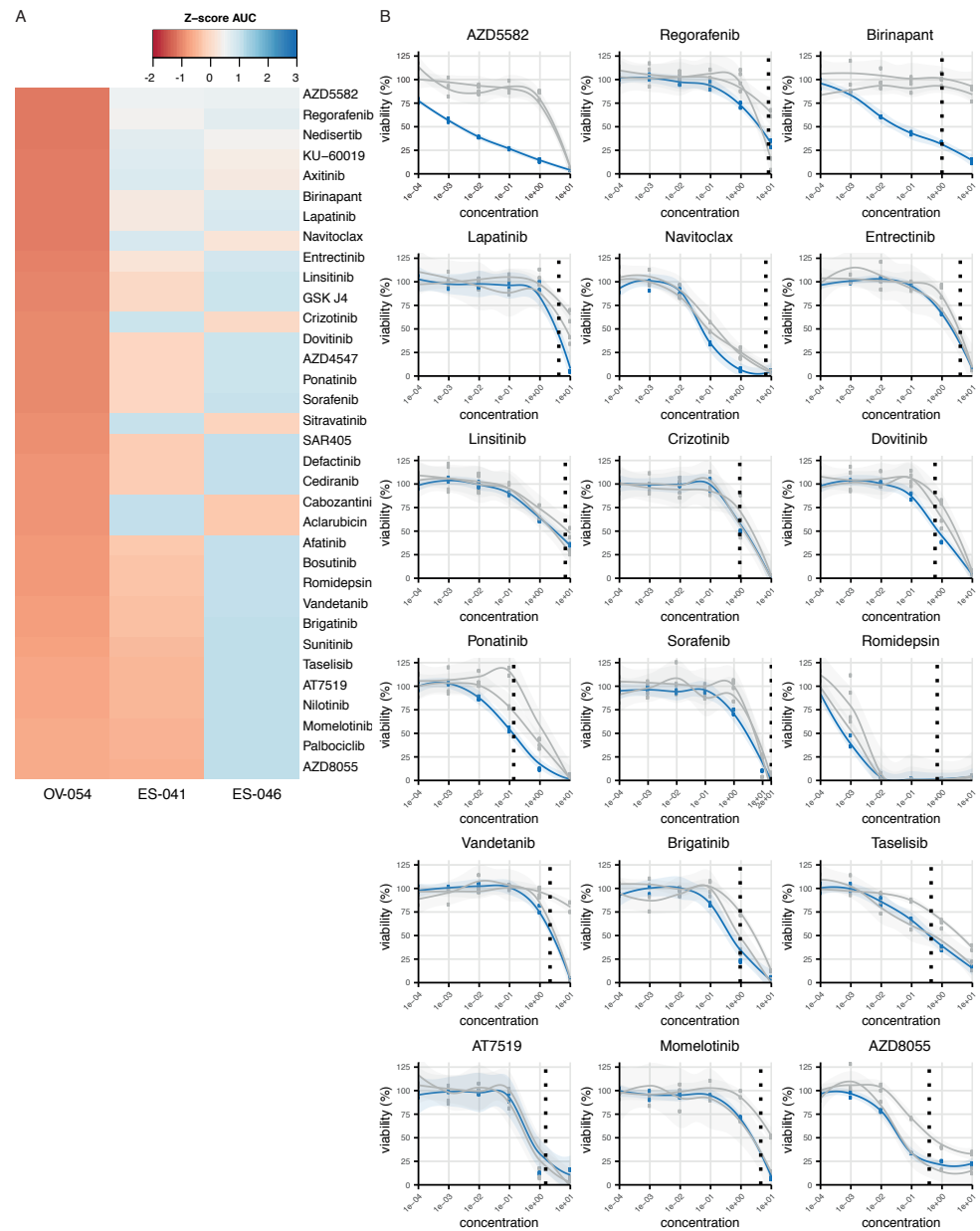


Figure 6: Compound screen on OV-054 DSRCT cells reveals compounds that affect cell viability. A) Heatmap depicting the most sensitive compounds for OV-054 DSRCT compared to two Ewing sarcoma models (ES-041 and ES-046) colors represent AUC Z-scores. B) Graphs depicting cell viability of OV-054 DSRCT (blue) and the two Ewing sarcoma models (gray) upon a 5-day incubation with different drug concentrations (μM). Known plasma concentrations are shown with the vertical dashed line.

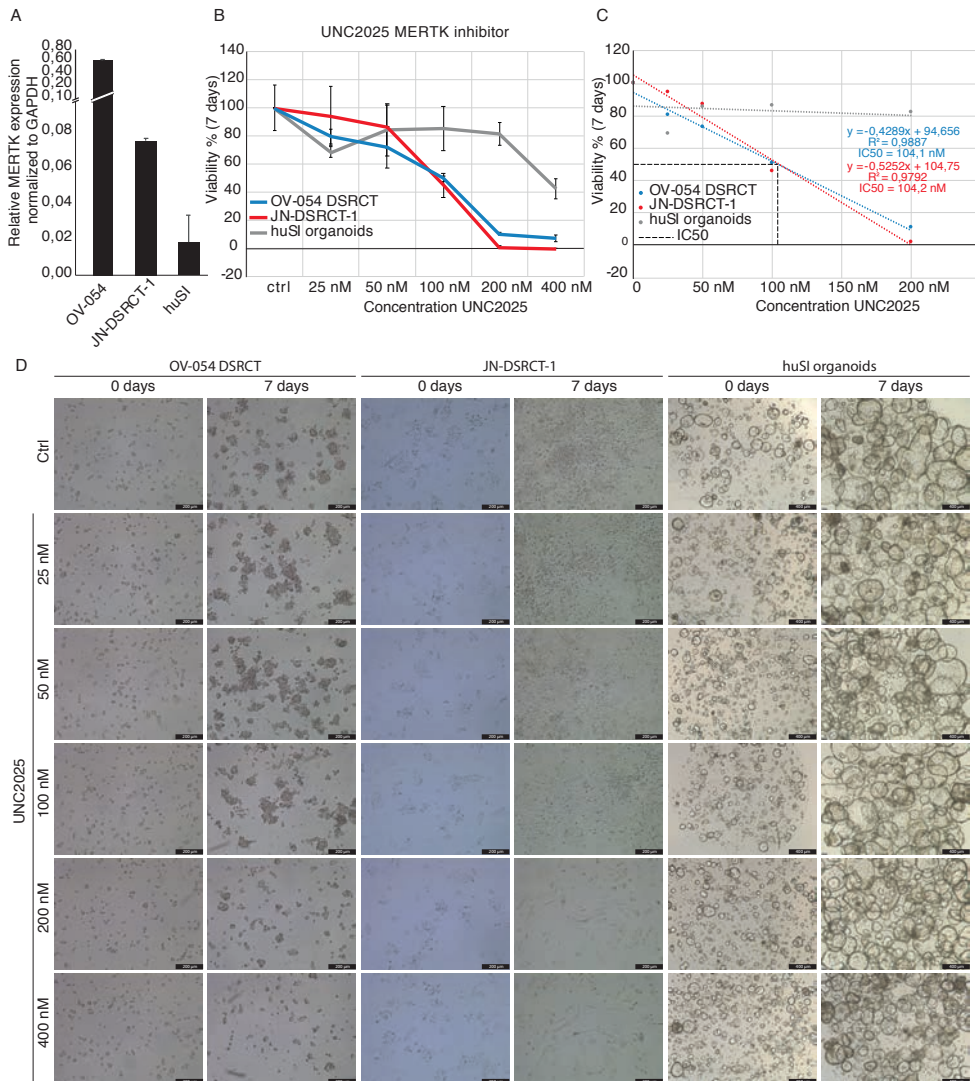


Figure 7: MERTK inhibitor UNC2025 affects DSRCT cell expansion *in vitro*. A) Barplot depicting relative MERTK expression in OV-054, JN-DSRCT-1 and huSI organoids, normalized to GAPDH as determined by qPCR. B) Graph depicting cell viability of OV-054 DSRCT, JN-DSRCT-1 and huSI organoids upon 7 days administration of 0, 25, 50, 100, 200 and 400 nM UNC2025. C) Graph depicting IC50 of UNC2025 on both OV-054 DSRCT and JN-DSRCT-1 cells 7 days post UNC2025 administration. D) Representative pictures of OV-054 DSRCT, JN-DSRCT-1 and huSI organoids *in vitro* at day 0 and day 7 after administration of 0, 25, 50, 100, 200, and 400 nM UNC2025, scale bars: 200 μ m (OV-054 and JN-DSRCT) and 400 μ m (huSI organoids).

OV-054 DSRCT cells *in vitro* in a dose dependent manner (Fig. 7B,D) and a similar effect was found in the JN-DSRCT-1 cell line (Fig. 7B,D). In both DSRCT cell lines, the IC₅₀ of UNC2025 was around 104 nM (Fig. 7C), in line with a previous study of UNC2025 mediated MERTK inhibition in leukemia (DeRyckere *et al*, 2017). Normal human small intestinal (huSI) organoids were exposed to UNC2025 as a control and were only affected by UNC2025 at the highest concentration of 400 nM (Fig. 7B,D). Together this suggested that MERTK is an important driver for cell proliferation in DSRCT and a potential therapeutic target.

Discussion

Using a primary DSRCT patient-derived 2D and 3D cell culture system, we were able to characterize the molecular mechanisms driven by the DSRCT-specific EWS-WT1 fusion protein and the effect of inhibition of the target gene *MERTK* on cell expansion. DSRCT is a highly aggressive and rare soft tissue sarcoma, characterized by a chromosomal translocation resulting in the *EWS-WT1* gene fusion. Expression of *EWS-WT1* presumably regulates genetic targets responsible for oncogenesis in DSRCT. The 5-year event-free survival rate is 18% (Zhang *et al*, 2015), showing the urgency of novel therapies to improve the outcomes for DSRCT patients.

OV-054 DSRCT cells *in vitro* grow as nests of small round cells with large nuclei, typically also seen in DSRCT tissue (Gerald & Rosai, 1989). Both 2D and 3D culture conditions of OV-054 DSRCT consist of a homogeneous cell population exhibiting similarities to the transcriptional profile of the original tumor. The *EWS-WT1* fusion is expressed similarly under 2D and 3D culture conditions. This novel DSRCT *in vitro* model can be used to investigate molecular pathways driving this rare sarcoma type and further explore therapeutic options, which is urgently needed to improve the poor prognosis of this sarcoma.

To explore molecular mechanisms of EWS-WT1, we used an shRNA knock-down approach on our primary DSRCT *in vitro* model. When the genes were compared that were affected upon shRNA-mediated knock-down of *EWS-WT1* with similar gene sets previously described for the JN-DSRCT-1 and BER cell lines (Gedminas *et al*, 2020), we indeed find overlap in up- and downregulated genes. Of note, *ASCL1* was downregulated upon *EWS-WT1* knock-down, which was previously described as a direct target of the gene fusion (Kang *et al*, 2014). This confirms that these genes are (in)direct targets of the EWS-WT1 fusion and likely play a role in tumor development and progression.

Gedminas and colleagues show similarities between the molecular mechanisms of EWS-FLI1 in Ewing sarcoma and EWS-WT1 in DSRCT, despite their different DNA-binding domains (Gedminas *et al*, 2020). These common features include dysregulation of the DNA damage response, an alteration in the E2F transcription factor family members and modulation of other pathways, including TGF β and IGF/mTOR signaling. While the mechanism behind these common features is not clear, DSRCT cells show a striking dependence on *ERG* expression. This is a close

family member of *FLI1* and upregulated by *EWS-WT1* in DSRCT (Gedminas et al, 2020). Interestingly, Franzetti and colleagues found that a knock-down of *EWS-FLI1* expression in Ewing sarcoma affected cell dynamics (Franzetti et al, 2017). Major changes were observed in dynamics of the actin cytoskeleton and cell-to-cell adhesions shifted to cell-matrix adhesion, associated with an increase of cell migration and invasion potential *in vivo*. The dynamical changes of the actin cytoskeleton and a shift from cell-cell adhesion to cell-matrix adhesion shown in the Ewing sarcoma model are similar to the observations we found in DSRCT upon knock-down of *EWS-WT1* *in vitro*. In our study, knock-down of *EWS-WT1* in DSRCT cells affects cell shape and cell propagation. We found several cell migration genes and cell-cell adhesion genes to be affected upon *EWS-WT1* knock-down. Thus, despite the differences in DNA binding motifs of *EWS-FLI1* and *EWS-WT1*, underlying mechanisms driving Ewing sarcoma and DSRCT are possibly similar.

Because of the rarity of DSRCT, this sarcoma is often excluded from clinical trials. Currently, there are 10 clinical trials ongoing or completed that involve DSRCT patients and just one of these clinical trials included an RTK-targeting compound, i.e. sorafenib (ClinicalTrials.gov Identifier: NCT01946529). Unfortunately, the interim analysis of this clinical trial determined that the therapy did not meet the anticipated response, therefore the trial was stopped. To discover novel therapeutic entities, we performed a medium-throughput drug screen on the established preclinical OV-054 DSRCT *in vitro* model. 201 different compounds were included in the drug screen for DSRCT cell viability. The compounds to which the OV-054 DSRCT cells were sensitive included several drugs targeting regulators of apoptosis and many drugs targeting RTKs and downstream pathways of RTKs, including the PI3K-AKT and mTOR signaling pathways. Our data suggests that regulation of apoptosis is important in DSRCT cells and that RTK-driven pathways are key players in DSRCT tumor progression. Therefore, other compounds that target RTKs or downstream pathways of RTKs might show a more effective response, either alone or in combination with current standard chemotherapy.

MERTK expression levels in OV-054 DSRCT are decreased upon knock-down of *EWS-WT1*, showing that this gene is likely regulated by the fusion protein. *MERTK* has several downstream signaling pathways, including MAPK/ERK, PI3K/AKT, and JAK/STAT, regulating multiple biological processes (Lee-Sherick et al, 2013; Brandao et al, 2013; Graham et al, 2014). *MERTK* is involved in multiple malignancies, including leukemia, glioma, melanoma, and rhabdomyosarcoma (Schlegel et al, 2013; Graham et al, 2014), while it has been described as novel therapeutic target in several of these malignancies (Schlegel et al, 2013). Here we show that *MERTK* inhibition with small molecule inhibitor UNC2025 affects propagation of OV-054 DSRCT cells *in vitro*, providing a rationale for investigating *MERTK* as a therapeutic target in DSRCT by small molecule inhibitors such as UNC2025.

Methods

Patient derived DSRCT specimen

Surgically resected tissue was obtained from a DSRCT patient at the Amsterdam UMC with informed consent. Tumor material was washed with Advanced Dulbecco's Modified Eagle's Medium F12 (AdDMEM-F12) (Thermo Fisher Scientific, #12634010) supplemented with 1% pen/strep (Thermo Fisher Scientific, #15140122), 1% Glutamax (Thermo Fisher Scientific, #35050038), 1% Hepes (Thermo Fisher Scientific, #15630056) and minced into tumor pieces using scalpels and mechanically disrupted by pipetting up and down before plating into suspension cell culture plates.

Cell culture

The patient-derived OV-054 DSRCT cell line was maintained in DSRCT medium, containing Advanced Dulbecco's Modified Eagle's Medium F12 (AdDMEM-F12) (Thermo Fisher Scientific, #12634010) supplemented with 1% pen/strep (Thermo Fisher Scientific, #15140122), 1% Glutamax (Thermo Fisher Scientific, #35050038), 1% N2 (Gibco, #17502048), 1% Hepes (Thermo Fisher Scientific, #15630056), 2% B27 (Gibco, #12587010), 0.25% NAC (Sigma Aldrich, #A9165), 50 ng/mL FGF2 (Peprotech, #100-18B), 50 ng/mL EGF (Peprotech, #AF-100-15), 10 ng/mL IGF1 (Peprotech, #100-11), 10 ng/mL Rho Kinase Inhibitor (Abmole, #M1817), 10 ng/mL BMP4 (Peprotech, #120-05ET) and 0.1% BME (Gibco, #31350-010). Cells were incubated at 37°C with 5% CO₂ and passaged 1:5 every 10 days using TrypLE Express Enzyme (Thermo Fisher Scientific, #12605010).

HEK293T cells were maintained in Dulbecco's Modified Eagle's Medium (Thermo Fisher Scientific, #31966-047) supplemented with 10% Fetal Calf Serum (FCS) (Gibco), 1% pen/strep (Thermo Fisher Scientific, #15140122) and 1% Hepes (Thermo Fisher Scientific, #15630056). Cells were incubated at 37°C with 5% CO₂ and passaged 1:20 every 3-4 days using TrypLE Express Enzyme (Thermo Fisher Scientific, #12605010).

Single cell RNA sequencing

OV-054 DSRCT cells were digested using TrypLE Express Enzyme (Thermo Fisher Scientific, #12605010) and mechanically dissociated by pipetting up and down. 2D and 3D OV-054 DSRCT cells were subsequently sorted for DAPI negative cells using the FACSJazz (BD bioscience) and SH800S Cell Sorter (SONY), respectively. Single DSRCT cells were sorted into a 384-well plate for SORT-seq performed by Single Cell Discoveries B.V. (Muraro et al, 2016). Cluster analysis was performed using RaceID3 (Herman et al, 2018). *WT1* reads represent *EWS-WT1* fusion expression, since wild-type *WT1* is not expressed in OV-054 DSRCT cells.

Comparison R2 dataset

The DSRCT patient described in this paper is included in the INFORM study (Tilburg et al, 2021) and available microarray data was analyzed in R2 (www.r2.amc.nl). Two gene-sets were created from the gene expression list of the original DSRCT patient: high-expressed genes (Z-score >1) and low-expressed genes (Z-score <-1). Average read counts of the genes in these gene-sets were collected from the here generated scRNAseq data of the 2D and 3D cultured DSRCT cells.

Introduction shRNAs into OV-054 DSRCT cells

shRNAs targeting the *EWS-WT1* breakpoint or *WT1* exon 8-10 and a non-targeting shRNA were cloned into PLKO-Tet-On Vector (Addgene, #21915)(Supplemental table 1). shRNAs were introduced in the patient-derived OV-054 DSRCT cells using lentiviral transduction. Cells were selected by addition of 0.5 µg/mL puromycin (InvivoGen, #ant-pr-1) to the culture medium. Transcription of shRNAs was induced with 1.0 µg/mL doxycycline (Thermo Fisher Scientific, #564-25-0).

RNA isolation, PCR, and qPCR

RNA isolation was performed using Direct-zol RNA MicroPrep Kit (Zymo Research, R2062) according to the manufacturer's protocol. cDNA synthesis was performed using SuperScript III reverse transcriptase (Thermo Fisher Scientific, # 12574026) and random primers (Promega, #C1181). q-PCR was performed using iQTM SYBR Green Supermix (BIO-RAD, #1708882). *EWS-WT1* was amplified from cDNA by the primers: FW: 3'-TCCTACAGCCAAGCTCAAGTC-5' and REV: 3'-ACCTTCGTTCA-CAGTGGTTG-5'. *MERTK* was amplified from cDNA by the primers FW: 3'-GTGTC-CAAGGGAGTGCAG-5' and REV: 3'-CTCAGCGGATCAGCTTCC-5'. Cq-values were normalized to *GAPDH*, amplified by the primers: FW: 3'-CACATCGCTCA-GACACCATG-5' and REV: 3'-TGACGGTGCCATGGAATTTG-5'. For PCR and sequencing of the *EWS-WT1* breakpoint the same primers were used as mentioned above for the q-PCR. The reverse primer was used for sequencing of the fusion breakpoint by MacroGen Europe B.V..

RNA Sequencing

RNA samples of OV-054 DSRCT cells upon induction of shRNA 2, 3, and NT were paired-end sequenced by MacroGen Europe B.V., using Illumina TruSeq stranded total RNA library construction with Ribo-Zero Gold and Novaseq6000 S4 2x 150bp. To allow for distinguishing between reads that derived from *EWS-WT1* fusion transcripts, wild-type *EWSR1* transcripts or wild-type *WT1* transcripts the hg38 reference transcriptome was obtained from Ensembl and edited. Therefore, the full length *EWSR1* was split into 5'*EWSR1* (exon 1-7) and 3'*EWSR1* (exon 8-17) and full length *WT1* was split into 5'*WT1* (exon 1-7) and 3'*WT1* (exon 8-10). Paired-end sequencing reads were aligned to this edited reference transcriptome using Burrows-Wheeler

Aligner software package (BWA-0.7.17) (Li & Durbin, 2009).

Time-lapse imaging and particle analysis

OV-054 DSRCT cells with shRNA 3 and NT shRNA were induced with DOX, 24 hours prior to live imaging. Live imaging was performed using the Leica DMi8, while incubated at 37°C and 5% CO₂. Images were taken every 2 min from representative areas in each well for 16 hours in total (24-40hr post DOX). Cell counts and cell area from pictures of DOX-induced and non-induced shRNAs in OV-054 DSRCT cells were analyzed using particle analysis in ImageJ. The number of segments represent the number of cells, and the segment areas represent the area of each cell. Cell migration and cell adhesion genes were identified using the DAVID gene annotation tool (Huang *et al*, 2009a, 2009b). Cell-matrix interactions were quantified using the cell counter tool in ImageJ.

Medium-throughput compound screen

Two days prior to the addition of compounds, 5x10³ OV-054 DSRCT cells were seeded per well in 384-well plates. A panel of 201 drugs and DMSO controls were added to the 384-well plates in different concentrations using the Beckman Coulter Biomek i7 Hybrid liquid handling workstation. After 5 days of exposure of the compounds, cell viability was measured with CellTiter-Glo Assay (Promega) using the Spectra-max i3x luminescence microplate reader. Values were normalized to DMSO. AUC Z-scores were calculated by (AUC-AUC_{avg})/st.dev for OV-054 DSRCT cultures and two Ewing cultures (ES-046 and ES-041). Relevant plasma concentrations from previous phase I and II trials (Supplemental table 2) were plotted to compare the viability curves.

UNC2025 screen

OV-054 DSRCT cells, JN-DSRCT-1 cells, and control human small intestinal (huSI) organoids were incubated with different concentrations of MERTK inhibitor UNC2025 (Seleckchem, #S7576): 25, 50, 100, 200 or 400 nM was added to the culture medium. 7 days after addition of UNC2025, representative pictures were taken, and cells were treated with TrypLE Express Enzyme (Thermo Fisher Scientific, #12605010) and counted. Viability of huSI organoids were measured by organoid size using representative pictures and the area measurement tool in ImageJ.

References

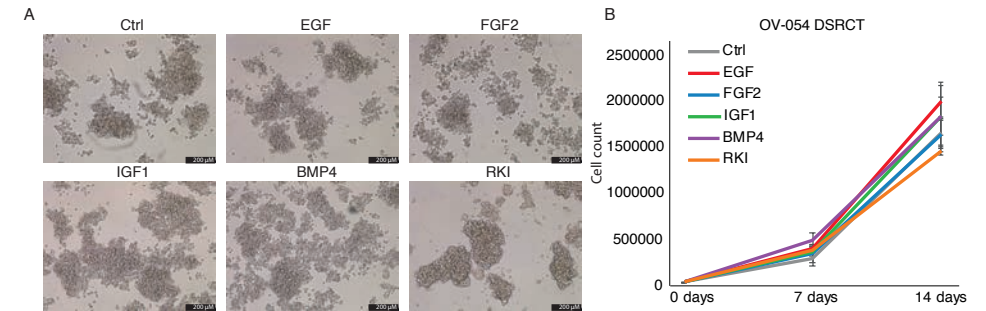
- Bedi S, Khan SA, AbuKhader MM, Alam P, Siddiqui NA & Husain A (2018) A comprehensive review on Brigatinib – A wonder drug for targeted cancer therapy in non-small cell lung cancer. *Saudi Pharm J* 26: 755–763
- Bleijns M, Wetering M, Clevers H & Drost J (2019) Xenograft and organoid model systems in cancer research. *EMBO J* 38: 1–11
- Bulbul A, Fahy BN, Xiu J, Rashad S, Mustafa A, Husain H & Hayes-jordan A (2017) Desmoplastic Small Round Blue Cell Tumor : A Review of Treatment and Potential Therapeutic Genomic Alterations. *Sarcoma* 2017: 1-12
- Chen EX, Hotte S, Hirte H, Siu LL, Lyons J, Squires M, Lovell S, Turner S, McIntosh L & Seymour L (2014) A Phase I study of cyclin-dependent kinase inhibitor, AT7519, in patients with advanced cancer: NCIC Clinical Trials Group IND 177. *Br J Cancer* 111: 2262–2267
- DeRyckere D, Lee-Sherick AB, Huey MG, Hill AA, Tyner JW, Jacobsen KM, Page LS, Kirkpatrick GG, Eryildiz F, Montgomery SA, et al (2017) UNC2025, a MERK small-molecule inhibitor, is therapeutically effective alone and in combination with methotrexate in leukemia models. *Clin Cancer Res* 23: 1481–1492
- Franzetti GA, Laud-Duval K, Van Der Ent W, Brisac A, Irondele M, Aubert S, Dirksen U, Bouvier C, De Pinieux G, Snaar-Jagalska E, et al (2017) Cell-to-cell heterogeneity of EWSR1-FLI1 activity determines proliferation/migration choices in Ewing sarcoma cells. *Oncogene* 36: 3505–3514
- Gedminas JM, Chasse MH, McBairty M, Beddows I, Kitchen-Goosen SM & Grohar PJ (2020) Desmoplastic small round cell tumor is dependent on the EWS-WT1 transcription factor. *Oncogenesis* 9: 1–8
- Gerald WL & Haber DA (2005) The EWS – WT1 gene fusion in desmoplastic small round cell tumor. *Sem. in Cancer Biol.* 15: 197–205
- Gerald WL & Rosai J (1989) Case 2 desmoplastic small cell tumor with divergent differentiation. *Pediatr Pathol* 9: 177–183
- Graham DK, Deryckere D, Davies KD & Earp HS (2014) The TAM family: Phosphatidylserine-sensing receptor tyrosine kinases gone awry in cancer. *Nat Rev Cancer* 14: 769–785
- Hayes-jordan A, Laquaglia MP & Modak S (2016) Management of Desmoplastic Small Round Cell Tumor. *Semin Pediatr Surgery* 25: 299–304
- Herman JS, Sagar & Grün D (2018) FateID infers cell fate bias in multipotent progenitors from single-cell RNA-seq data. *Nat Methods* 15: 379–386
- Hingorani P, Dinu V, Zhang X, Lei H, Shern JF, Park J, Steel J, Rauf F, Parham D, Gastier-Foster J, et al (2020) Transcriptome analysis of desmoplastic small round cell tumors identifies actionable therapeutic targets: a report from the Children’s Oncology Group. *Sci Rep* 10: 1–12
- Huang DW, Sherman BT & Lempicki RA (2009a) Systematic and integrative analysis of large gene lists using DAVID bioinformatics resources. *Nat Protoc* 4: 44–57
- Huang DW, Sherman BT & Lempicki RA (2009b) Bioinformatics enrichment tools: Paths toward the comprehensive functional analysis of large gene lists. *Nucleic Acids Res* 37: 1–13
- Juric D, Krop I, Ramanathan RK, Wilson TR, Ware JA, Sanabria Bohorquez SM, Savage HM, Sampath D, Salphati L, Lin RS, et al (2017) Phase I dose-escalation study of taselisib, an oral PI3K inhibitor, in patients with advanced solid tumors. *Cancer Discov* 7: 704–715
- Kang HJ, Park JH, Chen WP, Kang SI, Moroz K, Ladanyi M & Lee SB (2014) EWS-WT1 oncoprotein activates neuronal reprogramming factor ASCL1 and promotes neural differentiation. *Cancer Res* 74: 4526–4535
- Kang YK, Yoo C, Ryoo BY, Lee JJ, Tan E, Park I, Park JH, Choi YJ, Jo J, Ryu JS, et al (2013) Phase II study of dovitinib in patients with metastatic and/or unresectable gastrointestinal stromal tumors after failure of imatinib and sunitinib. *Br J Cancer* 109: 2309–2315
- Karnieli E, Werner H, Rauscher FJ, Benjamin LE & LeRoith D (1996) The IGF-I receptor gene promoter is a molecular target for the Ewing’s sarcoma-Wilms’ tumor 1 fusion protein. *J Biol Chem* 271: 19304–19309
- Kim J, Lee K & Pelletier J (1998) The desmoplastic small round cell tumor t(11;22) translocation produces EWS/WT1 isoforms with differing oncogenic properties. *Oncogene* 16: 1973–1979
- Li H & Durbin R (2009) Fast and accurate short read alignment with Burrows-Wheeler transform. *Bioinformatics* 25: 1754–1760
- Liston DR & Davis M (2017) Clinically relevant concentrations of anticancer drugs: A guide for nonclinical studies. *Clin Cancer Res* 23: 3489–3498

- Macauley VM, Middleton MR, Eckhardt SG, Rudin CM, Juergens A, Gedrich R, Gogov S, McCarthy S & Poondru S (2017) Erlotinib in Patients with Advanced Solid Tumors. *Clin Cancer Res* 22: 2897–2907
- Markides CSA, Coil DR, Luong LH, Mendoza J, Kozielski T, Vardeman D & Giovanella BC (2013) Desmoplastic small round cell tumor (DSRCT) xenografts and tissue culture lines: Establishment and initial characterization. *Oncol Lett* 5: 1453–1456
- Meneses-Lorente G, Bentley D, Guerini E, Kowalski K, Chow-Maneval E, Yu L, Brink A, Djebli N, Mercier F, Buchheit V, et al (2021) Characterization of the pharmacokinetics of entrectinib and its active M5 metabolite in healthy volunteers and patients with solid tumors. *Invest New Drugs* 39: 803–811
- Muraro MJ, Dharmadhikari G, Grün D, Groen N, Dielen T, Jansen E, van Gurp L, Engelse MA, Carloti F, de Koning EJP, et al (2016) A Single-Cell Transcriptome Atlas of the Human Pancreas. *Cell Syst* 3: 385–394.e3
- Naing A, Aghajanian C, Raymond E, Olmos D, Schwartz G, Oelmann E, Grinsted L, Burke W, Taylor R, Kaye S, et al (2012) Safety, tolerability, pharmacokinetics and pharmacodynamics of AZD8055 in advanced solid tumors and lymphoma. *Br J Cancer* 107: 1093–1099
- Nishio J, Iwasaki H, Ishiguro M, Ohjimi Y, Fujita C, Yanai F, Nibu K, Mitsudome A, Kaneko Y & Kikuchi M (2002) Establishment and characterization of a novel human desmoplastic small round cell tumor cell line, JN-DSRCT-1. *Lab Invest* 82: 1175–1182
- Schlegel J, Sambade MJ, Sather S, Moschos SJ, Tan AC, Winges A, DeRyckere D, Carson CC, Trembath DG, Tentler JJ, et al (2013) MERTK receptor tyrosine kinase is a therapeutic target in melanoma. *J Clin Invest* 123: 2257–2267
- Wilson WH, O'Connor OA, Czuczman MS, LaCasce AS, Gerecitano JF, Leonard JP, Tulpule A, Dunleavy K, Xiong H, Chiu YL, et al (2010) Navitoclax, a targeted high-affinity inhibitor of BCL-2, in lymphoid malignancies: A phase 1 dose-escalation study of safety, pharmacokinetics, pharmacodynamics, and antitumor activity. *Lancet Oncol* 11: 1149–1159
- Zhang S, Zhang Y, Yu YH & Li J (2015) Results of multimodal treatment for desmoplastic small round cell tumor of the abdomen and pelvis. *Int J Clin Exp Med* 8: 9658–9666
- Zheng J, Xin Y, Zhang J, Subramanian R, Murray BP, Whitney JA, Warr MR, Ling J, Moorehead L, Kwan E, et al (2018) Pharmacokinetics and disposition of momelotinib revealed a disproportionate human metabolite - Resolution for clinical development. *Drug Metab Dispos* 46: 237–247
- Zhu X, Trueman S, Straubinger RM & Jusko WJ (2018) Physiologically-based pharmacokinetic and pharmacodynamic models for gemcitabine and birinapant in pancreatic cancer xenografts. *J Pharmacokin Pharmacodyn* 45: 733–746

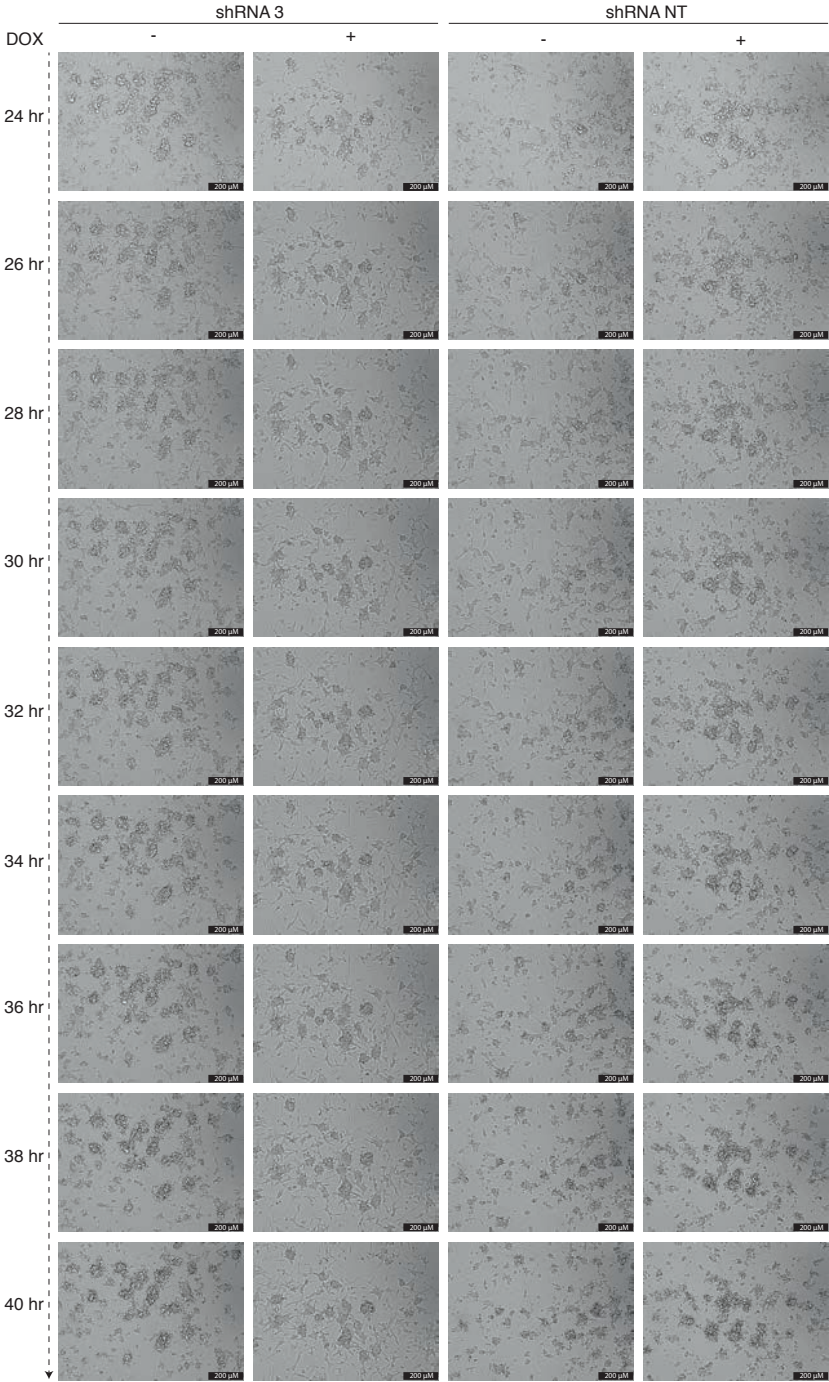
Supplemental figures

shRNA 2	FW: CCGGCACAACATGCATCAGAGAAACCTCGAGGTTTCTCTGATGCATGTTGTGTTTT REV:AATTAAAAACACAACATGCATCAGAGAAACCTCGAGGTTTCTCTGATGCATGTTGTG
shRNA 3	FW: CCGGCAGCAGAGTGAGAAACCATACCTCGAGGTATGGTTTCTCACTCTGCTGTTTT REV:AATTAAAAACAGCAGAGTGAGAAACCATACCTCGAGGTATGGTTTCTCACTCTGCTG
shRNA 4	FW: CCGGATCAGAGAAACATGACCAAACCTCGAGGTTTGGTCATGTTTCTCTGATTTTT REV:AATTAAAAATCAGAGAAACATGACCAAACCTCGAGGTTTGGTCATGTTTCTCTGAT
shRNA 5	FW: CCGGCAGCAGAGTGAGAAACCATACTCGAGTATGGTTTCTCACTCTGCTGCTTTTT REV:AATTAAAAAGCAGCAGAGTGAGAAACCATACTCGAGTATGGTTTCTCACTCTGCTGC
shRNA 6	FW: CCGGTCTCGTTCAGACCAGCTCAAACCTCGAGTTTGAGCTGGTCTGAACGAGATTTTT REV:AATTAAAAATCTCGTTCAGACCAGCTCAAACCTCGAGTTTGAGCTGGTCTGAACGAGA
shRNA NT	FW:CCGGATCTCGCTTGGGCGAGAGTAAGCTCGAGCTTACTCTCGCCCAAGCGAGATTTTTT REV:AATTAAAAATCTCGCTTGGGCGAGAGTAAGCTCGAGCTTACTCTCGCCCAAGCGAGAT

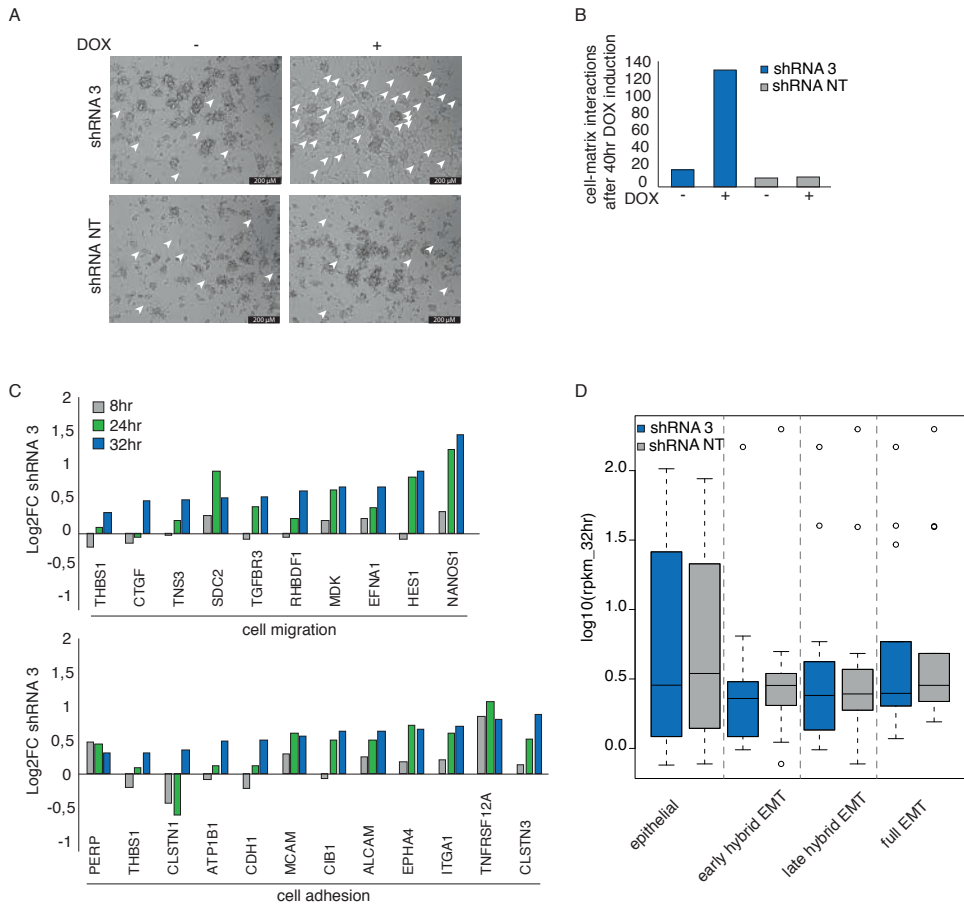
Supplemental table 1: shRNA sequences targeting the breakpoint of *EWS-WT1* (shRNA 3 and 5), *WT1* exon 8-10 (shRNA 2, 4 and 6), and a non-targeting (shRNA NT).



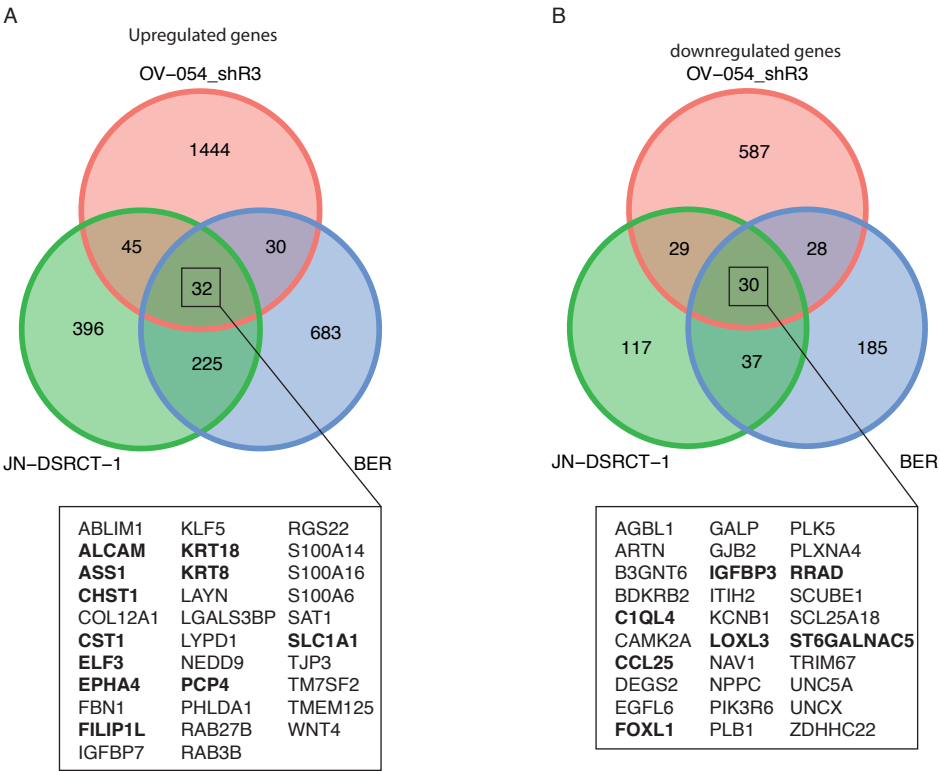
Supplemental figure 1: Effect growth factors on DSRCT cultures. A) Representative pictures of OV-054 DSRCT cells with EGF, FGF2, IGF1, BMP4, and RKI. B) Expansion curve OV-054 DSRCT cells with different growth factors.



Supplemental Figure 2: Time-lapse DSRCT upon *EWS-WT1* knock-down 24-40 hours of DOX-induction. Scale bar is 200 μ M.



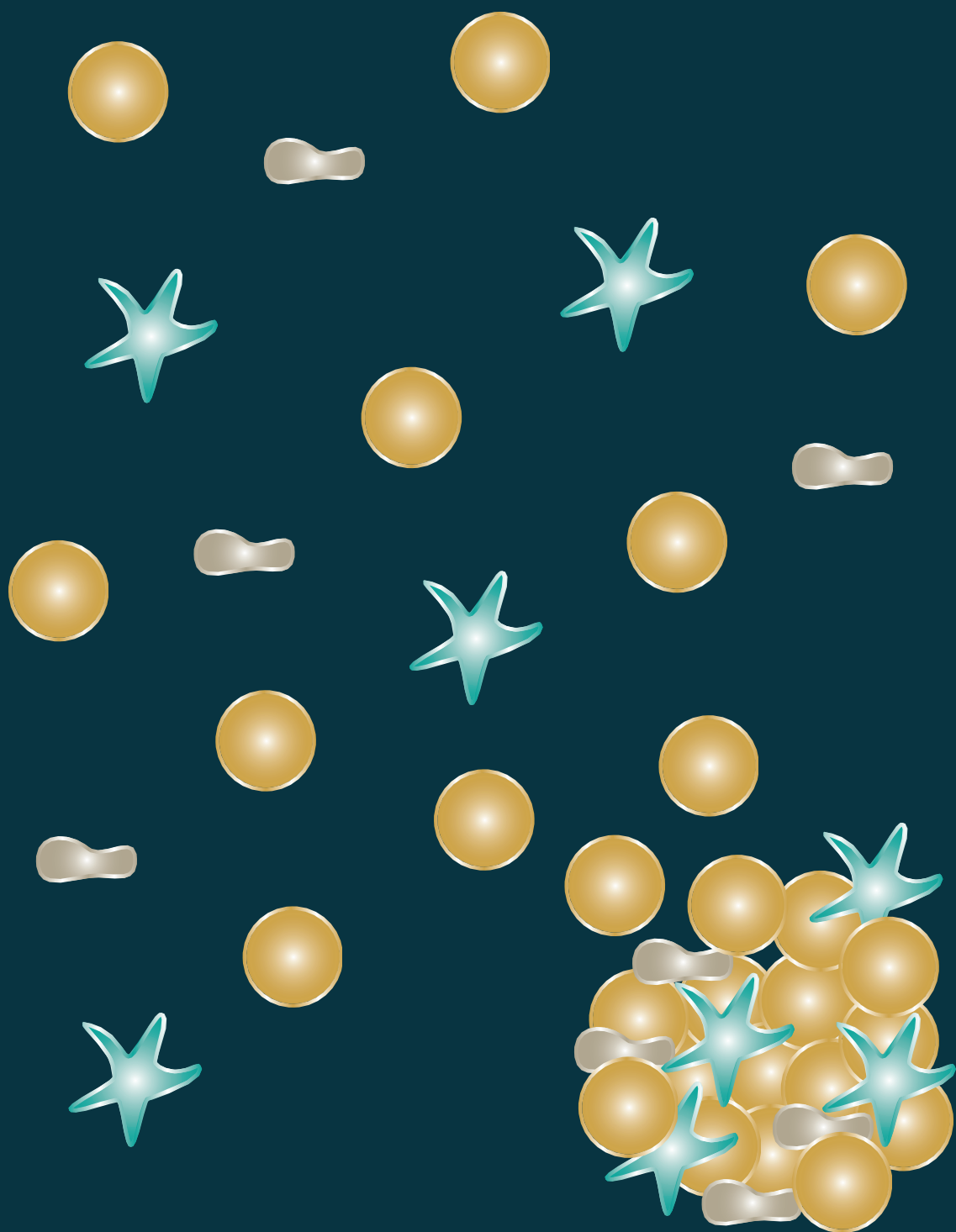
Supplemental Figure 3: Changes in cell-matrix interactions and expression of cell migration and cell adhesion genes upon *EWS-WT1* knock-down. A) Pictures depicting OV-054 DSRCT cells upon 40 hrs of DOX induction of shRNA 3 or shRNA NT, arrows indicate cell-matrix interactions. scale-bar is 200 μ M. B) Bar plot depicting quantification of cell-matrix interactions upon 40 hrs of DOX induction of shRNA 3 or shRNA NT. C) Bar plot depicting log₂FC of cell migration and cell adhesion genes upon 8, 24, and 32 hours DOX-induction of shRNA 3. These genes were affected with both shRNA 2 and shRNA 3 mediated *EWS-WT1* knock-down and identified using DAVID gene annotation tool (Huang *et al*, 2009a, 2009b). D) boxplot depicting average expression EMT genesets (Pastushenko & Blanpain, 2019) in OV-054 DSRCT cells upon 32 hrs DOX induction of shRNA 3 and shRNA NT.



Supplemental Figure 4: Comparison of EWS-WT1 target genes in OV-054 with shRNA3-mediated KD of EWS-WT1 to the JN-DSRCT-1 and BER cell lines (Gedminas *et al*, 2020). A) Venn diagram depicting overlapping upregulated genes upon knock-down of EWS-WT1. B) Venn diagram depicting overlapping downregulated genes upon knock-down of EWS-WT1.

Compound	Plasma concentration (uM)	Reference
Regorafenib	8,1	Liston & Davis (2017)
Birinapant	1,0	Zhu <i>et al.</i> (2018)
Lapatinib	4,2	Liston & Davis (2017)
Navitoclax	6,6	Wilson <i>et al.</i> (2010)
Entrectinib	4,0	Meneses-lorente <i>et al.</i> (2021)
Linsitinib	6,9	Macaulay <i>et al.</i> (2017)
Crizotinib	0,9	Liston & Davis (2017)
Dovitinib	0,6	Kang <i>et al.</i> (2013)
Ponatinib	0,1	Liston & Davis (2017)
Sorafenib	20,1	Liston & Davis (2017)
Romidepsin	0,7	Liston & Davis (2017)
Vandetanib	2,2	Liston & Davis (2017)
Brigatinib	0,9	Bedi <i>et al.</i> (2018)
Taselisib	0,4	Juric <i>et al.</i> (2017)
AT7519	1,6	Chen <i>et al.</i> (2014)
Momelotinib	4,5	Zheng <i>et al.</i> (2018)
AZD8055	0,4	Naing <i>et al.</i> (2012)

Supplemental table 2: Plasma concentrations of effective compounds (Liston & Davis, 2017; Zhu *et al.*, 2018; Meneses-Lorente *et al.*, 2021; Macaulay *et al.*, 2017; Kang *et al.*, 2013; Bedi *et al.*, 2018; Juric *et al.*, 2017; Chen *et al.*, 2014; Zheng *et al.*, 2018; Naing *et al.*, 2012; Wilson *et al.*, 2010).



Chapter 5

Single cell atlas of Ewing sarcoma reveals subclonal evolution and its immune cell composition

Margit Bleijs^{1,*}, Lindy Visser^{1,*}, Thanasis Margaritis^{1,*},
Marc van de Wetering¹, Frank Holstege¹, Hans Clevers^{1,2}

1. Oncode Institute, Princess Maxima Center for Pediatric Oncology,
Utrecht, The Netherlands

2. Oncode Institute, Hubrecht Institute, Royal Netherlands Academy of Arts
and Sciences and University Medical Center, Utrecht, The Netherlands

* These authors contributed equally to this work

Abstract

Ewing sarcoma (ES) is the second most common bone and soft tissue sarcoma and occurs in adolescence and young adults. Previous studies have contributed to the understanding of cellular dynamics in ES, yet most of these studies are based on established cell lines and mouse models. Here, we analyze single cells from primary ES patient-derived tumor tissue and discover subclonal dynamics by inferred copy-number variation (CNV) analysis. Additionally, we reveal the composition of tumor-infiltrating immune cells in ES and the effect on immune cell states upon treatment. Notably, we find that a subset of T cells expresses the targetable immune checkpoint molecules TIGIT and CTLA4, indicating that the immunosuppressive ES tumor microenvironment (TME) can possibly be overcome by combinatorial inhibition of immune checkpoint molecules.

Introduction

Ewing sarcoma (ES) is an aggressive solid tumor that occurs in adolescence and young adults, often during the growth spurt (Ross *et al.*, 2013). This sarcoma arises in bone and soft tissue and is most frequently located in the pelvis, femur, tibia, ribs, thoracic wall, gluteal muscle, pleural cavities and cervical muscles (Grünewald *et al.*, 2018). The standard treatment of ES consists of chemotherapy, surgery and local radiation therapy (Le Deley *et al.*, 2014). The 5-year overall survival rate of ES patients is approximately 70%. Yet, when patients are diagnosed with metastatic or relapsed disease, the long-term survival rate declines to just around 20% (Kovar *et al.*, 2012; Le Deley *et al.*, 2014). Genetically, ES is characterized by a genomic translocation, which results in the expression of a gene fusion involving *EWSR1* and an ETS family transcription factor, most frequently *FLI1* (Ross *et al.*, 2013). The chimeric EWS-FLI1 transcription factor affects target gene expression in several ways, including through alteration of DNA methylation, histone modifications and noncoding RNA expression (Riggi *et al.*, 2021).

Several studies have contributed to the understanding of cellular dynamics in ES. Previous research showed the existence of an ES subpopulation that contains cancer stem cell properties including the capacity to initiate and sustain tumor growth (Suvà *et al.*, 2009). Another study leveraged the inverse relationship between cell pluripotency and miR-154 expression to discover a highly tumorigenic, metastasis-prone ES population as well as a poorly tumorigenic, non-metastatic component (Keskin *et al.*, 2021). Additionally, the EPHB2 receptor was reported as a prognostic marker and promotor of metastasis in ES patients (Keskin *et al.*, 2021). However, most of our current knowledge of ES biology is still based on studies using cell lines, which may only partially mirror the cellular states during tumor initiation and cellular dynamics during tumor progression.

Transcriptomic studies that are based on a mixture of cell populations lack the resolution to identify specific cell types and do not determine the complexity of intra-tumor heterogeneity. Recently, single-cell RNA-sequencing (scRNA-seq) has shown promising results in exploring the cellular architecture of several malignancies (Mereu *et al.*, 2020; Tirosh, Izar, *et al.*, 2016), and the composition of their tumor microenvironment (TME) (Lee *et al.*, 2020; Tirosh, Venteicher, *et al.*, 2016). Single cell RNA sequencing has been performed on ES cell lines and on a PDX model to reveal cell-to-cell heterogeneity of *EWS-FLI1* expression and its effect on ES progression (Aynaud *et al.*, 2020; Franzetti *et al.*, 2017). However, no studies have been published that investigate the architecture of primary ES tumor specimens at the single cell level. In this study, we provide a comprehensive analysis of 18 ES samples from 11 different patients. We provide a single cell atlas of primary ES and identify subclonal dynamics during ES tumor progression. Additionally, we identify the composition of tumor infiltrating immune cells.

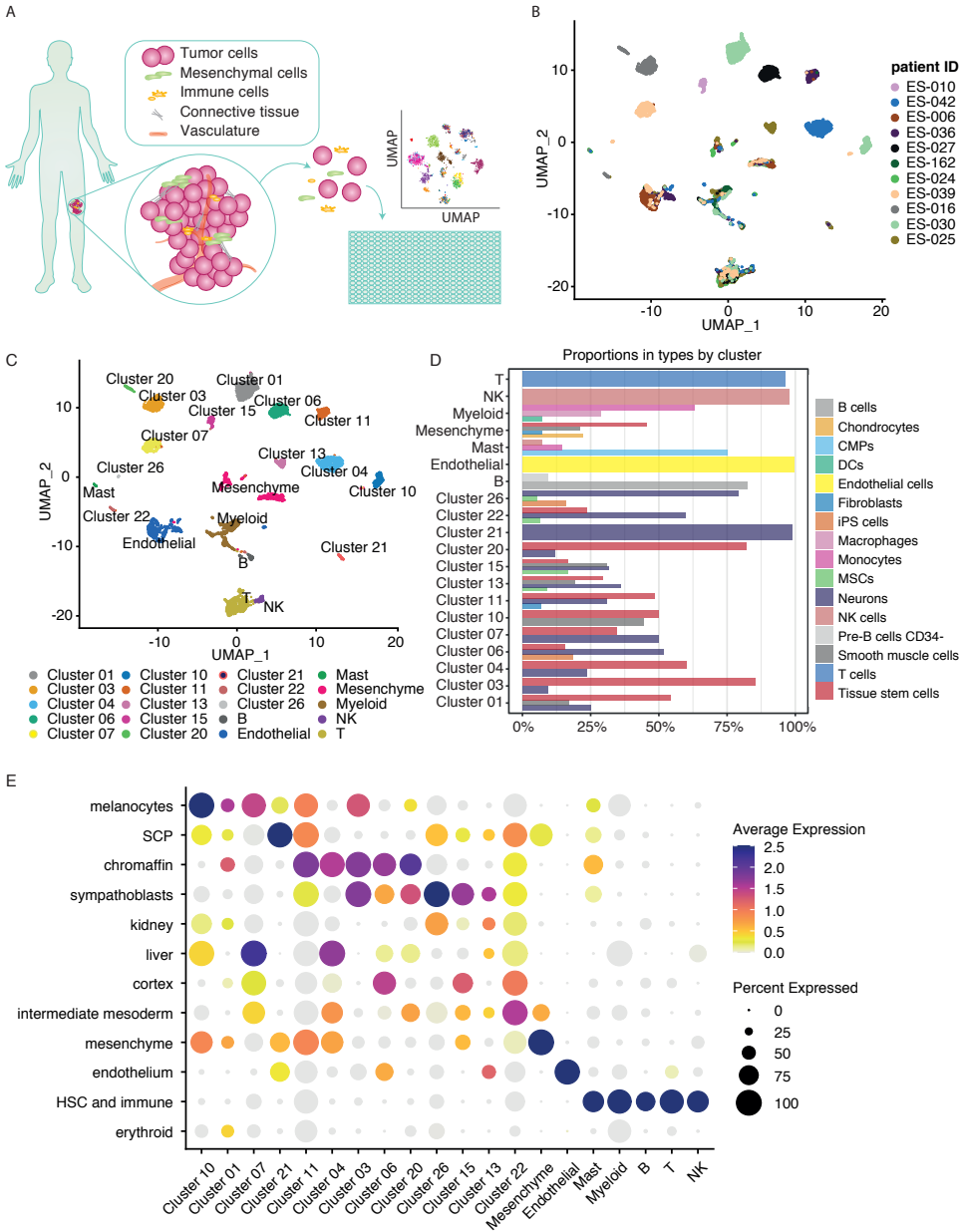
Results

Single cell architecture of primary Ewing sarcoma

To explore the cellular composition of ES, 18 primary ES samples were obtained from 11 individual patients under informed consent. The primary ES material was digested into a single cell suspension and sorted for single cell RNA sequencing (scRNA-seq), using the CEL-Seq2 protocol (Hashimshony *et al.*, 2016; Muraro *et al.*, 2016) (Fig. 1A). The expression profiles of the cells in the different patients were dimensionally reduced using Uniform Manifold Approximation and Projection (UMAP) (Fig. 1B). Unbiased clustering analysis using the Louvain algorithm identified 20 distinct cell clusters (Fig. 1C). To annotate the different cell clusters that were present in the single cell datasets, the expression profiles of single cells from primary ES tumor tissue were compared to the expression profiles of known cell types (Fig. 1D). As expected, clusters that consisted of cells from multiple patient samples were annotated as non-cancer cell populations and included immune cells, endothelial cells, and mesenchymal cells. By contrast, the predicted ES cell populations of individual patients mostly formed separate clusters (Fig. 1B-C).

These predicted ES cell populations expressed several genes known to be upregulated in ES, including the diagnostic marker *CD99* and the EWS-FLI1 candidate target genes *CAV1*, *CCND1*, *HES1*, and *KDSR* (Supp. Fig. 1A) (Aynaoud *et al.*, 2020; Town *et al.*, 2016). A gene set enrichment analysis (comparing the differentially-expressed genes of the predicted tumor and healthy clusters – MsigDB-C2) showed a high resemblance of the tumor clusters to published datasets involving Ewing-family tumors and target genes of the EWS-FLI1 fusion (Hu-Lieskovan *et al.*, 2005; Staeger *et al.*, 2004) (Supp. Fig. 1B), indicating their ES cell identity. Interestingly, the ES cells of some of the individual patients clustered into several subpopulations, e.g. patient ES-030 in clusters 01 and 10 and patient ES-025 in clusters 13 and 21, indicative of intra-tumor heterogeneity (Fig. 1B).

The gene expression profiles of the ES cell clusters were bearing signs of mixed lineage, combining characteristics of neural cells, induced pluripotent stem cells (iPSCs), mesenchymal stem cells (MSCs), smooth muscle cells, and tissue stem cells (Fig. 1D). Tumor cell cluster 21, which largely consist of cells from patient ES-025, showed a very high resemblance to neurons, expressing neural markers such as *SOX10* and *NGFR*, while also expressing the mesenchymal marker *COL1A1* (Supp. Fig. 2A). Additionally, approximately 30% of the cells in this cluster were in the S or G2M cell cycle stage (Supp. Fig. 2B), which indicated that cluster 21 is not comprised of healthy, post-mitotic neurons but represented ES tumor cells with striking neural resemblance. To delve deeper into this, we compared the transcription profiles of each cluster to different neural-crest derivative states present during human embryonic development (Fig. 1E) (Kameneva *et al.*, 2021). As expected, the immune cells, endothelial cells and mesenchymal cells resembled their corresponding cell types during human embryonic development, while the ES tumor clusters showed a



greater overlap to the four annotated neural-crest derived cell types from the Kameleva dataset, including melanocytes, Schwann cell precursors (SCP), chromaffin cells, and sympathoblasts. Several ES tumor cell clusters showed a high resemblance to chromaffin cells (Cluster 01, 03, 04, 06, 11, and 20); some clusters showed a high resemblance to sympathoblasts (Cluster 13, 15, and 26); some clusters were more similar to melanocytes (Cluster 07 and 10), while Cluster 21 showed a striking resemblance to SCPs (Fig. 1E). These neural-crest-like features fit with a neural crest-origin of ES, which is consistent with one of the hypotheses for the ES cell-of-origin in the literature (von Levetzow *et al.*, 2011).

Subclonal evolution in Ewing sarcomas

Pediatric cancers are characterized by complex chromosomal aberrations, which can result in copy number variations (CNV) throughout the genome (L. Cheng *et al.*, 2019). To identify genetic dynamics of tumor cell populations in our single cell sequencing data, inferCNV analysis was performed on the scRNAseq data of primary ES (Fig. 2A). The clusters of mesenchymal cells, endothelial cells and immune cells were plotted as a reference for the presence of CNVs as these cell clusters did not harbor amplifications or losses of chromosomes in their genome. As expected, the ES tumor cell clusters showed amplifications and losses of chromosome arms (Fig. 2A), confirming their tumor cell identity. The observed CNVs based on this analysis are in line with the frequently-observed CNVs in ES using whole genome sequencing approaches, such as the gains in chromosome 1q, 2q, and 8 (Grünwald *et al.*, 2018). Overall, the tumor cell clusters harbored relatively few CNVs (on average approximately 6 CNVs per patient) compared to other bone tumors, such as osteosarcoma (on average approximately 19 CNVs per patient)(Fig 2A) (Zhou *et al.*, 2020). Interestingly, some ES tumor cell clusters showed subclonal variances in their CNV profile (Fig. 2A, Supp. Fig 3-5). As expected, the sub-clustering of ES cells from patient ES-030 (Fig. 1B) was accompanied by genetic differences in CNVs (Supp. Fig. 3). Often, an increase in CNVs occurs upon chemotherapy exposure (L. Cheng *et al.*, 2019), which could explain the subclonality in this patient. Additionally, variations in CNVs were also observed in two individual treatment-naïve ES samples, including in ES-025 and the biopsy of ES-039 (Supp. Fig. 4-5). This could indicate the occurrence of subclonal evolution during ES progression. The SCP-like subpopulations of ES-025 (Cluster 21) lacked the CNVs found in most ES cells from this patient (Fig. 2B, Supp. Fig. 4), suggesting that this might be an early ES cell population that does not harbor CNVs yet. Moreover, while the biopsy material of ES patient ES-039 contained multiple subclonal genetic events (Fig. 2C, Supp. Fig. 5), the resection material from the same patient, which was obtained 4,5 months later and received initial chemotherapeutic treatment (6x Vincristine/Isofosfamide/Doxorubicin/Etoposide), lacked most of the CNVs that were accumulated in the biopsy (Fig. 2C, Supp. Fig. 5). This could indicate that ES cells in this patient that harbor CNVs were more sensitive to chemotherapeutic treatment rather than that cells without CNVs had an

advantage in clonal evolution during ES progression.

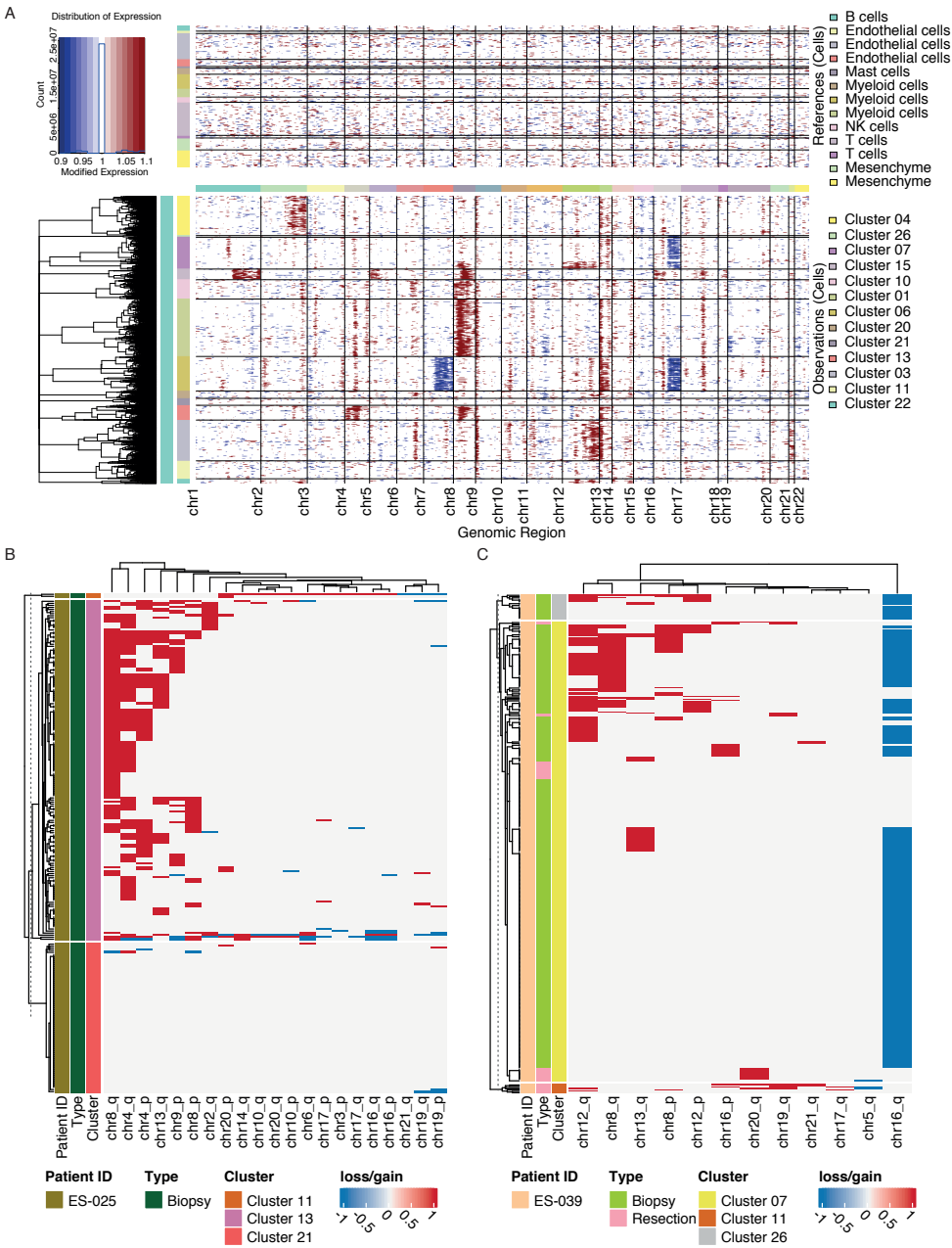


Figure 2: CNVs in Ewing sarcoma and subclonal evolution. A) Heatmap depicting CNV profiles of each cell inferred from inferCNV analysis; chromosomes are lined up on the horizontal axis and cell clusters on the vertical axis. Immune-, endothelial-, and mesenchymal cells on the upper panel were used as reference healthy cell clusters.

Heatmaps depicting phylogenetic evolution tree by gains and losses of chromosome arms in the tumor cells of patient ES-025 (B) and patient ES-039 (C). Inferred CNVs were averaged across chromosome arms and scaled based on the healthy cells. Z-scores over 2.5 were assigned as gains (red) while below -2.5 were assigned as losses (blue).

Immune cell composition in Ewing sarcoma

Tumor-infiltrating immune cells are important components of the TME as they can both promote or inhibit cancer progression (Morales *et al.*, 2020). Several immune cell populations were identified in ES tumors, including T cells, NK cells, myeloid cells, mast cells, and B cells (Fig. 1D, Supp. Fig. 6D). The composition of immune cell populations varied among different Ewing sarcoma patients (Supp. Fig. 6A-E). When comparing treatment-naïve versus treatment-exposed ES samples, we found a small, non-significant increase in T lymphocyte populations and a decrease in macrophages in treatment-exposed samples (Supp. Fig. 6F). Next, the myeloid- and T-cell populations were further analyzed to identify their stimulatory or anti-tumor cell state.

Heterogeneity of tumor-infiltrating myeloid cells

The myeloid population is comprised of a variety of cell types, including macrophages and dendritic cell types. In primary Ewing sarcomas, we found five macrophage populations and two dendritic cell populations (Fig. 3A). The macrophage populations included naïve macrophages (Mq_M0), expressing *S100A8*, *VCAN*, and *FCN1*; macrophages expressing high levels of the chemokine ligands *CCL3* and *CCL4* (Mq_CCL3); macrophages expressing high levels of the glycoprotein *GPNNMB* (Mq_GPNNMB); macrophages with a low expression of Apolipoprotein E (*APOE*; Mq_APOE_low), and a macrophage population expressing high levels of *PPARG* and *FABP4* (Mq_PPARG) (Fig. 3A-D). The *FABP4+PPARG+* macrophage population was previously identified as an alveolar macrophage population in the lung (Aran *et al.*, 2019). Indeed, we found this population of macrophages specifically in patient sample ES-042 (Fig. 3A-B), which was resected from the thoracic area. Macrophages can display a variety of activation states, described as classically (M1) or alternatively (M2) activated cells (Engblom *et al.*, 2016). M1-macrophages typically produce proinflammatory cytokines, which attract NK cells, T cells, and immature dendritic cells (Wang *et al.*, 2009). Accordingly, the chemokine expressing Mq_CCL3 population showed a proinflammatory signature and a high M1 score compared to other macrophage populations (Fig. 3E, Supp. Fig. 7A-G). The Mq_CCL3 cluster was dominated by cells derived from patient ES-025 and ES-026 (Fig. 3B), indicating that these patients had an enrichment of the proinflammatory M1-macrophage population, while most ES patients had a low abundance of proinflammatory M1-macrophages.

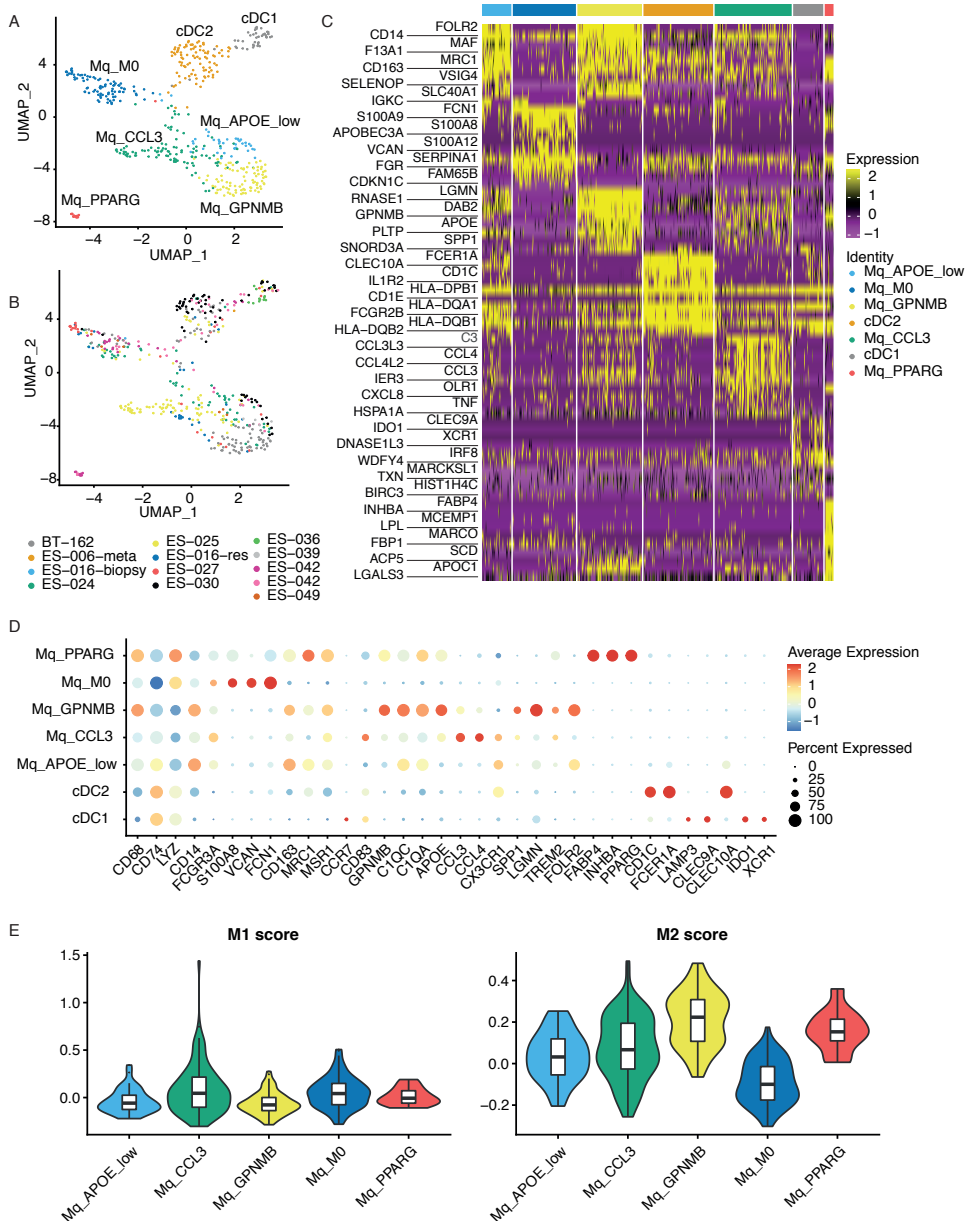


Figure 3: Myeloid cell composition in Ewing sarcoma. A) UMAP depicting myeloid cell clustering. B) UMAP depicting patient contribution to myeloid cell clusters. C) Heatmap depicting differentially expressed genes in myeloid cell populations. D) Dot plot depicting marker gene expression per myeloid cell population. E) Violin plots depicting M1 and M2 macrophage scores.

On the contrary, a higher abundance of *GNPMB*+ anti-inflammatory M2 cells were found in the majority of the ES patients. *GNPMB* was previously described to induce cancer stemness and metastasis (Liguori et al., 2021). Accordingly, *GNPMB*+ macrophage populations presented with a high M2 score and a high anti-inflammatory signature (Fig. 3E, Supp. Fig. 7A-G). Interestingly, the alveolar *FABP4*+*PPARG*+ macrophage population also showed a high anti-inflammatory M2 score (Fig. 3E, supp. Fig. 7A-G). When comparing the pro-inflammatory and anti-inflammatory scores of macrophage populations in post- versus pre-treated ES samples, a small, non-significant increase was observed in both pro-inflammatory and anti-inflammatory macrophages (Supp. Fig. 7D-G). Gene-set enrichment analysis showed an increase in IFN- α -NF- κ B signaling, inflammatory response, IL6-JAK-STAT3 signaling, and Toll-like-receptor signaling pathways in treatment-naïve ES samples (Supp. Fig. 7H), indicating an increased pro-inflammatory response in pre-treated ES. Additionally, treatment-exposed ES samples showed increased Fc γ R-mediated phagocytosis (Supp. Fig. 7H), which is expected as chemotherapy-induced necrotic cells are cleared by phagocytosis (Brouckaert et al., 2004).

Dendritic cells (cDCs) are specialized antigen-presenting cells, which play a key role in the initiation and regulation of the innate and adaptive immune systems. In the TME, DCs can present specific tumor-associated antigens on their MHC molecules to initiate T cell responses (Wculek et al., 2020). DCs are comprised of different cell types, including cDC1 and cDC2 subsets, which were both found in primary ES (Fig. 3A). The cDC2 population, expressing high levels of *CD1C*, *FCER1A*, and *CLEC10A*, is crucial for CD4+ T cell responses and can activate CD8+ T cells (Fig. 3D) (Binnewies et al., 2019; Wculek et al., 2020). The cDC1 population, expressing cell surface markers *LAMP3*, *CLEC9A*, and *XCR1*, is involved in CD8+ T cell-type and Th1 cell-type immunity and correlates with beneficial prognosis in cancer. However, the cDC1 population also expressed *IDO1* (Fig. 3D), which is an enzyme that degrades the essential amino acid tryptophan and is a potent suppressor of T cell responses (Mellor & Munn, 2004). To overcome IDO-mediated immune suppression, various compounds, that inhibit IDO, such as Epacadostat, are being explored in clinical trials (Kristeleit et al., 2017).

Heterogeneity of tumor-infiltrating lymphocytes

Tumor-infiltrating T lymphocytes comprise of a variety of cell types and states with different functional properties. Several T cell populations were identified in primary ES, including naïve T cells (T_naïve), gamma-delta T cells (T_gd), CD8+ T cells (T_CD8), regulatory T cells (T_CD4_FOXP3), and several subsets of CD4+ T cells (Fig. 4A-D). CD8+ T-cells were characterized with a high expression of granzymes *GZMA*, *GZMH*, and *GZMK*, as well as chemokine ligand *CCL5* (Fig. 4D), indicating their cytotoxic properties. A subset of these CD8+ T-cells, however, also expressed exhaustion markers *TIGIT* and *LAG3* (Fig. 4D-E), indicating suppression of the T cell response. CD4+ T cells were characterized by high expression of cyto-

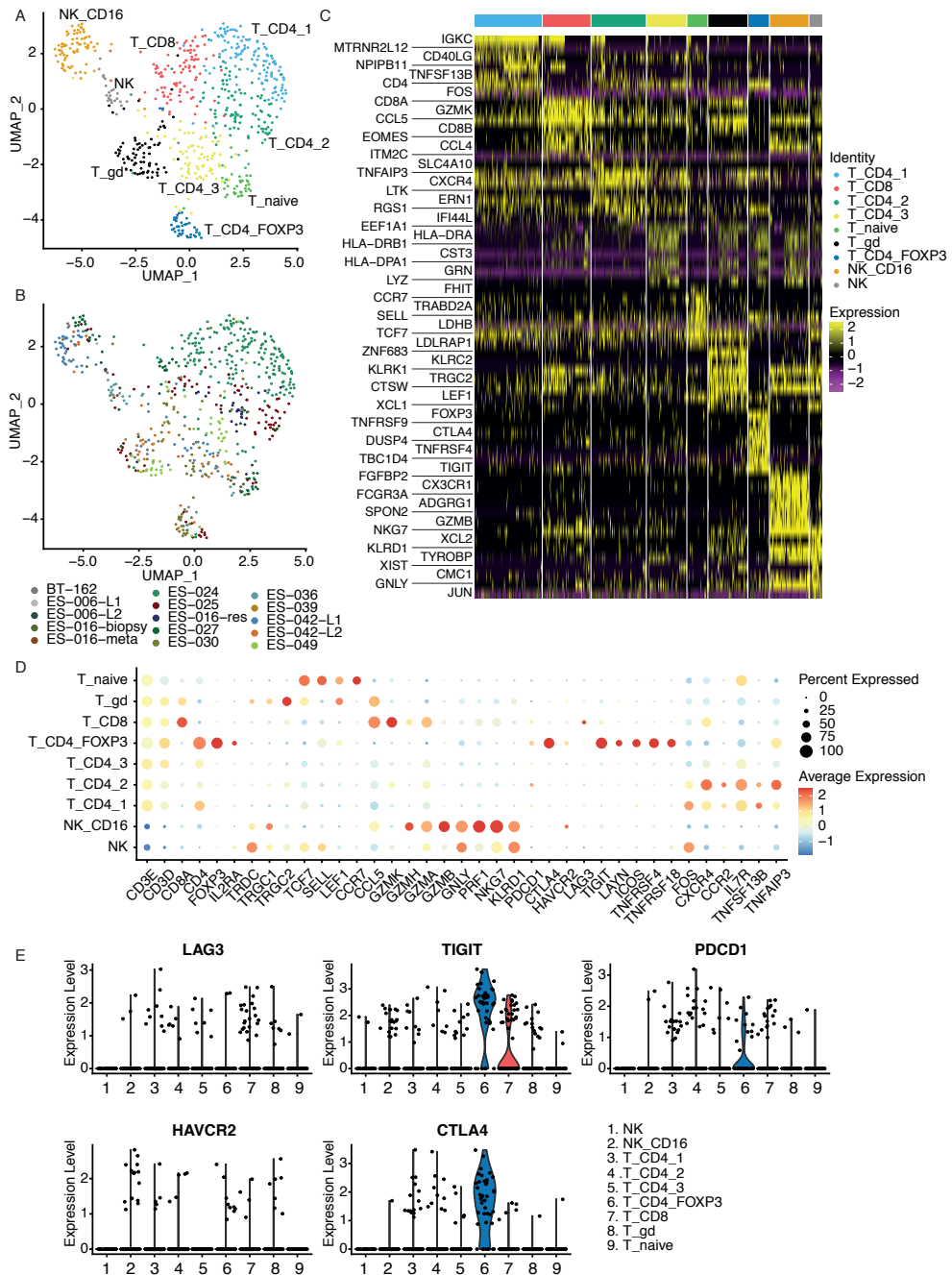


Figure 4: T- and NK cell composition in Ewing sarcoma. A) UMAP depicting T- and NK cell clustering. B) UMAP depicting patient contribution to T- and NK cell clusters. C) Heatmap depicting differentially expressed genes in T- and NK cell populations. D) Dot plot depicting marker gene expression per cell population. E) Violin plots depicting expression of immune checkpoint molecules per cluster.

toxic granzyme marker *GZMA*, chemokine receptor *CXCR8*, and the costimulatory molecules *TNFAIP3* and *TNFSF13B* (Fig. 4D). The *CD4+FOXP3+* T cells additionally expressed the costimulatory surface molecules *TNFRSF4* and *TNFRSF18*, while they also highly expressed exhaustion markers *TIGIT*, *CTLA4*, and *PDCD1*. Gene-set enrichment analysis of effector T cells in post- versus pre-treated samples showed an increased response to the pro-inflammatory cytokines IFN γ , IFN- α , and NF- κ B in treatment-naïve primary Ewing sarcoma (Supp. fig. 8G). However, when comparing the cytotoxic and exhaustion scores of effector T cells in the same sample groups no significant difference was observed (Supp. fig. 8A-F).

Finally, two distinct NK cell populations were identified expressing high levels of NK cell markers *GNLY* and *NKG7* (Fig. 4D). The NK cell population was marked by high expression of *TRDC*, *TCF7*, and the adhesion molecule *SELL* (Fig. 4D), while the *NK_CD16* cell population was characterized by a high expression of various granzymes, including *GZMA*, *GZMB*, and *GZMH* (Fig. 4D), suggesting that they possess cytotoxic properties.

Discussion

Understanding the cellular dynamics regulating ES tumor maintenance and progression is key for the development of effective cancer therapies. Several studies have contributed to the understanding of cellular dynamics in ES (Keskin *et al.*, 2021; Suvà *et al.*, 2009). However, most studies that address ES biology are based on established cell lines or transplanted mouse models. While these studies give important insights in mechanisms underlying ES tumor progression, they lack the architecture of the original tumor, including the surrounding TME. In this study, we provide a single cell atlas of primary ES tumor samples to reveal subclonal genetic events during ES progression and the contribution of immune cells in the TME. Finally, we identify targetable immune checkpoint genes that may account for the immune suppressive nature of the TME in ES.

Phylogenetic branching evolution, based on CNVs in canonical aberrations and oncogenes, is a fundamental principle of genetic variation in pediatric solid tumors (Andersson *et al.*, 2020). A recent study shows that genetic heterogeneity in Wilms tumor, neuroblastoma, and rhabdomyosarcoma (RMS) is more prevalent in aggressive tumors compared to clinically favorable tumors (Andersson *et al.*, 2020). Mutations that occur earlier in tumor progression are likely to be present in all tumor cells, while mutations occurring later during tumor growth are likely to be present in subclones of tumor cells. Interestingly, genomic signatures that differentiate prognostic subgroups in neuroblastoma and RMS emerge earlier during tumor progression than they do in Wilms tumors, indicating that some pediatric solid tumors are born bad, while others grow worse over time (Andersson *et al.*, 2020). In our study, inferCNV analysis revealed that subclonal genetic events were already present in two individual treatment-naïve diagnostic ES samples. This suggests that ES are born bad, similar to neuroblastoma and RMS. However, the small SCP-like

cell subpopulation of ES-025 lacks the CNVs found in most of the cells from this patient, suggesting that ES can also grow worse over time. Single cell WGS would allow reconstruction of phylogenetic trees to get a more detailed overview of clonal evolution of ES tumor cells.

The cell-of-origin of ES remains a matter of debate. The neural-crest-like characteristics of ES cells as reported here suggests that this sarcoma is neural-crest derived, which is in line with previous research showing that introduction of *EWS-FLI1* fusion gene expression in neuroblastoma cells results in a switch from the neuroblastoma differentiation program to that of ES/primitive neuroectodermal tumors (PNET) (Rorie *et al.*, 2004). This would imply that neural-crest derivative cells acquiring the *EWS-FLI1* fusion can transform to ES cells. However, another study shows that introduction of the *EWS-FLI1* fusion gene in primary human MSCs can also trigger the ES initiation program (Riggi *et al.*, 2008). In our data, ES cell clusters resembled various neural-crest derivatives (Kameneva *et al.*, 2021). Several ES cell clusters resembled sympathoblasts and chromaffin cells, while some ES cell clusters resembled melanocytes. Interestingly, lineage specification of neural-crest cells towards melanocytes appears earlier in development than lineage specification towards neurons and mesenchymal progenitors (Soldatov *et al.*, 2019). This suggests that the founder cell of ES is an early neural crest cell, stuck in development. Moreover, one of the markers of the neural-crest derived mesenchymal lineage is *Fli1* (Soldatov *et al.*, 2019). Hence, acquisition of the *EWS-FLI1* fusion gene could interfere with differentiation of neural-crest cells towards mesenchymal progenitors. However, we cannot exclude the possibility that ES originates from mesenchymal cells that have acquired the oncogenic gene fusion or a de-differentiation of late neural-crest derivative because of secondary effects, such as the recurrent CNVs.

Tumor progression can be both stimulated and inhibited by components in the TME, including the immune cell populations. Various immunotherapeutic approaches for the treatment of ES have shown limited efficacy, which may be due to the lack of specific surface antigens and to the immunosuppressive TME (Morales *et al.*, 2020). Indeed, we find that both anti-inflammatory M2 macrophages and exhausted T cells are abundant in ES. Interestingly, targetable immune checkpoint molecules, including *CTLA4* and *TIGIT*, are expressed in a subset of the T cell populations. This suggests that therapeutic approaches based on immune checkpoint inhibition could be effective in ES patients. However, as these immune checkpoint molecules were expressed in a subset of ES patients, only those would benefit from such treatment. Regulatory T cells that express *CTLA4* can induce IDO-competent DCs to express *IDO*, which subsequently leads to suppression of T cell responses (Mellor & Munn, 2004). We propose that therapies targeting the immune checkpoint molecules *CTLA4* and *TIGIT* in combination with IDO inhibitors might be beneficial for a subset of ES patients. The prevalence of immune suppressive M2 macrophages in ES negatively affects the efficacy of immunotherapies. The relative decrease in M2 macrophages upon chemotherapy, could be indicative for more effective im-

mune checkpoint inhibition following standard chemotherapy. Additionally, a recent study shows that the combination of TIGIT blockade with IL-15 mediated NK- and T- cell stimulation amplifies tumor cell killing of soft tissue sarcomas (Judge *et al.*, 2020). Together this suggests that the immunosuppressive nature of the ES TME might be overcome by combinatory inhibition of immune checkpoint molecules.

Methods

Patient derived Ewing sarcoma specimen

Surgically resected tissue was obtained from Ewing sarcoma patients at the Princess Máxima Center with informed consent. Tumor material was washed with basal medium containing Advanced Dulbecco's Modified Eagle's Medium F12 (AdDMEM-F12) (Thermo Fisher Scientific, #12634010) supplemented with 1% pen/strep (Thermo Fisher Scientific, #15140122), 1% Glutamax (Thermo Fisher Scientific, #35050038), 1% Hepes (Thermo Fisher Scientific, #15630056) and minced into tumor pieces. The tumor pieces were washed with AdDMEM-F12 and a part of the tumor pieces were frozen into AdDMEM-F12, supplemented with 50% Fetal Calf Serum (FCS) (Gibco, #16140071) and 10% Dimethyl Sulfoxide (DMSO) (Sigma-Aldrich, #D8418).

Whole genome/exome DNA sequencing

150 ng of total DNA was used for library preparation using the KAPA HyperPlus kit (Roche), according to the manufacturer's instructions. Libraries from tumor and normal tissue were pooled in a 3:1 ratio, with a total of 7 tumor/normal pairs per S4 sequencing kit. Libraries were sequenced using 2x150 cycles on a NovaSeq 6000 (Illumina). The WGS sequencing data was processed as per the GATK 4.0 workflow for variant calling, using a wdl and cromwell based workflow. Reads were aligned to GRCh38 using Burrows-Wheeler Aligner software package (BWA-0.7.13) (Li & Durbin, 2009), and QC was performed using FastQC (version 0.11.5) and picard-Tools (version 2.20.1). Somatic variants were identified using Mutect2 from GATK v4.1 and annotated using Vep (version v92). Similarly, CNA's were identified using GATK v4.1.

Tissue dissociation and single cell RNA sequencing

Tumor pieces were minced using scalpels and mechanically disrupted by pipetting up and down. Single cells were taken off and kept apart on ice. Left over tissue clumps were digested at 37°C using digestion buffer, containing basal medium supplemented with 1 mg/mL Collagenase1A (Sigma-Aldrich, #C9891) and 100 U/mL DNase I (Roche, #4716728001) to prevent cells clumping. Tissue clumps were digested at 37°C, for three 10 min rounds; after each round single cells were taken collected and kept on ice and fresh digestion buffer was added to the left-over clumps. After digestion, Red Blood Cell lysis buffer (Sigma-Aldrich, #11814389001) was applied for 5 min at RT to lyse the red blood cells. The single cells were washed with FACS buffer, containing PBS supplemented with 2% FCS, 2 mM EDTA and 100 U/mL DNase I. The cells were stained for 30 min at RT with Human CD45 PE-conjugated Antibody (R&D Systems, #FAB1430P-100) in FACS buffer.

Prior to sorting, single cell suspensions were stained at RT in 5 μ M DRAQ5 and 1 μ M

DAPI (Sigma-Aldrich, #D9542). Viable single cells were sorted based on forward / side-scatter properties, DAPI-, DRAQ5-, and CD45 staining as shown in Supp. Fig. 9 (gating strategy) using FACS (SONY SH800S Cell Sorter) into 384-well plates (Bio-Rad) containing 10 μ L of mineral oil (Sigma) and 50 nL of RT primers. Libraries were prepared using the Sort-seq method (Muraro et al., 2016) and subjected to paired-end sequencing with 75-bp length using the Illumina NextSeq500 sequencer.

Mapping and filtering

The Sharq pipeline was used to process the sequencing data as previously described (Candelli *et al.*, n.d.). Mapping was performed using STAR (version 2.6.1), on the Genome Reference Consortium GRCh38. Read assignment was performed with featureCounts (version 1.5.2), using a gene annotation based on GENCODE version 26.

External RNA controls (ERCCs) and transcripts mapping to the mitochondrial genome were removed from all cells. The same for transcripts of genes identified based on high correlation with the hemoglobin genes expression, as previously described by Hanemaaijer et al. (Hanemaaijer *et al.*, 2021). To avoid contamination, wells where the inserts were mapping over 15-fold to non-exonic as compared to exonic regions, cells with mitochondrial-encoded transcripts over 80% of nuclear transcripts, cells expressing over 5% of their total transcriptome erythroid marker genes were removed. To improve cross-sample comparisons, ambient mRNA contamination in individual cells was estimated and removed using DecontX (Yang *et al.*, 2020). DecontX was run for all samples (batches) individually. Removal of cells with less than 800 transcripts was repeated on the decontaminated counts matrix.

scRNA-seq analysis

Unique transcript counts were normalized using sctransform (Hafemeister & Satija, 2019) and analyzed using the Seurat R package (version 4.0.0) (Butler *et al.*, 2018). From the top 3000 variable genes, genes associated with cell cycle phase, dissociation stress (heat shock and chaperone proteins according to GO:0006986), sex (*XIST*, *TSIX*, and Y chromosome-specific genes), and activity (ribosomal protein genes according to GO:0022626) were removed from the list of variable genes to avoid biases in cell clustering, as described before (Hanemaaijer *et al.*, 2021). The first 30 principal components were used both to calculate dimensionality reduction using the UMAP technique and to perform clustering with a resolution of 1 and the Louvain algorithm.

Cell cycle states were annotated using the CellCycleScoring function of Seurat. Differential expression analysis was performed with the FindMarkers Seurat (Butler *et al.*, 2018) function for different clusters, using the Wilcoxon test with 1.5-fold change expression cutoff and 5% Bonferroni multiple testing corrected statistical significance cutoff. Only positive markers were considered.

Module scores for the external human fetal scRNA-seq dataset (Kameneva *et al.*, 2021) were calculated using the AddModuleScore function of Seurat with

the following modifications: only genes present in both datasets were kept for the external dataset, followed by filtering of the low quality cells with fewer than 800 transcripts. The top 20 genes of each ES dataset cluster after removal of the contaminating genes were used for the calculation. For the myeloid composition analysis, the module scores were calculated based on M1 and M2 gene signatures from Cheng *et al.* (S. Cheng *et al.*, 2021) and on the pro- and anti-inflammatory gene signatures from Wauters *et al.* (Wauters *et al.*, 2021). For the T and NK composition analysis, the exhausted and cytotoxic genes signatures were used from Jerby-Arnon *et al.* (Jerby-Arnon *et al.*, 2018) and Tirosh *et al.* (Tirosh, Izar, *et al.*, 2016).

Cell annotation using external data

The healthy cell clusters, including immune cells, endothelial cells, and mesenchyme were annotated using SingleR (version 1.2.4) (Aran *et al.*, 2019) with the Human Primary Cell Atlas dataset (Mabbott *et al.*, 2013), consisting of 713 microarray samples. Marker genes were used for further refining the cell annotations.

Copy Number Variation analysis

We identified malignant cells by inferring the somatic large-scale chromosomal copy number alterations using infercnv (version 1.6.0). We used the endothelial, mesenchyme and immune cells as a healthy reference. The gene ordering file, which contains the chromosomal start and end position for each gene, was created from ENSEMBL using the biomaRt R package (version 2.46.3) (Durinck *et al.*, 2009). To run infercnv, we used the following parameters: a cutoff of 0.1, clustered cells into the annotated clusters, denoised the output and applied an i3 hidden Markov model.

For the phylogenetic analysis, InferCNV scores were averaged across chromosome arms and then scaled and centered (i.e. z-transformed) based on the healthy cell clusters. Z-scores over 2.5 were assigned as gains (red, while z-scores below -2.5 were assigned as losses (blue).

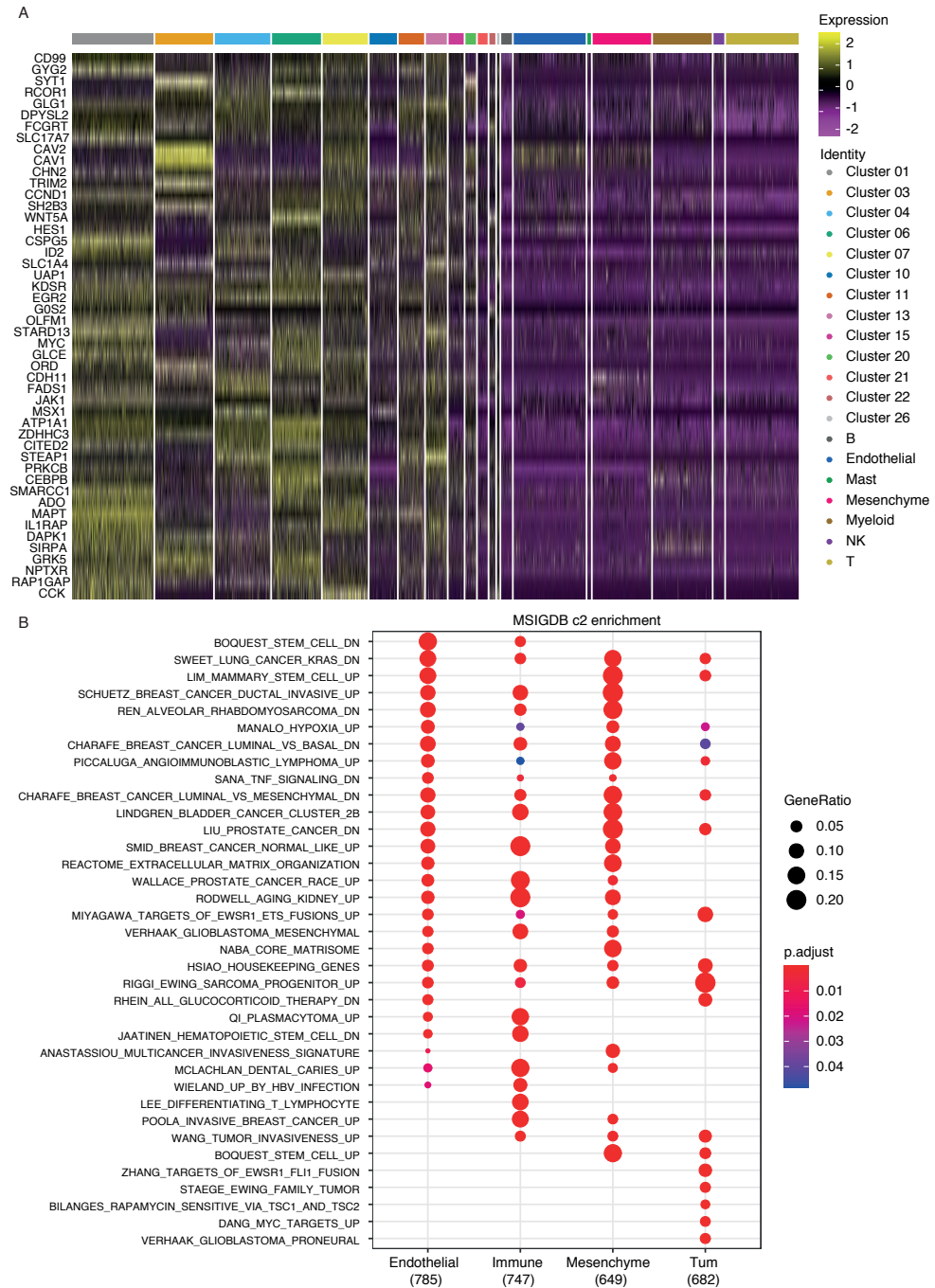
References

- Andersson, N., Bakker, B., Karlsson, J., Valind, A., Mengelbier, L. H., Spierings, D. C. J., Foijer, F., & Gisselsson, D. (2020). Extensive clonal branching shapes the evolutionary history of high-risk pediatric cancers. *Cancer Research*, 80(7), 1512–1523.
- Aran, D., Looney, A. P., Liu, L., Wu, E., Fong, V., Hsu, A., Chak, S., Naikawadi, R. P., Wolters, P. J., Abate, A. R., Butte, A. J., & Bhattacharya, M. (2019). Reference-based analysis of lung single-cell sequencing reveals a transitional profibrotic macrophage. *Nature Immunology*, 20(2), 163–172.
- Aynaud, M., Mirabeau, O., Gruel, N., Grossetête, S., Boeva, V., Durand, S., Surdez, D., Saulnier, O., Zaidi, S., Gribkova, S., Fouché, A., Kairov, U., Raynal, V., Tirode, F., Grünewald, T. G. P., Bohec, M., Baulande, S., Janoueix-Lerosey, I., Vert, J.-P., ... Zinovyev, A. (2020). Transcriptional Programs Define Intratumoral Heterogeneity of Ewing Sarcoma at Single-Cell Resolution. *Cell Reports*, 30(6), 1767–1779.e6.
- Binnewies, M., Muij, A. M., Pollack, J. L., Combes, A. J., Hardison, E. A., Barry, K. C., Tsui, J., Ruhland, M. K., Kersten, K., Abushawish, M. A., Spasic, M., Giurintano, J. P., Chan, V., Daud, A. I., Ha, P., Ye, C. J., Roberts, E. W., & Krummel, M. F. (2019). Unleashing Type-2 Dendritic Cells to Drive Protective Antitumor CD4+ T Cell Immunity. *Cell*, 177(3), 556–571.e16.
- Brouckaert, G., Kalai, M., Krysko, D. V., Saelens, X., Vercammen, D., Ndlovu, Matladi, Haegeman, G., D'Herde, K., & Vandenabeele, P. (2004). Phagocytosis of Necrotic Cells by Macrophages Is Phosphatidylserine Dependent and Does Not Induce Inflammatory Cytokine Production. *Molecular Biology of the Cell*, 15(3), 1089–1100.
- Butler, A., Hoffman, P., Smibert, P., Papalexi, E., & Satija, R. (2018). Integrating single-cell transcriptomic data across different conditions, technologies, and species. *Nature Biotechnology*, 36(5), 411–420.
- Candelli, T., Lijnzaad, P., Muraro, M. J., Kerstens, H., Oudenaarden, A. Van, Margaritis, T., & Holstege, F. (2018). Sharq A versatile preprocessing and QC pipeline for Single Cell RNA-seq. *BioRxiv* <https://doi.org/10.1101/250811>
- Cheng, L., Pandya, P. H., Liu, E., Chandra, P., Wang, L., Murray, M. E., Carter, J., Ferguson, M., Saadatza-deh, M. R., Bijangi-Visheshsaraei, K., Marshall, M., Li, L., Pollok, K. E., & Renbarger, J. L. (2019). Integration of genomic copy number variations and chemotherapy-response biomarkers in pediatric sarcoma. *BMC Medical Genomics*, 12(S1), 23.
- Cheng, S., Li, Z., Gao, R., Xing, B., Gao, Y., Yang, Y., Qin, S., Zhang, L., Ouyang, H., Du, P., Jiang, L., Zhang, B., Yang, Y., Wang, X., Ren, X., Bei, J. X., Hu, X., Bu, Z., Ji, J., & Zhang, Z. (2021). A pan-cancer single-cell transcriptional atlas of tumor infiltrating myeloid cells. *Cell*, 184(3), 792–809.e23.
- Durinck, S., Spellman, P. T., Birney, E., & Huber, W. (2009). Mapping identifiers for the integration of genomic datasets with the R/ Bioconductor package biomaRt. *Nature Protocols*, 4(8), 1184–1191.
- Engblom, C., Pfirschke, C., & Pittet, M. J. (2016). The role of myeloid cells in cancer therapies. *Nature Reviews Cancer*, 16(7), 447–462.
- Franzetti, G. A., Laud-Duval, K., Van Der Ent, W., Brisac, A., Irondele, M., Aubert, S., Dirksen, U., Bouvier, C., De Pinieux, G., Snaar-Jagalska, E., Chavrier, P., & Delattre, O. (2017). Cell-to-cell heterogeneity of EWSR1-FLI1 activity determines proliferation/migration choices in Ewing sarcoma cells. *Oncogene*, 36(25), 3505–3514.
- Grünewald, T. G. P., Cidre-Aranaz, F., Surdez, D., Tomazou, E. M., De Álava, E., Kovar, H., Sorensen, P. H., Delattre, O., & Dirksen, U. (2018). Ewing sarcoma. *Nature Reviews Disease Primers*, 4(5).
- Hafemeister, C., & Satija, R. (2019). Normalization and variance stabilization of single-cell RNA-seq data using regularized negative binomial regression. *Genome Biology*, 20(1), 1–15.
- Hanemaaijer, E. S., Margaritis, T., Sanders, K., Bos, F. L., Candelli, T., Al-Saati, H., van Noesel, M. M., Meyer-Wentrup, F. A. G., van de Wetering, M., Holstege, F. C. P., & Clevers, H. (2021). Single-cell atlas of developing murine adrenal gland reveals relation of Schwann cell precursor signature to neuroblastoma phenotype. *Proceedings of the National Academy of Sciences of the United States of America*, 118(5).
- Hashimshony, T., Senderovich, N., Avital, G., Klochendler, A., de Leeuw, Y., Anavy, L., Gennert, D., Li, S., Livak, K. J., Rozenblatt-Rosen, O., Dor, Y., Regev, A., & Yanai, I. (2016). CEL-Seq2: Sensitive highly-multiplexed single-cell RNA-Seq. *Genome Biology*, 17(1), 1–7.
- Hu-Lieskovan, S., Zhang, J., Wu, L., Shimada, H., Schofield, D. E., & Triche, T. J. (2005). EWS-FLI1 fusion protein up-regulates critical genes in neural crest development and is responsible for the observed phenotype of Ewing's family of tumors. *Cancer Research*, 65(11), 4633–4644.
- Jerby-Arnon, L., Shah, P., Cuoco, M. S., Rodman, C., Su, M. J., Melms, J. C., Leeson, R., Kanodia, A., Mei, S., Lin, J. R., Wang, S., Rabasha, B., Liu, D., Zhang, G., Margola, C., Ashenberg, O., Ott, P. A.,

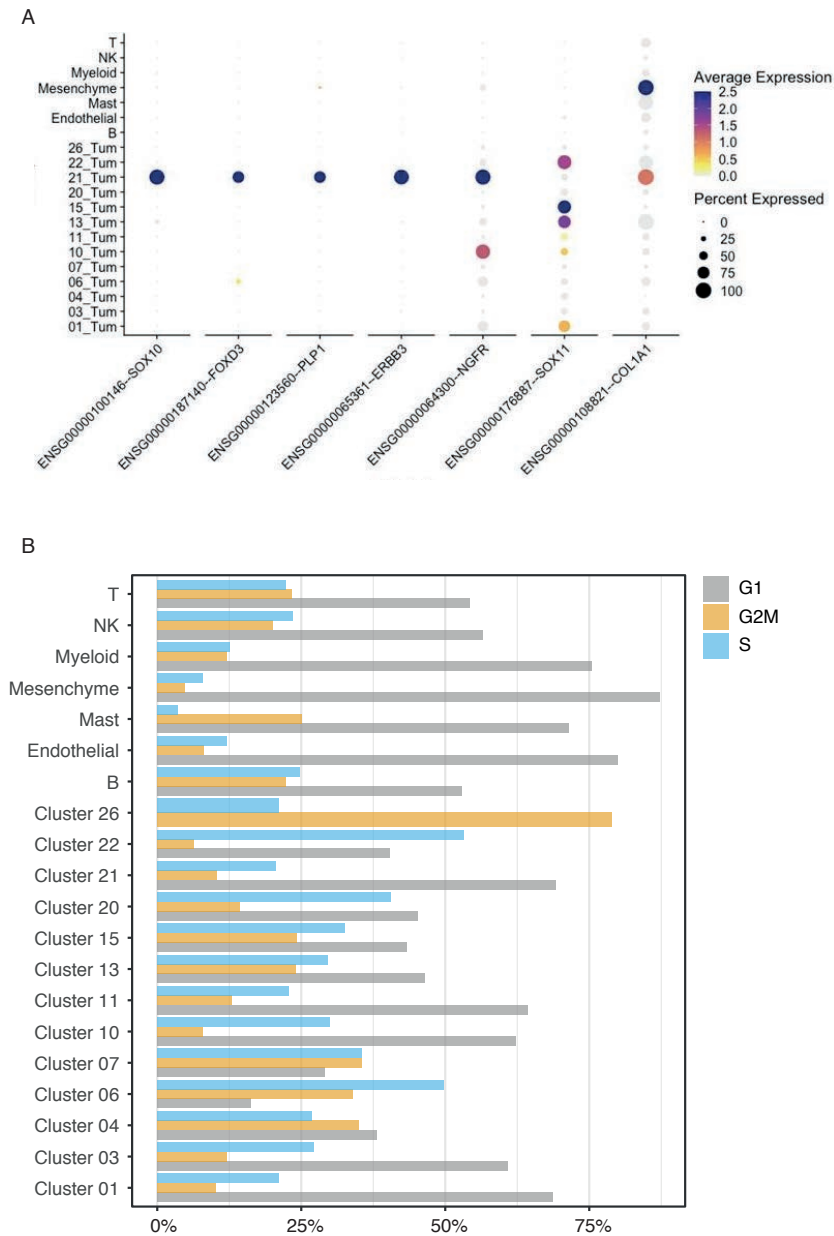
- Buchbinder, E. I., Haq, R., ... Regev, A. (2018). A Cancer Cell Program Promotes T Cell Exclusion and Resistance to Checkpoint Blockade. *Cell*, 175(4), 984-997.e24.
- Judge, S. J., Darrow, M. A., Thorpe, S. W., Gingrich, A. A., O'Donnell, E. F., Bellini, A. R., Sturgill, I. R., Vick, L. V., Dunai, C., Stoffel, K. M., Lyu, Y., Chen, S., Cho, M., Rebhun, R. B., Monjaze, A. M., Murphy, W. J., & Canter, R. J. (2020). Analysis of tumor-infiltrating NK and T cells highlights IL-15 stimulation and TIGIT blockade as a combination immunotherapy strategy for soft tissue sarcomas. *Journal for ImmunoTherapy of Cancer*, 8(2), 1-17.
- Kameneva, P., Artemov, A. V., Kastriti, M. E., Faure, L., Olsen, T. K., Otte, J., Erickson, A., Semsch, B., Andersson, E. R., Ratz, M., Frisén, J., Tischler, A. S., de Krijger, R. R., Boudierlique, T., Akkuratova, N., Vorontsova, M., Gusev, O., Fried, K., Sundström, E., ... Adameyko, I. (2021). Single-cell transcriptomics of human embryos identifies multiple sympathoblast lineages with potential implications for neuroblastoma origin. *Nature Genetics*, 53(5), 694-706.
- Keskin, T., Rucci, B., Cornaz-Buros, S., Martin, P., Fusco, C., Broye, L., Cisarova, K., Perez, E. M., Letovanec, I., La Rosa, S., Cherix, S., Diezi, M., Renella, R., Provero, P., Suvà, M. L., Stamenkovic, I., & Riggi, N. (2021). A live single-cell reporter assay links intratumor heterogeneity to metastatic proclivity in Ewing sarcoma. *Science Advances*, 7(27), eabf9394.
- Kovar, H., Alonso, J., Aman, P., Aryee, D. N. T., Ban, J., Burchill, S. A., Burdach, S., De Alava, E., Delattre, O., Dirksen, U., Fourtouna, A., Fulda, S., Helman, L. J., Herrero-Martin, D., Pancras, P. C., Kontny, U., Lawlor, E. R., Lessnick, S. L., Lombart-Bosch, A., ... Ladenstein, R. (2012). The first European interdisciplinary Ewing sarcoma research summit. *Frontiers in Oncology*, 2 MAY(May), 1-11.
- Kristeleit, R., Davidenko, I., Shirinkin, V., El-Khouly, F., Bondarenko, I., Goodheart, M. J., Gorbunova, V., Penning, C. A., Shi, J. G., Liu, X., Newton, R. C., Zhao, Y., Maleski, J., Leopold, L., & Schilder, R. J. (2017). A randomised, open-label, phase 2 study of the IDO1 inhibitor epacadostat (INCB024360) versus tamoxifen as therapy for biochemically recurrent (CA-125 relapse)-only epithelial ovarian cancer, primary peritoneal carcinoma, or fallopian tube cancer. *Gynecologic Oncology*, 146(3), 484-490.
- Le Deley, M. C., Paulussen, M., Lewis, I., Brennan, B., Ranft, A., Whelan, J., Le Teuff, G., Michon, J., Ladenstein, R., Marec-Bérard, P., Van Den Berg, H., Hjorth, L., Wheatley, K., Judson, I., Juergens, H., Craft, A., Oberlin, O., & Dirksen, U. (2014). Cyclophosphamide compared with ifosfamide in consolidation treatment of standard-risk Ewing sarcoma: Results of the randomized noninferiority Euro-EWING99-R1 trial. *Journal of Clinical Oncology*, 32(23), 2440-2448.
- Lee, H. W., Chung, W., Lee, H. O., Jeong, D. E., Jo, A., Lim, J. E., Hong, J. H., Nam, D. H., Jeong, B. C., Park, S. H., Joo, K. M., & Park, W. Y. (2020). Single-cell RNA sequencing reveals the tumor microenvironment and facilitates strategic choices to circumvent treatment failure in a chemorefractory bladder cancer patient. *Genome Medicine*, 12(1), 1-21.
- Liguori, M., Digifico, E., Vacchini, A., Avigni, R., Colombo, F. S., Borroni, E. M., Farina, F. M., Milanese, S., Castagna, A., Mannarino, L., Craparotta, I., Marchini, S., Erba, E., Panini, N., Tamborini, M., Rimoldi, V., Allavena, P., & Belgiovine, C. (2021). The soluble glycoprotein NMB (GPNMB) produced by macrophages induces cancer stemness and metastasis via CD44 and IL-33. *Cellular and Molecular Immunology*, 18(3), 711-722.
- Mabbott, N. A., Baillie, J. K., Brown, H., Freeman, T. C., & Hume, D. A. (2013). An expression atlas of human primary cells: Inference of gene function from coexpression networks. *BMC Genomics*, 14(1).
- Mellor, A. L., & Munn, D. H. (2004). IDO expression by dendritic cells: Tolerance and tryptophan catabolism. *Nature Reviews Immunology*, 4(10), 762-774.
- Mereu, E., Lafzi, A., Moutinho, C., Ziegenhain, C., McCarthy, D. J., Álvarez-Varela, A., Batlle, E., Sagar, Grün, D., Lau, J. K., Boutet, S. C., Sanada, C., Ooi, A., Jones, R. C., Kaihara, K., Brampton, C., Talaga, Y., Sasagawa, Y., Tanaka, K., ... Heyn, H. (2020). Benchmarking single-cell RNA-sequencing protocols for cell atlas projects. *Nature Biotechnology*, 38(6), 747-755.
- Morales, E., Olson, M., Iglesias, F., Dahiya, S., Luetkens, T., & Atanackovic, D. (2020). Role of immunotherapy in Ewing sarcoma. *Journal for ImmunoTherapy of Cancer*, 8(2), 1-16.
- Muraro, M. J., Dharmadhikari, G., Grün, D., Groen, N., Dielen, T., Jansen, E., van Gurp, L., Engelse, M. A., Carlotti, F., de Koning, E. J. P., & van Oudenaarden, A. (2016). A Single-Cell Transcriptome Atlas of the Human Pancreas. *Cell Systems*, 3(4), 385-394.e3.
- Riggi, N., Suvà, M. L., & Stamenkovic, I. (2021). Ewing's Sarcoma. *New England Journal of Medicine*, 384(2), 154-164.
- Riggi, N., Suvà, M. L., Suvà, D., Cironi, L., Provero, P., Tercier, S., Joseph, J. M., Stehle, J. C., Baumer, K., Kindler, V., & Stamenkovic, I. (2008). EWS-FLI-1 expression triggers a ewing's sarcoma initiation

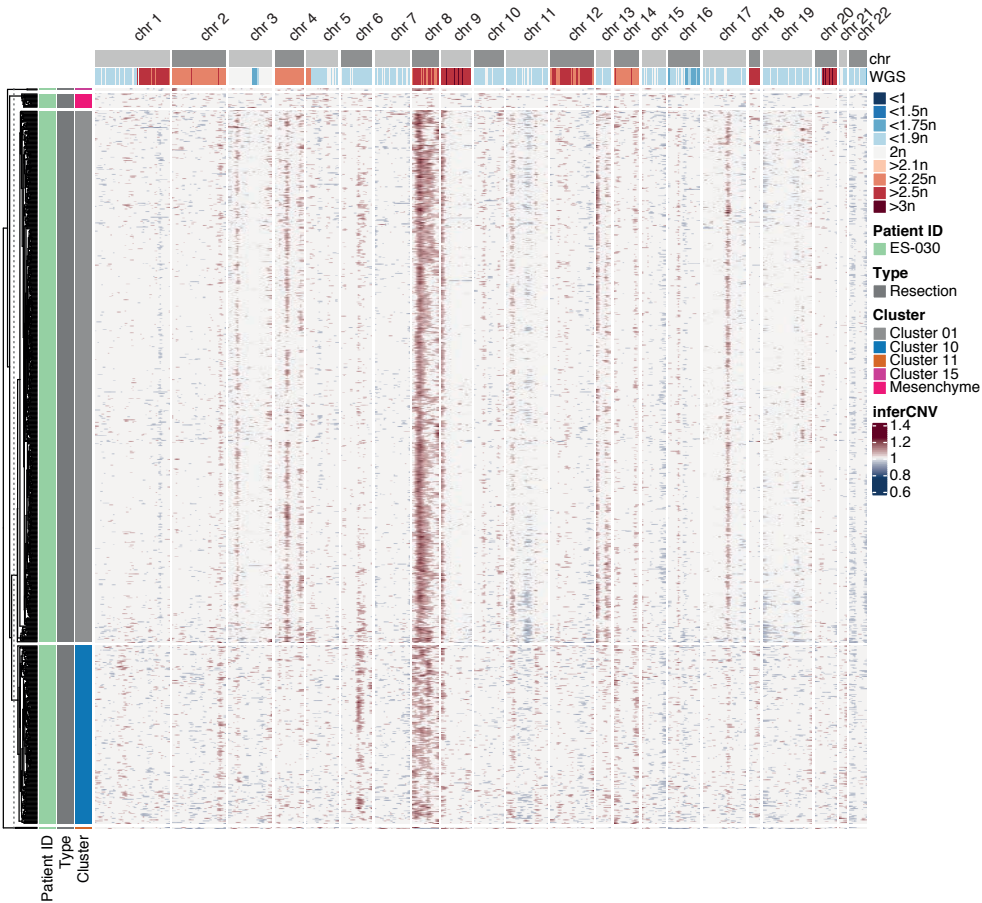
- program in primary human mesenchymal stem cells. *Cancer Research*, 68(7), 2176–2185.
- Rorie, C. J., Thomas, V. D., Chen, P., Pierce, H. H., O'Bryan, J. P., & Weissman, B. E. (2004). The Ews/Fli-1 Fusion Gene Switches the Differentiation Program of Neuroblastomas to Ewing Sarcoma/Peripheral Primitive Neuroectodermal Tumors. *Cancer Research*, 64(4), 1266–1277.
- Ross, K. A., Smyth, N. A., Murawski, C. D., & Kennedy, J. G. (2013). The biology of ewing sarcoma. *ISRN Oncology*, 2013(1), 759725.
- Soldatov, R., Kaucka, M., Kastriti, M. E., Petersen, J., Chontorotzea, T., Englmaier, L., Akkuratova, N., Yang, Y., Häring, M., Dyachuk, V., Bock, C., Farlik, M., Piacentino, M. L., Boismoreau, F., Hilscher, M. M., Yokota, C., Qian, X., Nilsson, M., Bronner, M. E., ... Adameyko, I. (2019). Spatiotemporal structure of cell fate decisions in murine neural crest. *Science*, 364(6444).
- Staeger, M. S., Hutter, C., Neumann, I., Foja, S., Hattenhorst, U. E., Hansen, G., Afar, D., & Burdach, S. E. G. (2004). DNA microarrays reveal relationship of Ewing family tumors to both endothelial and fetal neural crest-derived cells and define novel targets. *Cancer Research*, 64(22), 8213–8221.
- Suvà, M. L., Riggi, N., Stehle, J. C., Baumer, K., Tercier, S., Joseph, J. M., Suvà, D., Clément, V., Provero, P., Cironi, L., Osterheld, M. C., Guillou, L., & Stamenkovic, I. (2009). Identification of cancer stem cells in Ewing's sarcoma. *Cancer Research*, 69(5), 1776–1781.
- Tirosh, I., Izar, B., Prakadan, S. M., Wadsworth, M. H., Treacy, D., Trombetta, J. J., Rotem, A., Rodman, C., Lian, C., Murphy, G., Fallahi-Sichani, M., Dutton-Regeister, K., Lin, J. R., Cohen, O., Shah, P., Lu, D., Genshaft, A. S., Hughes, T. K., Ziegler, C. G. K., ... Garraway, L. A. (2016). Dissecting the multicellular ecosystem of metastatic melanoma by single-cell RNA-seq. *Science*, 352(6282), 189–196.
- Tirosh, I., Venteicher, A. S., Hebert, C., Escalante, L. E., Patel, A. P., Yizhak, K., Fisher, J. M., Rodman, C., Mount, C., Filbin, M. G., Neftel, C., Desai, N., Nyman, J., Izar, B., Luo, C. C., Francis, J. M., Patel, A. A., Onozato, M. L., Riggi, N., ... Suvà, M. L. (2016). Single-cell RNA-seq supports a developmental hierarchy in human oligodendroglioma. *Nature*, 539(7628), 309–313.
- Town, J., Pais, H., Harrison, S., Stead, L. F., Bataille, C., Bunjobpol, W., & Zhang, J. (2016). Exploring the surfaceome of Ewing sarcoma identifies a new and unique therapeutic target. *Proceedings of the National Academy of Sciences of the United States of America*, 113(1).
- von Levetzow, C., Jiang, X., Gwyne, Y., von Levetzow, G., Hung, L., Cooper, A., Hsu, J. H. R., & Lawlor, E. R. (2011). Modeling initiation of ewing sarcoma in human neural crest cells. *PLoS ONE*, 6(4), 1–10.
- Wang, D., DuBois, R. N., & Richmond, A. (2009). The role of chemokines in intestinal inflammation and cancer. *Current Opinion in Pharmacology*, 9(6), 688–696. <https://doi.org/10.1016/j.coph.2009.08.003>
- Wauters, E., Van Mol, P., Garg, A. D., Jansen, S., Van Herck, Y., Vanderbeke, L., Bassez, A., Boeckx, B., Malengier-Devlies, B., Timmerman, A., Van Brussel, T., Van Buyten, T., Schepers, R., Heylen, E., Dauwe, D., Doooms, C., Gunst, J., Hermans, G., Meersseman, P., ... Lambrechts, D. (2021). Discriminating mild from critical COVID-19 by innate and adaptive immune single-cell profiling of bronchoalveolar lavages. *Cell Research*, 31(3), 272–290.
- Wculek, S. K., Cueto, F. J., Mujal, A. M., Melero, I., Krummel, M. F., & Sancho, D. (2020). Dendritic cells in cancer immunology and immunotherapy. *Nature Reviews Immunology*, 20(1), 7–24.
- Yang, S., Corbett, S. E., Koga, Y., Wang, Z., Johnson, W. E., Yajima, M., & Campbell, J. D. (2020). Decontamination of ambient RNA in single-cell RNA-seq with DecontX. *Genome Biology*, 21(1), 57.
- Yu, G., Wang, L. G., Han, Y., & He, Q. Y. (2012). ClusterProfiler: An R package for comparing biological themes among gene clusters. *OMICS A Journal of Integrative Biology*, 16(5), 284–287.
- Zhou, Y., Yang, D., Yang, Q., Lv, X., Huang, W., Zhou, Z., Wang, Y., Zhang, Z., Yuan, T., Ding, X., Tang, L., Zhang, J., Yin, J., Huang, Y., Yu, W., Wang, Y., Zhou, C., Su, Y., He, A., ... Hu, H. (2020). Single-cell RNA landscape of intratumoral heterogeneity and immunosuppressive microenvironment in advanced osteosarcoma. *Nature Communications*, 11(1), 1–17.

Supplemental figures

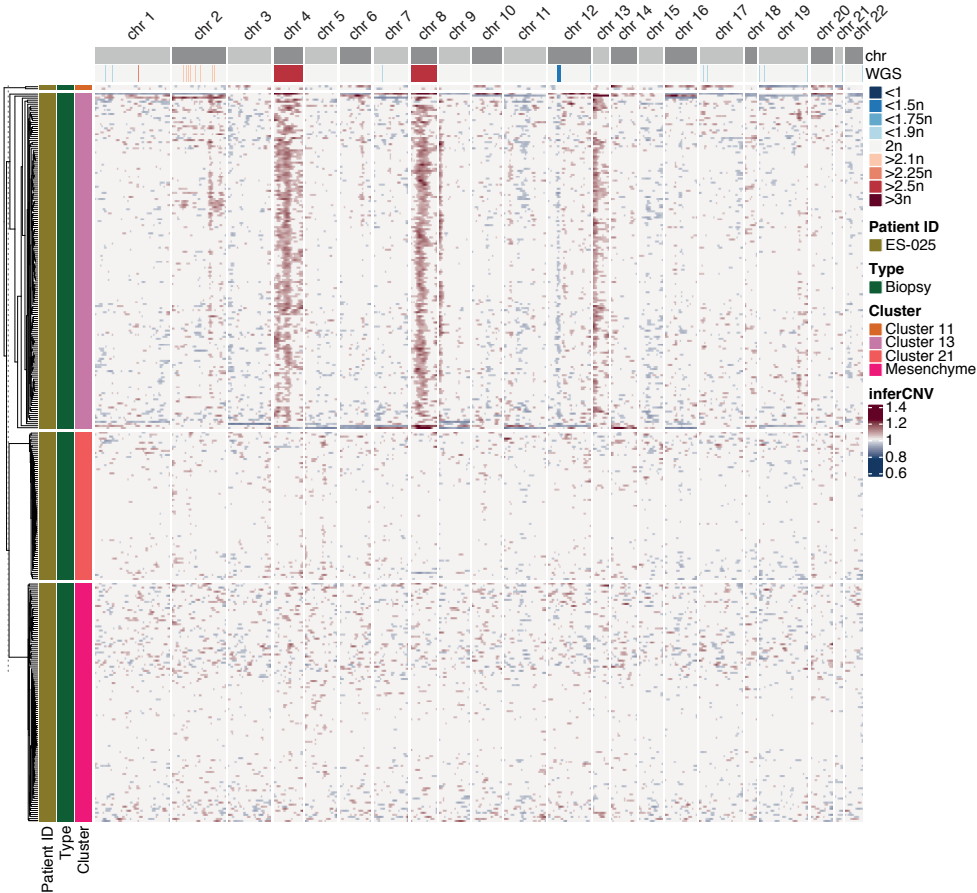


Supplemental figure 1: Identification Ewing sarcoma tumor cells clusters. A) Heatmap depicting expression of Ewing-associated genes, based on Hu-Lieskovan *et al.* (Hu-Lieskovan *et al.*, 2005) in tumor- and healthy cell populations. B) Dot plot depicting enrichment scores of tumor- and healthy cell populations to publicly available signatures from Molecular Signature Database (MSigDB-c2). The enrichments were calculated using the `compareCluster` function from the `clusterProfiler` R package (Yu *et al.*, 2012).

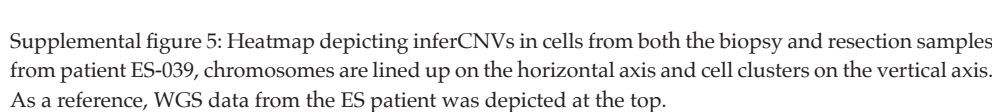


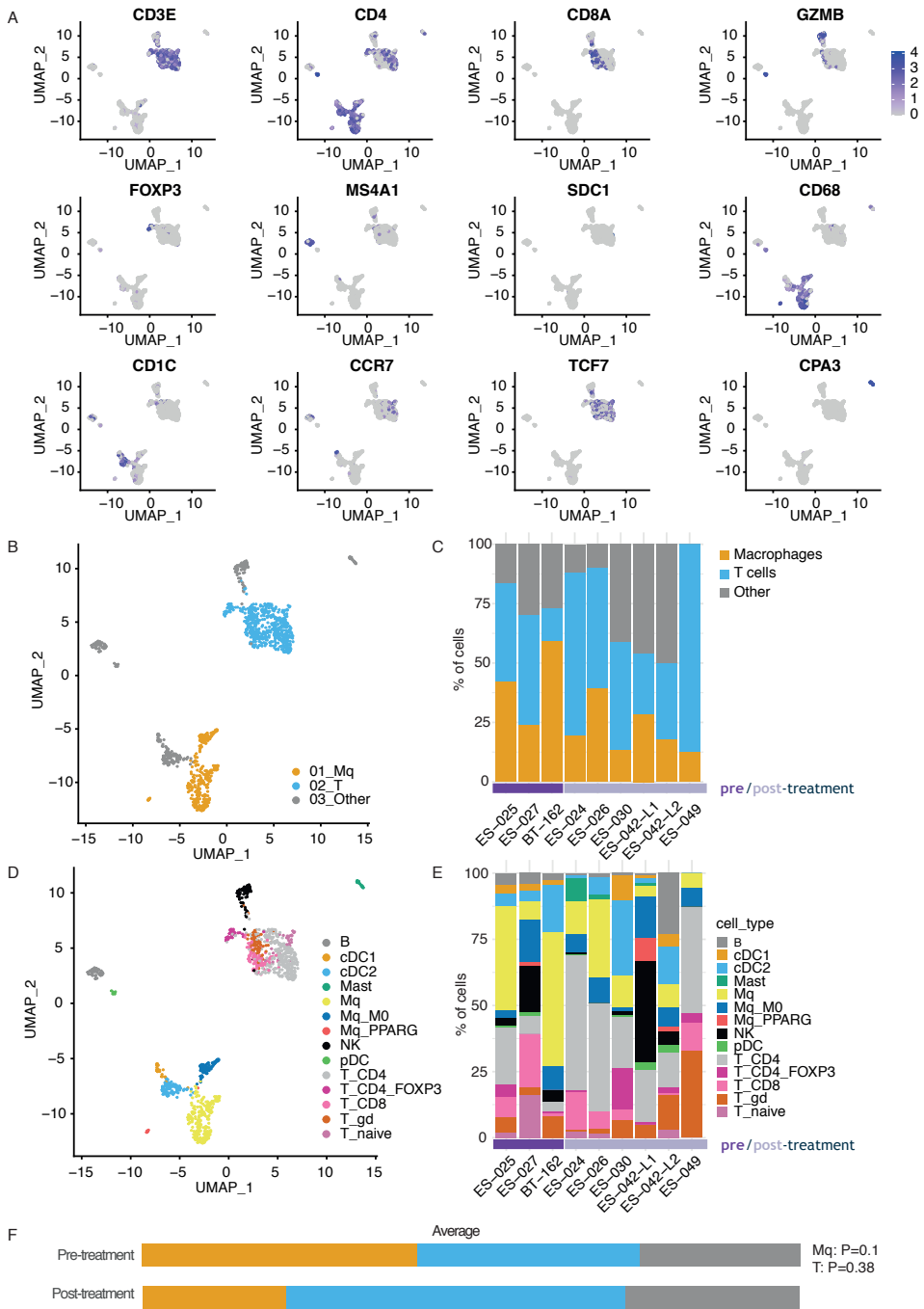


Supplemental figure 3: Heatmap depicting inferCNVs in the cells of a resection sample of patient ES-030, chromosomes are lined up on the horizontal axis and cell clusters on the vertical axis. As a reference, WGS data from the ES patient was depicted at the top.

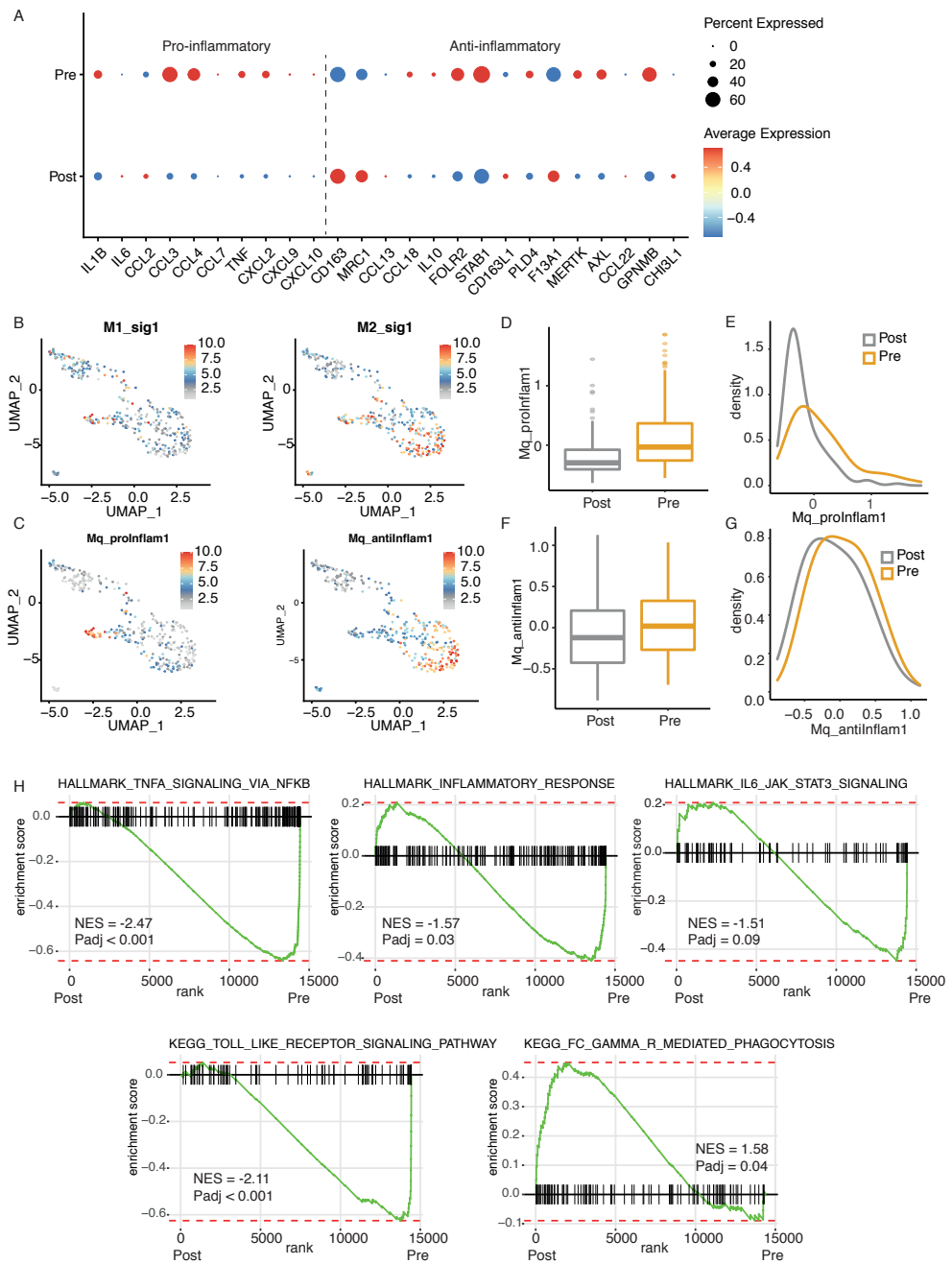


Supplemental figure 4: Heatmap depicting inferCNVs in the cells coming from a biopsy sample of patient ES-025, chromosomes are lined up on the horizontal axis and cell clusters on the vertical axis. As a reference, WGS data from the ES patient was depicted at the top.

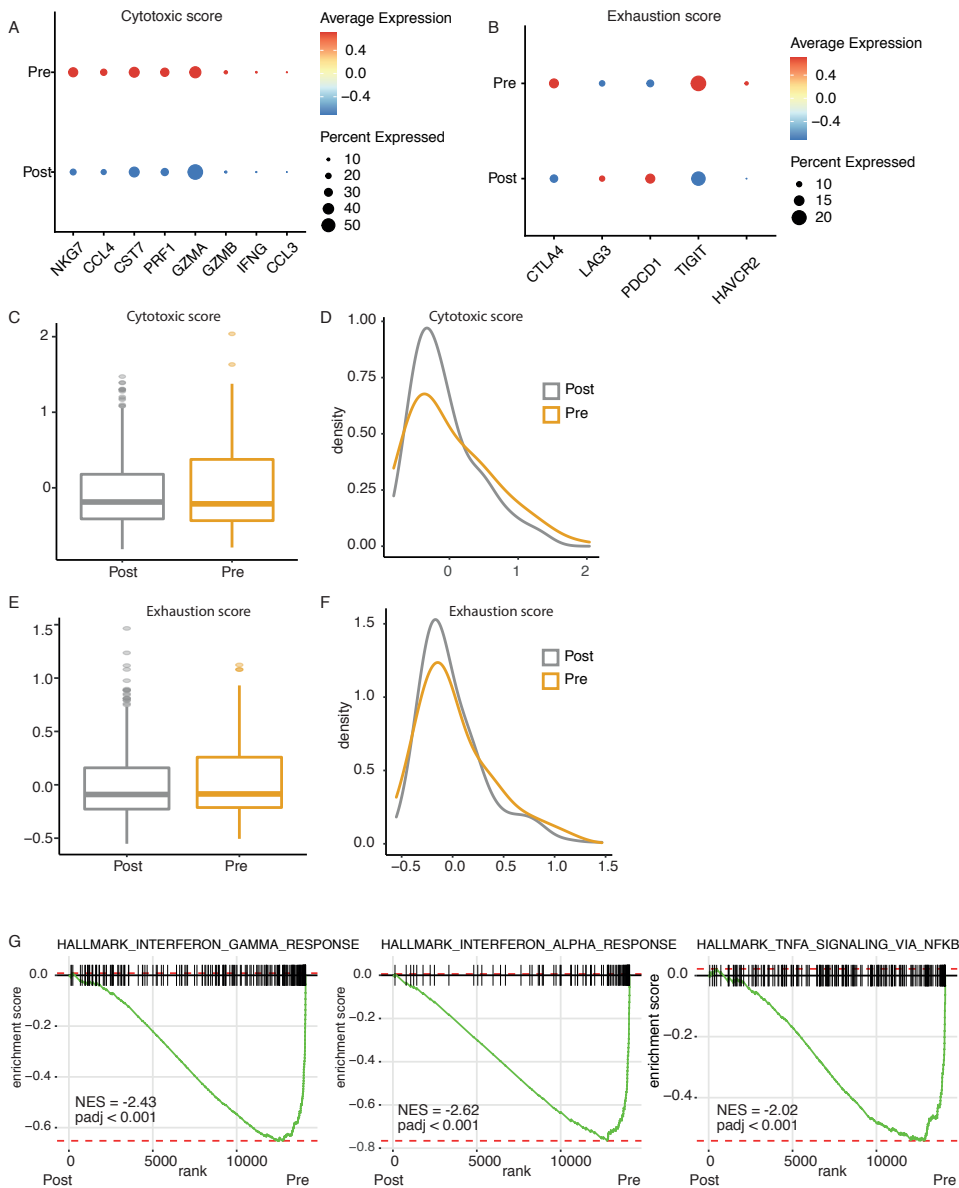




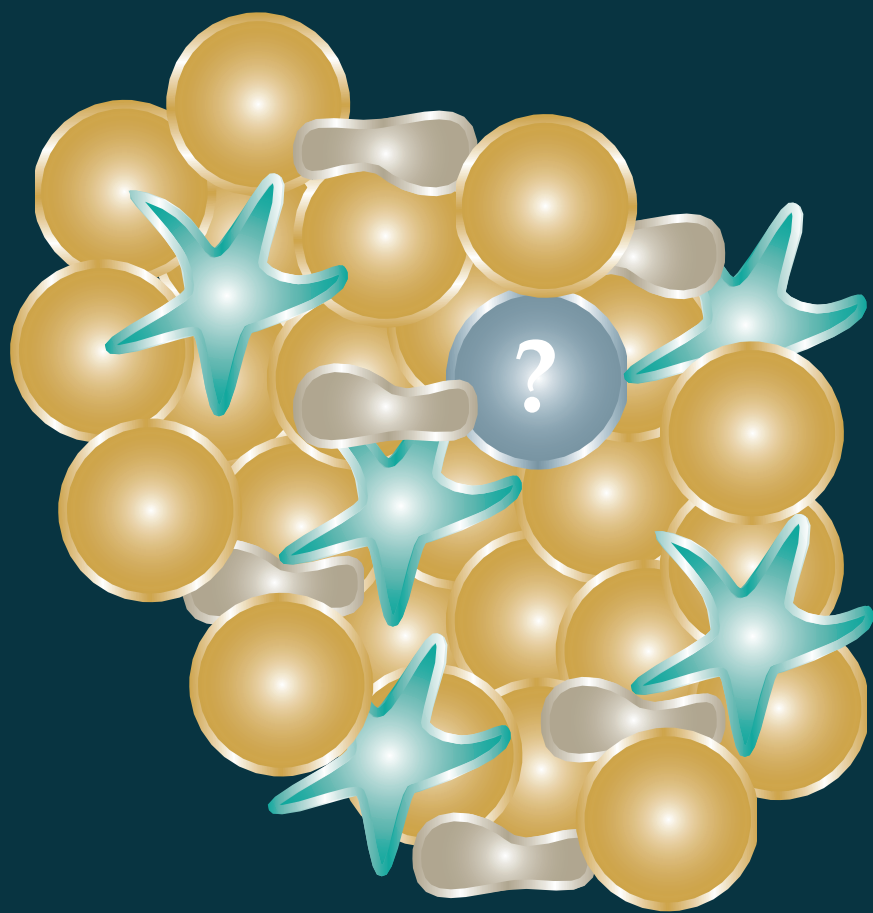
Supplemental figure 6: Immune cell composition in treatment-naïve and treatment-exposed Ewing sarcoma samples. A) UMAPs depicting immune cell marker expression B) UMAP depicting immune cell clusters. C) Bar plot depicting contribution of immune cell populations to pre- and post-treatment Ewing sarcoma samples. D) UMAP depicting immune cell subclusters. E) Bar plot depicting contribution of immune cell subpopulations to pre- and post-treatment Ewing sarcoma samples.



Supplemental figure 7: Pro-inflammatory M1 signature and anti-inflammatory M2 signature expression in macrophage populations pre- and post- treatment. A) Dot plot depicting marker expression of pro-inflammatory and anti-inflammatory scores in pre- versus post-treatment samples. B) UMAPS depicting expression of M1- and M2-signature in macrophages. C) UMAPS depicting expression of pro- and anti-inflammatory scores in macrophages. D) Box plot depicting pro-inflammatory score in post- versus pre-treatment samples. E) Graph depicting distribution of the pro-inflammatory score in post- versus pre-treatment samples. F) Box plot depicting anti-inflammatory score in post- versus pre-treatment samples. G) Graph depicting distribution of the anti-inflammatory score in post- versus pre-treatment samples. H) Graphs depicting enrichment scores of signaling pathway activities in post- vs pre-treatment samples.



Supplemental figure 8: Cytotoxic and exhaustion module scores of effector T-cells in pre- vs post-treatment samples. A) Dot plot depicting gene expression of genes involved in the cytotoxic module score. B) Dot plot depicting gene expression of genes involved in the exhaustion module score. C) Box plot depicting cytotoxic module score in effector T-cells from post- vs pre-treatment samples. D) Graph depicting distribution of cytotoxic module score in effector T-cells from post- vs pre-treatment samples. E) Box plot depicting exhaustion module score in effector T-cells from post- vs pre-treatment samples. F) Graph depicting distribution of exhaustion module score in effector T-cells from post- vs pre-treatment samples. G) Graphs depicting gene set enrichment analysis on pre-ranked differentially expressed genes using the R package Fast Gene Set Enrichment Analysis (fgsea, version 1.14.0) and Molecular Signature Database (MsigDB version 7.2), comparing post- vs pre-treatment samples.



Chapter 6

General Discussion

Margit Bleijs¹

1. Oncode Institute, Princess Maxima Center for Pediatric Oncology,
Utrecht, The Netherlands

Introduction

In the Netherlands, 650 children are diagnosed with pediatric cancer each year. Due to the discovery of chemotherapy in the past century the cure rate of these pediatric cancers has increased to 75% (DeVita & Chu, 2008; Saletta *et al*, 2014). However, still 1 out of 4 children diagnosed with pediatric cancer cannot yet be cured, underlining the need for better understanding of cancer initiation and progression in children to develop effective treatment options. Preclinical cancer models are essential to study the mechanisms driving tumor progression and to explore therapies that can affect tumor growth and survival (Bleijns *et al*, 2019). In this thesis, we have reviewed the promises and challenges of different preclinical models in cancer research (**chapter 2**). Additionally, we have described the establishment of preclinical *in vitro* models of Ewing sarcoma (**chapter 3**) and an Ewing-like desmoplastic small round cell tumor (DSRCT) (**chapter 4**). These *in vitro* models allowed for compound screens to explore therapeutic options and for investigating the molecular mechanisms driving tumor growth. Moreover, we have described the single cell architecture of primary Ewing sarcoma tissue (**chapter 5**), which reveals intra-tumor heterogeneity and subclonal genetic evolution. Furthermore, we have characterized the immune cell composition in Ewing sarcoma and explored the expression of potentially targetable immune checkpoint molecules. Inhibition of immune checkpoint molecules could overcome the immune-suppressive tumor microenvironment (TME) in a subset of Ewing sarcoma patients. Together, the studies described in this thesis contribute to a better understanding of mechanisms driving rare pediatric solid tumors and to explore therapeutic approaches. In this chapter, the promises and challenges of the preclinical approaches used in this thesis are discussed, including patient-derived tumor organoid (PDO) *in vitro* models, compounds screens and single cell RNA sequencing.

The limitations of *in vitro* model systems

Most *in vitro* preclinical studies are based on established 2D cell lines. While established cell lines have provided valuable insights on tumor development and mechanisms of therapeutic actions (Sos *et al*, 2009; Greshock *et al*, 2010), they are unable to recapitulate the complexity of the tumor architecture. Cell lines lack both the phenotypic and genetic heterogeneity found in the original tumors. Recently, 3D PDO *in vitro* models have shown promising results in recapitulating the architecture of the tumor tissue they derived from (Huang *et al*, 2015; van de Wetering *et al*, 2015; Nanki *et al*, 2018; Sachs *et al*, 2018; Yan *et al*, 2018). Additionally, PDO models allow for the generation of a living biobank as they can be expanded indefinitely and cryopreserved. Organoid models can be established with a great success rate from epithelial tissues and carcinomas since the required environmental factors in epithelial stem cell niches are well studied (Kretzschmar & Clevers, 2016). This allows the mimicking of the stem cell niche *in vitro* by addition of the appropriate growth factors. Successful establishment of carcinoma PDO models and organoids derived from

their healthy epithelial counterparts are highly valuable for exploring therapeutic options that affects tumor cell viability without affecting the healthy epithelial cells (van de Wetering *et al*, 2015).

While adult cancers are mostly carcinomas and epithelial in origin, pediatric cancers often include leukemias and solid tumors. Establishment of PDO models from solid tumors remains challenging, hampering preclinical research. Additionally, the cell-of-origin and its environmental factors remain unknown for many pediatric cancers. Which makes it challenging to identify the appropriate growth factors required in the culture medium composition to initiate PDO growth *in vitro*. The lack of knowledge on the cell-of-origin of Ewing sarcoma and Ewing-like sarcomas also makes it impossible to establish *in vitro* cultures of healthy counterparts from which solid tumors arise.

Besides the addition of growth factors in the culture medium to mimic the original microenvironment, cells themselves also excrete soluble factors and extracellular vesicles to communicate and stimulate growth (Vis *et al*, 2020). Therefore, when culture medium is exchanged important secreted components by the cells are removed and cells need to recover their auto- and paracrine communication. Hence, the culture medium of PDO *in vitro* models has to be refreshed only partially to limit the disturbance of essential cell-cell communication. Additionally, it is key that cells are seeded in the right density to allow them to create the correct concentrations of their own microenvironmental factors. Additionally, previous studies show that cell-densities *in vitro* can affect cell responses to compounds as well as intracellular trafficking by lipid composition changes (Vital-Reyes *et al*, 2006; Kavaliauskiene *et al*, 2014).

Another major challenge of establishing PDO *in vitro* models is to remain the heterogeneity of cells present in the original tumor, considering that selective pressure is inevitable in all preclinical models (Bleijs *et al*, 2019). Cultured tumor cells that have a faster cell cycle rate have a growth advantage *in vitro*. Differences in cell cycle rates of *in vitro* models can affect the response to cytotoxic compounds that target cell cycle mechanisms, such as DNA replication. While *in vitro* PDO cultures acquire a higher cell cycle rate, they subsequently accumulate genetic mutations faster. Considering that genomic mutations that arise during DNA replication are unavoidable (Tomasetti & Vogelstein, 2015), these *in vitro* preclinical models might deviate from their original tumor tissue. Genetic aberrations also accumulate during tumor progression in the patient. For example, an increase in genetic aberrations often occurs upon exposure to chemotherapy (Cheng *et al*, 2019). However, in **chapter 5** we have shown that subclonal genetic events can also occur during Ewing sarcoma tumorigenesis in treatment-naïve patients. In Ewing sarcoma patients the genetic subclonal evolution includes copy number variations (CNVs), such as the frequently-observed gains in chromosome 1q, 2q, and 8 (Grünwald *et al*, 2018), rather than single base substitutions that leave a mutational footprint. A previous study shows that increased mutation rates in human pluripotent and adult stem cells as a conse-

quence of *in vitro* culturing leaves a mutational footprint related to oxidative stress (Kuijk *et al*, 2020). Indicating that the mutational profile accumulated *in vitro* differs from the genetic aberrations during tumor progression in the patient. This might result in different responses to therapeutic compounds.

The low number of PDTO models of pediatric sarcomas indicate the difficulty of *in vitro* establishment. Apart from our OV-054 DSRCT *in vitro* model, only two other *in vitro* models have been published (Nishio *et al*, 2002; Gedminas *et al*, 2020; Markides *et al*, 2013). The fact that so few DSRCT tumors were able to expand *in vitro*, suggests that the essential surrounding growth factors are still unknown. The DSRCT models that were able to expand *in vitro* likely harbor underlying genetic events that allow the cells to grow independent of their microenvironmental factors in culture. Apart from the *EWS-WT1* fusion driver event, secondary genomic alterations are rarely described for DSRCTs. However, a recent study performed genomic profiling on a cohort of 83 DSRCT patients. They observed recurrent secondary somatic alterations in *FGFR4*, *ARID1A*, *TP53*, *MSH3*, and *MLL3* in 82% of the DSRCT patients (Chow *et al*, 2020). This percentage of secondary events is significantly greater than previously reported (Jiang *et al*, 2014; Bulbul *et al*, 2017) and might have both prognostic and therapeutic implications. Further genetic studies are needed to investigate whether these secondary genomic alterations in DSRCT patients enable the tumor cells to expand independent of their microenvironmental factors. This could give insights on mechanisms driving DSRCT progression and subsequently might increase the success rate of *in vitro* model establishment of this rare sarcoma type.

While PDTO models cannot reflect the full complexity of the tumor composition as they lack critical components of the TME, including tumor-stroma interactions and the vasculature, these model systems are a promising tool for several translational applications, including personalized compound screens, as reviewed in **chapter 2**.

Promises and challenges of drug screens and clinical trials

Preclinical anti-cancer agents that enter clinical trials frequently fail to acquire regulatory approval due to insufficient safety or inefficacy. This indicates a limited predictive value of current preclinical models. Moreover, unsuccessful chemotherapy is often the result of drug resistance and is a major cause of mortality (de Groot *et al*, 2020). In the medium-throughput compound screens performed on Ewing sarcoma and DSRCT PDTO models, described in **chapter 3** and **chapter 4**, a panel of 201 single compounds are tested. These compound screens can indicate whether targeted drugs are effective in the killing of tumor cells. Additionally, these screening results give insights in important signaling pathways that likely regulate tumor progression. For example, receptor tyrosine kinase (RTK) driven signaling pathways seem to be important for DSRCT cell expansion (**chapter 4**). However, these single compound screens cannot predict whether multiple compounds work synergisti-

cally and strengthen their effect or whether combinations of compounds inhibit the desired effect. A previous study explored combination therapies for several organoid lines and identified unique drug combinations for individual patients with a uterine carcinosarcoma (Pauli *et al*, 2017). For example, they showed that HDAC inhibitor Vorinostat sensitized the PDTO *in vitro* model of one patient to PI3K inhibitors, including Buparlisib. Additionally, a combination screen indicated that Buparlisib sensitized the PDTO *in vitro* model from another patient to two HDAC inhibitors, Vorinostat and Belinostat, and to the PARP inhibitor Olaparib (Pauli *et al*, 2017). These results show the importance of exploring the effect of drug combinations in a patient-specific manner to enhance the clinical response. Further research on Ewing sarcoma and Ewing-like sarcoma *in vitro* preclinical models is needed to explore the effect of combination therapies in a personalized manner. Additionally, as discussed in **chapter 2**, the combination of high-throughput screens using PDTO *in vitro* models and validation of compounds in patient-derived tumor xenograft (PDTX) *in vivo* models can greatly improve the prediction of clinical responses to therapeutic approaches.

Clinical trials involving children face several challenges, including the small numbers of children eligible for entering trials, the low prevalence of many childhood diseases and ethical concerns. As a consequence of the lack of specific trial-based data in children results are commonly extrapolated from studies in adults. However, children have a different range of diseases and metabolize medical compounds differently, resulting in unpredictable clinical responses (Caldwell *et al*, 2004; Joseph *et al*, 2015). Approximately two thirds of all medications often prescribed for children have insufficient evidence regarding dosing, safety, and efficacy (Martinez-Castaldi *et al*, 2008). Fortunately, the need for clinical trials in children has been increasingly recognized by the scientific community as it resulted in significant improvements in their health care. As a result of clinical trials, the 5-year overall survival of childhood acute lymphoblastic leukemia improved from 25% to more than 70% (Chessells, 1992; Caldwell *et al*, 2004). Increased recognition lead to new legislation in some countries making trials of therapeutic approaches mandatory in children as well as adults before these are approved in the clinic (Caldwell *et al*, 2004). Currently, almost 300 clinical trials that include Ewing sarcoma patients are listed in the clinical trial database (<https://clinicaltrials.gov>), which indicates the improving efforts in exploring therapeutic options specific for rare pediatric sarcomas.

Caveats of single cell RNA sequencing

Single cell RNA sequencing adds remarkable resolution to cell biology research compared to traditional bulk sequencing, which reflects the average gene expression across thousands of cells. Single cell transcriptomics has been applied to various human tissues and cancers (Grün *et al*, 2015; Muraro *et al*, 2016; Zhou *et al*, 2020). Individual sequenced transcriptomes can be grouped and linked to specific cell types. Thereby, gene expression patterns of each cell type can be explored without contam-

ination from other cell types. This method allows for the discovery of meaningful cell-to-cell gene expression variability, which is very different from bulk sequencing. With traditional bulk sequencing, thousands of cells are pooled and analyzed as one. Consequently, the most prevalent cell type will dominate the data. Using single cell transcriptomics, each individual cell can potentially be identified as a separate cell type. This way, rare cell populations can be detected, which would otherwise go undetected between the thousands of different cells that surround them.

However, there are also limitations to the single cell sequencing technique. For example, the low quantities of starting material. A mammalian cell contains 50 picogram of total RNA, of which only 1 % (50 nanogram) is mRNA. Additionally, the conversion of mRNA to cDNA is never 100% efficient, thereby lowly expressed genes can be entirely lost from a cell. This often affects transcription factors that are expressed in low levels (Muraro *et al*, 2016). Moreover, annotating cell populations can be challenging. Clusters of cells can be linked to specific cell types by comparing their transcription profiles with datasets of known cell types or by looking at marker gene expression. This works well for healthy cell types, such as endothelial-, immune-, and mesenchymal cells. However, for cancer cells that lack specific markers this becomes more difficult. Ewing sarcoma and Ewing-like sarcoma cells are currently identified by the expression of their driving fusion gene. Apart from this fusion gene they lack specific markers that differentiate them from healthy cell types. During the PCR amplification step of the fragments, only the barcoded 3'-end fragments are amplified and subsequently paired-end sequenced. Therefore, only the *FLI1* part of the *EWS-FLI1* fusion transcripts are picked up with our single cell RNA sequencing approach, which makes it impossible to detect expression of the fusion gene. This complicates the annotation of Ewing tumor cells. Due to these limitations identification of Ewing tumor cell clusters relies on the expression of *EWS-FLI1* candidate target genes and/or the presence of copy number variations (CNVs).

While single cell RNA sequencing has some caveats, it allows to dissect the tumor architecture with great resolution. This allows to find tumor subpopulations that have not been described before, such as the small subpopulations of tumor cells in patient ES-025, described in **chapter 5**, that lack the CNVs observed in most of the cells from this patient and show a striking resemblance to neural crest derived Schwann cell precursor (SCP) cells. This could be an early Ewing sarcoma cell population that does not harbor CNVs yet, indicating that Ewing sarcomas could originate from early neural-crest derivatives.

The unidentified cell-of-origin of Ewing sarcoma

The origin of Ewing sarcoma remains a matter of debate. In general, Ewing sarcoma cells are characterized with neuroectodermal characteristics. Therefore, Ewing sarcoma was thought to be derived from early neural-crest cells. This is consistent with the striking resemblance of Ewing sarcoma cells to early neural-crest derivatives that we observed in **chapter 5**. Introduction of *EWS-FLI1* expression in neuroblas-

toma cells changes their differentiation program to Ewing sarcoma tumors (Rorie *et al*, 2004). Indicating that Ewing sarcoma could indeed be derived from neural-crest derivatives. Other studies, however, show evidence of a mesenchymal origin of Ewing sarcoma (Tirode *et al*, 2007). As introduction of *EWS-FLI1* expression in primary human mesenchymal stem cells induces a gene expression profile with remarkable similarity to that of Ewing sarcomas (Riggi *et al*, 2008). This may recapitulate the initial steps of Ewing sarcoma development. In our data, described in **chapter 5**, the expression profile of Ewing sarcoma cell clusters resembled various neural-crest derivatives, including sympathoblast cells, chromaffin cells, and melanocytes (Kamenova *et al*, 2021). The lineage specification of neural-crest cells towards melanocytes occurs earlier in development than the lineage specification towards neurons and mesenchymal progenitors (Soldatov *et al*, 2019), suggesting that the Ewing sarcoma cell-of-origin could be an early neural-crest cell that gets stuck in development. Moreover, one of the markers of the neural-crest derived mesenchymal lineage in mouse is *Fli1* (Soldatov *et al*, 2019). Therefore, the genomic translocation resulting in the *EWS-FLI1* fusion gene may interfere with differentiation of neural-crest cells towards mesenchymal progenitors.

Ewing sarcoma mostly occurs in adolescence during the growth spurt and is often seen in athletic children and young adults. Therefore, symptoms are frequently mistaken for growth pain or sports injuries. It could be that neural-crest derivatives that normally lay dormant after migration throughout the body during embryonic development get activated upon injury during the growth spurt. If these cells acquire the oncogenic *EWS-FLI1* translocation they might transform and become Ewing sarcoma cells. However, we cannot exclude the hypothesis that mesenchymal stem cells that acquire the *EWS-FLI1* fusion can dedifferentiate and transform towards neural-crest-like Ewing sarcoma cells. Further research is therefore needed to investigate the true cell-of-origin of Ewing sarcoma.

Future perspective

The establishment of PDTO *in vitro* models of rare pediatric sarcomas, including Ewing sarcoma and Ewing-like sarcomas, is of high value for preclinical research. As these models allow for compound screening, they can predict clinical responses to therapeutic compounds in a personalized manner. Additionally, they allow for investigating into the molecular functions of the fusion genes driving these sarcomas and shed light on the mechanisms of tumor progression. Not only Ewing sarcoma and DSRCT are driven by a genomic translocation resulting in a fusion gene, as a variety of other rare pediatric sarcoma types are also characterized by fusion genes, including *BCOR*-fusion driven sarcomas, *CIC-DUX4* fusion driven sarcomas, and *PAX3/7-FOXO1* fusion driven rhabdomyosarcomas (Sbaraglia *et al*, 2020). All these fusion genes activate their specific target genes and signaling pathways essential for initiation and progression of different types of sarcomas. Identifying the molecular functions of different fusion genes can help to find effective targeted therapies for

specific pediatric sarcoma types.

Additionally, state-of-the-art techniques, such as whole genome sequencing (WGS) and RNA sequencing of primary tumor tissue enable the identification of molecular therapeutic targets for personalized treatment options (Tilburg *et al*, 2021). Moreover, with single cell RNA sequencing of primary tumor tissue rare cell types can be identified, for example a cancer stem cell population that is resistant for chemotherapy and responsible for tumor recurrence. Also, different cell types within the TME supporting tumor growth can be identified, like immune cells. In **chapter 5** we showed that a subset of T cells in the Ewing sarcoma TME presents with an immune-suppressive cell state that support tumor growth. These T cells express immune checkpoint molecules including *CTLA4* and *TIGIT*, which can be targeted by immune checkpoint inhibitors (Judge *et al*, 2020).

In conclusion, the studies described in this thesis improve preclinical studies of pediatric sarcomas. The preclinical *in vitro* models show the potential to identify molecules and pathways essential for tumor cell expansion and can predict the clinical response of targeted treatments. Establishment of preclinical *in vitro* models of a larger cohort, including all different types of rare pediatric sarcomas will benefit personalized patient care.

References

- Bleijns M, Wetering M, Clevers H & Drost J (2019) Xenograft and organoid model systems in cancer research. *EMBO J* 38: 1–11
- Bulbul A, Fahy BN, Xiu J, Rashad S, Mustafa A, Husain H & Hayes-Jordan A (2017) Desmoplastic Small Round Blue Cell Tumor: A Review of Treatment and Potential Therapeutic Genomic Alterations. *Sarcoma* 2017: 1–12
- Caldwell PHY, Murphy SB, Butow PN & Craig JC (2004) Clinical trials in children. *Lancet* 364: 803–811
- Cheng L, Pandya PH, Liu E, Chandra P, Wang L, Murray ME, Carter J, Ferguson M, Saadatzaheh MR, Bijangi-Visheshsaraei K, et al (2019) Integration of genomic copy number variations and chemotherapy-response biomarkers in pediatric sarcoma. *BMC Med Genomics* 12: 23
- Chessells JM (1992) Treatment of childhood acute lymphoblastic leukaemia: Present issues and future prospects. *Blood Rev* 6: 193–203
- Chow WA, Yee JK, Tsark W, Wu X, Qin H, Guan M, Ross JS, Ali SM & Millis SZ (2020) Recurrent secondary genomic alterations in desmoplastic small round cell tumors. *BMC Med Genet* 21: 1–8
- DeVita VT & Chu E (2008) A history of cancer chemotherapy. *Cancer Res* 68: 8643–8653
- Gedminas JM, Chasse MH, McBairty M, Beddows I, Kitchen-Goosen SM & Grohar PJ (2020) Desmoplastic small round cell tumor is dependent on the EWS-WT1 transcription factor. *Oncogenesis* 9: 1–8
- Greshock J, Bachman KE, Degenhardt YY, Jing J, Wen YH, Eastman S, McNeil E, Moy C, Wegrzyn R, Auger K, et al (2010) Molecular target class is predictive of in vitro response profile. *Cancer Res* 70: 3677–3686
- de Groot S, Röttgering B, Gelderblom H, Pijl H, Suzhai K & Kroep JR (2020) Unraveling the resistance of igf-pathway inhibition in ewing sarcoma. *Cancers (Basel)* 12: 1–18
- Grün D, Lyubimova A, Kester L, Wiebrands K, Basak O, Sasaki N, Clevers H & Van Oudenaarden A (2015) Single-cell messenger RNA sequencing reveals rare intestinal cell types. *Nature* 525: 251–255
- Grünewald TGP, Cidre-Aranaz F, Surdez D, Tomazou EM, De Álava E, Kovar H, Sorensen PH, Delattre O & Dirksen U (2018) Ewing sarcoma. *Nat Rev Dis Prim* 4
- Huang L, Holtzinger A, Jagan I, Begora M, Lohse I, Ngai N, Nostro C, Wang R, Muthuswamy LB, Crawford HC, et al (2015) Ductal pancreatic cancer modeling and drug screening using human pluripotent stem cell- and patient-derived tumor organoids. *Nat Med* 21: 1364–1371
- Jiang Y, Subbiah V, Janku F, Ludwig JA, Naing A, Benjamin RS, Brown RE, Anderson P & Kurzrock R (2014) Novel secondary somatic mutations in Ewing's sarcoma and desmoplastic small round cell tumors. *PLoS One* 9: 1–7
- Joseph PD, Craig JC & Caldwell PHY (2015) Clinical trials in children. *Br J Clin Pharmacol* 79: 357–369
- Judge SJ, Darrow MA, Thorpe SW, Gingrich AA, O'Donnell EF, Bellini AR, Sturgill IR, Vick L V., Dunai C, Stoffel KM, et al (2020) Analysis of tumor-infiltrating NK and T cells highlights IL-15 stimulation and TIGIT blockade as a combination immunotherapy strategy for soft tissue sarcomas. *J Immunother Cancer* 8: 1–17
- Kameneva P, Artemov A V., Kastriit ME, Faure L, Olsen TK, Otte J, Erickson A, Semsch B, Andersson ER, Ratz M, et al (2021) Single-cell transcriptomics of human embryos identifies multiple sympathoblast lineages with potential implications for neuroblastoma origin. *Nat Genet* 53: 694–706
- Kavaliuskiene S, Nymark CM, Bergan J, Simm R, Sylvänne T, Simolin H, Ekroos K, Skotland T & Sandvig K (2014) Cell density-induced changes in lipid composition and intracellular trafficking. *Cell Mol Life Sci* 71: 1097–1116
- Kretzschmar K & Clevers H (2016) Organoids: Modeling Development and the Stem Cell Niche in a Dish. *Dev Cell* 38: 590–600
- Kuijk E, Jager M, van der Roest B, Locati MD, Van Hoeck A, Korzelius J, Janssen R, Besselink N, Boymans S, van Boxtel R, et al (2020) The mutational impact of culturing human pluripotent and adult stem cells. *Nat Commun* 11
- Markides CSA, Coil DR, Luong LH, Mendoza J, Kozielski T, Vardeman D & Giovannella BC (2013) Desmoplastic small round cell tumor (DSRCT) xenografts and tissue culture lines: Establishment and initial characterization. *Oncol Lett* 5: 1453–1456
- Martinez-Castaldi C, Silverstein M & Bauchner H (2008) Child versus adult research: The gap in high-quality study design. *Pediatrics* 122: 52–57
- Muraro MJ, Dharmadhikari G, Grün D, Groen N, Dielen T, Jansen E, van Gurp L, Engelse MA, Carlotti F, de Koning EJP, et al (2016) A Single-Cell Transcriptome Atlas of the Human Pancreas. *Cell Syst* 3: 385–394.e3

- Nanki K, Toshimitsu K, Takano A, Fujii M, Shimokawa M, Ohta Y, Matano M, Seino T, Nishikori S, Ishikawa K, et al (2018) Divergent Routes toward Wnt and R-spondin Niche Independency during Human Gastric Carcinogenesis. *Cell* 174: 856-869.e17
- Nishio J, Iwasaki H, Ishiguro M, Ohjimi Y, Fujita C, Yanai F, Nibu K, Mitsudome A, Kaneko Y & Kikuchi M (2002) Establishment and characterization of a novel human desmoplastic small round cell tumor cell line, JN-DSRCT-1. *Lab Invest* 82: 1175-1182
- Pauli C, Hopkins BD, Prandi D, Shaw R, Fedrizzi T, Sboner A, Sailer V, Augello M, Puca L, Rosati R, et al (2017) Personalized in vitro and in vivo cancer models to guide precision medicine. *Cancer Discov* 7: 462-477
- Riggi N, Suvà ML, Suvà D, Cironi L, Provero P, Tercier S, Joseph JM, Stehle JC, Baumer K, Kindler V, et al (2008) EWS-FLI-1 expression triggers a ewing's sarcoma initiation program in primary human mesenchymal stem cells. *Cancer Res* 68: 2176-2185
- Rorie CJ, Thomas VD, Chen P, Pierce HH, O'Bryan JP & Weissman BE (2004) The Ews/Fli-1 Fusion Gene Switches the Differentiation Program of Neuroblastomas to Ewing Sarcoma/Peripheral Primitive Neuroectodermal Tumors. *Cancer Res* 64: 1266-1277
- Sachs N, de Ligti J, Kopper O, Gogola E, Bounova G, Weeber F, Balgobind AV, Wind K, Gracanin A, Begthel H, et al (2018) Resource A Living Biobank of Breast Cancer Organoids Resource A Living Biobank of Breast Cancer Organoids Captures Disease Heterogeneity. *Cell* 172: 373-386
- Saletta F, Seng MS & Lau LMS (2014) Advances in paediatric cancer treatment. *Transl Pediatr* 3: 156-15682
- Sbaraglia M, Righi A, Gambarotti M & Dei Tos AP (2020) Ewing sarcoma and Ewing-like tumors. *Virchows Arch* 476: 109-119
- Soldatov R, Kauka M, Kastriti ME, Petersen J, Chontorotzea T, Englmaier L, Akkuratova N, Yang Y, Häring M, Dyachuk V, et al (2019) Spatiotemporal structure of cell fate decisions in murine neural crest. *Science* (80-) 364
- Sos ML, Michel K, Zander T, Weiss J, Frommolt P, Peifer M, Li D, Ullrich R, Koker M, Fischer F, et al (2009) Predicting drug susceptibility of non - small cell lung cancers based on genetic lesions. *J Clin Invest* 119: 1727-1740
- Tilburg CM Van, Pfaff E, Pajtlar KW, Karin PS, Fiesel P, Jones BC, Prakash G, Stark S, Johann PD, Schramm K, et al (2021) The pediatric precision oncology INFORM registry : clinical outcome and benefit for patients with very high-evidence targets. *Cancer Discovery* 2021
- Tirode F, Laud-Duval K, Prieur A, Delorme B, Charbord P & Delattre O (2007) Mesenchymal Stem Cell Features of Ewing Tumors. *Cancer Cell* 11: 421-429
- Tomasetti C & Vogelstein B (2015) Variation in cancer risk among tissues can be explained by the number of stem cell divisions. *Science* (80-) 347: 78-81
- Vis MAM, Ito K & Hofmann S (2020) Impact of Culture Medium on Cellular Interactions in in vitro Co-culture Systems. *Front Bioeng Biotechnol* 8: 1-8
- Vital-Reyes VS, Rodríguez-Burford C, Oelschläger DK & Grizzle WE (2006) Cell density influences the effect of celecoxib in two carcinoma cell lines. *Biotech Histochem* 81: 51-54
- van de Wetering M, Francies HE, Francis JM, Bounova G, Iorio F, Pronk A, Van Houdt W, Van Gorp J, Taylor-Weiner A, Kester L, et al (2015) Prospective derivation of a living organoid biobank of colorectal cancer patients. *Cell* 161: 933-945
- Yan HHN, Siu HC, Law S, Ho SL, Yue SSK, Tsui WY, Chan D, Chan AS, Ma S, Lam KO, et al (2018) A Comprehensive Human Gastric Cancer Organoid Biobank Captures Tumor Subtype Heterogeneity and Enables Therapeutic Screening. *Cell Stem Cell* 23: 882-897
- Zhou Y, Yang D, Yang Q, Lv X, Huang W, Zhou Z, Wang Y, Zhang Z, Yuan T, Ding X, et al (2020) Single-cell RNA landscape of intratumoral heterogeneity and immunosuppressive microenvironment in advanced osteosarcoma. *Nat Commun* 11: 1-17



Addendum

Nederlandse samenvatting

List of publications

Curriculum vitae

Acknowledgement

Nederlandse samenvatting

In Nederland worden er per jaar 650 kinderen gediagnostiseerd met kinderkanker. De afgelopen 50 jaar zijn er veel nieuwe behandelingen ontwikkeld, waardoor 75% van deze patiënten kan worden genezen. Echter overlijdt nog steeds 1 op de 4 kinderen die gediagnostiseerd is met kinderkanker. Dit geeft aan dat er nog veel onderzoek gedaan moet worden om betere behandelmethoden te kunnen ontwikkelen.

Preklinische kweekmodellen zijn essentieel om het gedrag van tumorcellen te onderzoeken. Met de vernieuwende 3D kweekmethoden, organoïden genoemd, groeien de cellen als bolletjes dicht tegen elkaar aan. Hierdoor blijven cel-cel contacten en de verscheidenheid aan cel typen grotendeels behouden. De 3D organoïden kweekmodellen bootsen de originele tumor beter na in vergelijking met conventionele 2D cellijnen. Door de tumorcellen in kweekschaltes op te groeien, kunnen ze gebruikt worden voor het tegelijkertijd testen van heel veel verschillende medicijnen in een drugtest. Ook kunnen de cellen in een kweekschaltes genetische worden gemanipuleerd om de belangrijke moleculaire mechanismen te onderzoeken. In dit proefschrift beschrijven we het ontwikkelen van 3D organoïden kweekmodellen van zeldzame sarcomen die voorkomen bij kinderen; Ewing sarcoom en een Ewing-achtige desmoplastische kleine ronde celtumor, afgekort als DSRCT. De ontwikkelde organoïden kweekmodellen van Ewing sarcoom en DSRCT worden gebruikt voor drugtesten om nieuwe specifieke behandelingen te vinden waar deze sarcomen gevoelig voor zijn.

In **hoofdstuk 2** vergelijken we 3D organoïden kweekmodellen met preklinische muismodellen. 3D organoïden kweekmodellen zijn gemakkelijker te expanderen en daardoor geschikter om drugtesten op uit te voeren. Echter missen ze belangrijke omgevingsfactoren die rondom de tumor aanwezig zijn. In muismodellen groeien tumoren in een fysiologisch relevante omgeving, waardoor ze beter de reactie van de tumorcellen in de patiënt op medicijnen kunnen nabootsen. Het is van belang verschillende de preklinische modellen te combineren. Drugtesten op 3D organoïden kweekmodellen geven een goede indicatie voor welke medicijnen de tumorcellen gevoelig zijn. Muismodellen kunnen vervolgens worden gebruikt om een selectie van deze medicijnen te valideren in een fysiologisch relevante setting.

In **hoofdstuk 3** beschrijven we het ontwikkelen van Ewing sarcoom organoïden kweekmodellen. Deze kweekmodellen bootsen, zowel op genetisch niveau als op fenotypisch niveau, de tumor in de patiënt na. Drugtesten op deze kweekmodellen lieten zien dat Ewing sarcoom cellen specifiek gevoelig zijn voor HDAC-remmende medicijnen. Deze medicijnen blokkeren het eiwit histon-deacetylase (HDAC), wat ervoor zorgt dat bepaalde genen in de cellen wel of niet tot expressie worden gebracht. Hierdoor wordt de celdeling geremd en kunnen Ewing sarcoom cellen niet meer expanderen. Deze resultaten lieten zien dat Ewing sarcoom organoïden kweekmodellen kunnen worden ingezet om de gevoeligheid van de tumorcellen voor medicijnen te kunnen testen.

In **hoofdstuk 4** beschrijven we het ontwikkelen van een DSRCT organoïden kweekmodel, die de karakteristieke eigenschappen van de originele tumor nabootst. Drugtesten op dit kweekstelsel lieten zien dat DSRCT cellen gevoelig zijn voor verschillende medicijnen die receptor-tyrosinekinasen (RTK) blokkeren. RTKs vormen een groep membraanreceptoren die onder andere groeifactoren en hormonen kunnen herkennen. RTKs reguleren vele processen, zoals celdeling en apoptose. Ook spelen RTKs een belangrijke rol in het ontstaan en de ontwikkeling van verschillende soorten kanker. De resultaten van deze drugtesten lieten zien dat processen die gereguleerd worden door RTKs ook in DSRCT een belangrijke rol spelen.

Ewing sarcoom en DSRCT worden beide gekarakteriseerd door een translocatie in het genoom. Hierdoor zijn er stukken DNA, die coderen voor genen, met elkaar verwisseld en ontstaat er een fusiegen. Dit fusiegen komt tot expressie als een fusie-eiwit dat op verschillende manieren de cel kan dereguleren, waardoor de cel transformeert tot een kankercel. Ewing sarcoom wordt gedreven door het *EWS-FLI1* fusiegen, terwijl DSRCT wordt gedreven door het *EWS-WT1* fusiegen. Er is al veel onderzoek is gedaan naar de mechanismen van *EWS-FLI1* in Ewing sarcoom, maar de moleculaire functies van *EWS-WT1* in DSRCT zijn nog niet volledig in kaart gebracht. Om de mechanismen van *EWS-WT1* te onderzoeken hebben we de DSRCT organoïden kweekmodellen genetisch gemanipuleerd, waardoor de expressie van *EWS-WT1* kon worden geblokkeerd. Hierdoor konden we genen vinden die door *EWS-WT1* worden gereguleerd en bijdragen aan de agressieve karakteristieken van DSRCT cellen. Eén van deze *EWS-WT1* geregleerde genen is de RTK *MERTK*. Het specifiek remmen van *MERTK* in DSRCT cellen resulteerde in een verminderde cel expansie en apoptose. Dit toont aan dat *EWS-WT1* geregleerde *MERTK*-expressie belangrijk is voor DSRCT cellen en dat het remmen van *MERTK* mogelijk als nieuwe behandelingsmethode kan worden getest in DSRCT patiënten.

In **hoofdstuk 5** beschrijven we de compositie van verschillende celtypen in Ewing sarcomen. Door middel van het bestuderen van gen-transcriptie profielen van elke cel apart, hebben we in een aantal Ewing sarcoom patiënten cel subpopulaties gevonden. Dit toont aan dat niet alle Ewing sarcoom cellen hetzelfde zijn, maar er diverse subpopulaties van tumorcellen aanwezig zijn die genetische verschillen hebben en zich anders kunnen gedragen. Niet alleen de tumorcellen zelf, maar ook gezonde cellen in de omgeving van de tumor kunnen bijdragen aan de ontwikkeling van een tumor. Immune cellen kunnen bijvoorbeeld zowel een activerend effect als een remmend effect hebben op de tumorgroei. Bij sommige soorten kanker worden daarom immune checkpoint remmers gegeven. Deze behandeling helpt het natuurlijke afweersysteem weer te activeren om tumorcellen te herkennen en vernietigen. Ook in diverse Ewing sarcoom patiënten zagen we dat een aantal immune cel populaties immune checkpoint moleculen tot expressie brengen die het afweersysteem inactiveren. Mogelijk kunnen immune checkpoint remmers ook in deze patiënten het natuurlijke afweersysteem weer activeren en bijdragen aan de behandeling.

Samengevat dragen de onderzoeken die beschreven zijn in dit proefschrift bij aan het ontwikkelen van preklinische kweekmodellen voor onderzoek van verschillende zeldzame sarcomen die voorkomen bij kinderen. Deze kweeksystemen bootsen de originele tumor na en kunnen daardoor bijdragen aan het ontwikkelen van behandelmethoden waar Ewing sarcomen en DSRCT specifiek gevoelig voor zijn. Verdere ontwikkelingen van deze 3D organoïden kweekmodellen van verschillende soorten sarcomen zou het in de toekomst mogelijk kunnen maken om gepersonaliseerde behandelmethoden samen te stellen.

List of publications

Margit Bleijs, Marc van de Wetering, Hans Clevers, Jarno Drost (2019). Xenograft and organoid model systems in cancer research. *The EMBO Journal*. 38: 1–11

Kai Kretzschmar¹, Kim Boonenkamp¹, **Margit Bleijs**, Priyanca Asra, Mandy Koomen, Susana Chyva de Sousa Lopes, Barbara Giovanonne, Hans Clevers (2021). H. Troy / Tnfrsf19 marks epidermal 1 cells that govern interfollicular epidermal renewal and cornification. *Stem Cell Reports*. 16: 1-16

Submitted or in preparation

Margit Bleijs, Corine Pleijte, Sem Engels, Femke Ringnalda, Friederike Meyer-Wentrup, Marc van de Wetering, Hans Clevers. The molecular mechanisms driving DS-RCT cell expansion by the *EWS-WT1* fusion gene.

Margit Bleijs¹, Lindy Visser¹, Thanasis Margaritis¹, Frank Holstege, Marc van de Wetering, Hans Clevers. Single cell atlas of Ewing sarcoma reveals subclonal evolution and its immune composition.

Margit Bleijs¹, Femke Ringnalda¹, Laura Hiemcke-Jiwa, Kimberley Ober, Selma Eising, Hans Clevers. PDO models of Ewing sarcoma and Ewing-like sarcomas allow for medium-throughput drug screening.



Curriculum Vitae

Margit Bleijs was born on July 31st 1993 in Utrecht, The Netherlands. In 2010 she obtained her high school degree at the St. Gregorius College in Utrecht, after which she started the Bachelor's program Life Sciences – Molecular Biology at the University of Applied Sciences in Utrecht. During her Bachelor she first performed an internship in the Orthopedics department at the University Medical Center Utrecht, where she worked on the regeneration of cartilage by modulation of micro RNAs in osteoarthritic chondrocytes, under supervision of Dr. Lucienne Vonk. Next she performed an internship abroad in the lab of Prof. David Page at the Whitehead Institute (MIT), where she studied the association between a disruption in the ACRC gene and spermatogenic failure in men, under supervision of Dr. Michelle Carmell. During this period she has also worked on a small project at the Boston Children's Hospital (Harvard Medical School) focusing on fabricating and optimizing tri-layered scaffolds for the making of heart valves, under supervision of Dr. Nafiseh Massoumi. After she obtained her bachelor degree in 2014, she went back to the lab of Prof. David Page in Cambridge USA for a replication study on the association between a disruption in the ACRC gene and spermatogenic failure in men, in collaboration with Prof. Dr. Sjoerd Repping at the University Medical Center Amsterdam. In 2015, she started the Master's program Cancers, Stem Cells and Developmental Biology at Utrecht University, during which she performed her major internship in the lab of Prof. Dr. Hans Clevers at the Hubrecht Institute in Utrecht. Here, she studied the role of Troy-positive epidermal cells in murine skin renewal, under supervision of Dr. Kai Kretzschmar. Next, she performed her minor internship in the lab of Prof. Dr. Jacco van Rheenen at the Hubrecht Institute in Utrecht. There, she studied the dynamics of mammary tumor growth by intravital imaging, under supervision of Dr. Colinda Scheele. After these internships, she wrote a review article in the lab of Dr. Jarno Drost at the Princess Máxima Center in Utrecht, on patient-derived organoid and xenograft models in cancer research. She obtained her Master's degree in 2017, after which she joined the lab of Prof. Dr. Hans Clevers at the Princess Máxima Center in Utrecht to start a PhD on establishing preclinical models of rare pediatric sarcomas, including Ewing sarcoma and Ewing-like sarcomas, of which the results are presented in this thesis. In October 2021, Margit joined NWO as a program coordinator.

Acknowledgement

After 4 years it is time to complete this PhD chapter and move on to a new adventure. But before I move on, I would like to take the opportunity to thank many people that have helped me survive the past four years. I could not have finished this challenge without the help and mental support from a lot of people!

Allereerst wil ik **Hans** bedanken. Na een succesvolle stage in je grote Clev-ers groep in het Hubrecht Instituut, wilde ik de uitdaging aangaan om mijn PhD te starten in je nieuwe groep in het Prinses Máxima Centrum en ik ben dankbaar dat ik deze kans gekregen heb. Ik heb enorm veel geleerd de afgelopen jaren en ik ben dankbaar dat ik mij zo heb kunnen ontwikkelen. Bedankt voor alle kritische input en de snelle feedback op de hoofdstukken in dit proefschrift. Zonder **Marc** was ik nooit in dit mooie instituut terecht gekomen. Ik wil je daarom bedanken voor de kans om mijn PhD te doen in het Prinses Maxima Centrum. Een avontuur was het wel, dat begon met het opstarten van het lab in het Hubrecht Instituut. Later verhuizen we naar de nieuwbouw. In het huidige Prinses Maxima Centrum duurden het ook nog even voordat alle faciliteiten van de grond kwamen. Gelukkig is dit allemaal goed tot stand gekomen en draait het lab steeds beter. **Friederike**, vooral in het begin van mijn PhD ben je betrokken geweest bij het DSRCT project. Je klinische kijk op het project heeft me vooruit geholpen en ook je openheid over de kliniek van DSRCT patiënten heeft me geholpen bij het inzien hoe belangrijk het is om nieuwe behandelmethoden te ontwikkelen. Ik hoop dat mijn onderzoek iets kan bijdragen voor DSRCT patiënten in de toekomst.

Naast mijn promotor en co-promotoren wil ik graag mijn PhD- en leescom-missie bedanken: **Frank**, bedankt voor je eerlijke en goede adviezen. Dit heeft me erg geholpen de afgelopen jaren en me gestimuleerd om mijn proefschrift zonder verlenging af te ronden. **Niels**, bedankt voor de goede discussies tijdens mijn com-mittee meetings die me hielpen mijn projecten te prioriteren en deze vooruit hielpen. **Claudia**, thank you for joining my PhD committee when I was in desperate need of more support and for helping me getting back on track when I was sure to quit my PhD. By sharing your experiences on managing a PhD life you have encouraged me to complete this thesis. **Jan** en **Max**, bedankt voor jullie tijd en moeite om mijn proefschrift te lezen en beoordelen.

Most importantly, I would like to thank my paranimfs. **Evelyn**, you are one of my best colleagues friends. We started our PhD journey roughly at the same time in the Clev-ers group at the PMC and I couldn't have wished for a better PhD buddy. I'm glad we could encourage each other to keep struggling on. Thank you for all the scientific discussions, but even more for the much-needed wine & dines, VMT meet-ings and random hugs that kept me sane during the past four years. I could never have finished it without you!

Lisa, wij kennen elkaar al sinds onze bachelor studie en sleepte elkaar toen al door lastige tentamens heen (en vooral van en naar de kroeg). Daarna hebben we allebei een master afgerond en zijn bijna tegelijk begonnen aan onze PhD trajecten. Ik ben blij dat we tijdens al deze trajecten in dezelfde fases zaten en samen hoogtepunten konden vieren, maar ook voor elkaar klaar konden staan als er dieptepunten te verwerken waren. Bedankt voor alle peptalks onder het genot van een kopje koffie of glaasje wijn. Ik kijk ernaar uit om samen te beginnen met, jawel, dezelfde baan bij NWO!

Of course, I would like to thank all members and alumni of the Clevers lab at the PMC: **Femke**, enorm bedankt voor al je hulp de afgelopen jaren! Behalve dat je alles regelt in het lab en bestellingen doet als ik weer eens ‘olives’ nodig heb, heb je me ook super veel geholpen in de kweek. Zonder jou was hoofdstuk 3 (E.T.) nooit van de grond gekomen. Ik heb enorm veel van je geleerd en ga onze gezellige gesprekken en dansjes in de kweek missen! **Karin**, bedankt voor de gezelligheid in het lab en tijdens de borrels. Ik ga de ‘chicks with chicks’ kippenpraat op werk missen, maar ik hoop je in Houten nog vaak tegen te komen om kippenupdates te bespreken! Succes met alles en ik hoop dat er een keer een mooie NWO subsidie jouw kant op komt! **Evelyn**, thank you for the fun times in the lab, your input during the labmeetings and your incredible support! **Laurens** (DiCaprio), na een half jaar expansion drift richting mijn lab bench is het je gelukt, hij is van jou! Ik ga onze random stares en slappe lach in het lab missen! Succes met je PhD, het gaat je zeker lukken! **Seok-Young**, although our time in the lab together hasn’t been so long, I really enjoyed having you around. Thank you for teaching me a few words Korean and some of the Korean cuisine (although I still need to try the BBQ sauce!). Thank you for sharing the love for Schrobbelèr and remember: a shot of Schrobbelèr a day, keeps the PhDepression away! **Lin**, I’m glad you joined the lab in the PMC! Thank you for the fun times in the lab and at the borrels. I’ve learned a lot from your expertise in cloning and your input during the labmeetings. Good luck with everything! **Georg**, thank you for all your help with bioinformatic analyses and introducing me to the hpc drive. Good luck with your own group in Vienna! **Sophie**, bedankt voor je hulp en input bij de bioinformatic analyses van het DSRCT project. Ondanks dat we geen hele lange tijd samen hebben gewerkt, heb ik genoten van onze tijd in het lab samen. Ik ben blij dat je een leuke baan hebt gevonden bij Euretos! **Annemieke**, bedankt voor de snelle communicatie bij het inplannen van meetings en je hulp bij de laatste loodjes van het afronden van mijn PhD traject! Ook wil ik je bedanken voor het betrekken van de PMC Clevers groep bij activiteiten, zoals de Clevers BBQ!

Ook wil ik de master studenten bedanken die hebben bijgedragen aan mijn proefschrift: Allereerst **Nune**, jij liep al stage in de Clevers groep voordat ik begon met mijn PhD en je was voor mij meer een begeleider dan student. Ik wil je enorm bedanken voor het inwerken in het lab en het introduceren van het Ewing sarcoom



project. Ik ben blij dat je een mooie PhD plek hebt gevonden in het van Oudenaarden lab! Succes met deze uitdaging, het gaat je zeker lukken! **Corine**, bedankt voor het opzetten van het DSRCT project. Na heel wat trouble shooting is het gelukt de shRNAs te klonen en met succes, de knock-down werkt! Zonder jouw hulp was hoofdstuk 4 nooit van de grond gekomen! Succes met je verdere studeertraject! **Sem**, jij bent na Corine verder gegaan met het DSRCT project en hebt er nog extra shRNAs bij weten te kloneren die een knock-down geven en daarmee een waardevolle bijdrage geleverd aan hoofdstuk 4! Ik ben blij dat je een mooie baan hebt gevonden in het van Heesch lab op het PMC en we ook na je stage nog gezellig samen in de kweek hebben gezeten!

There are more people who significantly contributed to this thesis: **Thanasis**, thank you for all your help with the bioinformatics part of Chapter 5 and the fruitful discussions during meetings and borrels. I could never have finished the single cell manuscript without you! **Lindy**, bedankt voor alle hulp en je expertise op het gebied van immuuncellen! En vooral heel erg bedankt dat je tijdens je zwangerschapsverlof de tijd hebt genomen om data en figuren compleet te maken! **Laura**, bedankt voor alle immuno's en het meedenken met mijn Ewing projecten! I would also like to thank **the Sarcoma Group** for the fruitful discussions and the fun retreat.

A big thanks also goes out to all the amazing people I had the pleasure of meeting during the past 4 years at both the Princess Máxima Center and the Hubrecht Institute. My office mates at the Hubrecht Insistute **Marli** en **Mariël**, bedankt voor jullie gezelligheid in het Hubrecht office. Daar heb ik ook meegekregen hoe jullie je hebben ingezet om de nieuwbouw van het PMC en de verhuizing te realiseren. Respect en super bedankt! **Willemijn** bedankt dat je me hebt meegenomen naar de OK en pathologie waar ik veel van heb geleerd! **Jan** bedankt voor de gezelligheid en slechte humor in het office. **Lars**, zowel op het Hubrecht als het PMC hebben wij een office ruimte gedeeld, bedankt voor de gezelligheid en de nodige biertjes op zijn tijd. Ook nog bedankt voor het laten zien hoe de 'start'-knop werkt op de centrifuge ;). Heel veel succes met je post-doc in Zürich en super tof dat je even terug wilt komen om mijn back-up paranimf te zijn! And of course I would like to thank many more people from the office at the PMC: **Camilla**, thank you for your help with the drug screen analysis! **Irene**, wat zie jij er sportief uit vandaag ;), **Yvonne**, **Arianna**, **Juliane**, **Fransisco**, **Sofia**, **Sanne**, **Maroussia**, **Laura**, **Jarno**, **Valentina**, thank you all for the fun secret santa! Also **Jeff**, we started this journey at the same day! thank you for sharing a lot of legendary moments during the past four years. I can't wait to celebrate your defense! **Michael**, Thank you for joining the hESC project, although it was doomed from the start... Everything is awesome when your part of a team! **Eduard**, bedankt voor alle 384-well sorting platen! **Marian**, bedankt voor het regelen van de WGS data! **Tomasz**, thank you for the fun conversations at the FACS, **Tito**, **Philip**, **Terezinha**, **Lindy**, **Kaylee**, **Waleed**, **Michelle**, **Linda**, **Jennemieke**, **Karin**,

Bianca, Kimberley, Selma, Marlinde, Michael, Josephine, Axel, Eline, Karlijn, Niels, Arianne, Sjors, Rurika, Jurrian, Mark, Mark, Freek, Ruben, Flavia, Jordy, Wilco, Rico, Vera, Emma, Jessica, Florijn, Frank, Rijndert, Ravian, Hannah, Mario, Heggert, Thomas, Lisa, Irene, Claudia, Elvin, and many more... Thank you all for the fun times at the retreats, borrels, masterclasses and other memorable moments!

I would also like to thank current and former PhD students in the Clevers lab at the Hubrecht Institute: **Else, Joep, Cayetano, Fjodor, Frans, Jelte**, bedankt voor de nodige koffie momentjes en de gezellige BBQ, ik zie je nog wel in Houten! **Jens, Kadi**, thank you for giving me the honor of being your paranymph! **Kim**, bedankt voor het oppakken van het Troy project en het uitwerken tot een mooi paper! **Maarten**, bedankt voor al je CRISPR hulp! **Yorick, Adriana, Lulu, Carla, Marie**, thank you all for the fun lab outings, dinners, fun weekend at the Ardennes and of course all the live commentaries on the Eurovision song contest and important football games!

There are many more people to thank: **Louk, Anton, Eline, Elvin, Sanne, Juri** and **Disa Ronno** thank you for the fun times with the PhD committee 2020&2021. We have been laughing more than actually organizing events (which can only partially be blamed by the corona pandemic). I am looking forward to the next karaoke party!

The Wednesday night Florin Pubquiz was definitely one of the moments to look forward to every other week! Big thanks to the ever-enthusiastic team: **Captain Bas, Wim, Kim, Marit, Jeff, Annabel, Irene, Javi, Tim, Alex, Eduard, Lars, Reinier, Freek, Philip, Marc, Saman, Wouter, Eline, Gabi, Winnie**, and many others who occasionally joined!

There is no better way to release some PhD stress than chasing a ball for an hour every week! I would like to thank the futsal people that regularly or occasionally joined the futsal matches **Axel, Wim, Guy, Geert, Erik, Lucas, Mike, Louk, Freek, Nico, Enric, Jan, Lars, Bas, Winnie, Jens, Cayetano, Vlad, Sonja, Moritz, Muhammad, Marwan, Arwan, Samu, Pavol, Waleed, Manuel, Pieke, Jaap, Stijn, Jooske, Mike, Sanne, Michael, Nader, Niels, Mark** and many others...

But it doesn't stop there! I would like to thank all people from the PMC, Hubrecht, UMC and UU that were involved in masterclasses, retreats and legendary Ardennes-trips in any order: **Erik, Charlotte, Wouter, Wim, Bas, Ajit, Colinda, Lotte, Arianna, Laura, Anne, Clement, Caro, Wouter, Alex, Jimmy, Rob, Ravian, Rijndert, Hannah, Jeff, Evelyn, Annabel, Roxanne, Juliëtte, Naomi, Sander, Ilia, Ator, Lotte, Tim, Lars, Reinier, Gaby, Christa, Joe, Sonja, Spiros, Joris, Anton, Wessel**, and the many more people that I'm probably forgetting here!

Een van de hoogtepunten van mijn PhD was toch wel de Prinses Maxima rally die ik samen met **Sanne** en **Winnie** heb gereden. Bedankt voor de toffe tijd van de koekjesverkoop om genoeg geld op te halen tot het scheuren in de kever over het Formule 1 circuit!

The absolute highlight during my PhD was the HydraXIV summerschool. I would like to thank the members of the Hydra “party crew” **Kadi, Simon, Pablo** (uncle pablito), **Alessia, Elsa, Becky, Ben** (perfect specimen), and **Kim** for making this an amazing and unforgettable experience!

Nafise, azizam! Thank your being my career and life coach and dear friend. I’m happy and thankful that we stayed in touch after I have left Boston. Thank you for giving me the honor of being a bridesmaid at your wedding. I’m really happy I had the chance to visit you just before the pandemic! I would also like to send my love to **Cody** and **Tyler**. I can’t wait to visit you again! Lieve **Lotte**, wij hebben elkaar tijdens de master studie leren kennen en zijn vriendinnen gebleven door onze gezamenlijke liefde voor Amerika, country music en sushi! Ik hoop dat we snel nog een keer een tripje naar Dallas kunnen boeken! Bedankt voor je steun de afgelopen 4 jaar en heel veel succes met jouw PhD avontuur! Lieve **Maartje** en **Rolinda**, wij zijn al vriendinnen vanaf de middelbare school en jullie hebben dan ook in de afgelopen 10 jaar (bedankt voor het meetellen en herinneren Maart ;)) van mijn studeer periode heel wat van mijn emotionele achtbanen meegemaakt. Ik ben ontzettend blij en dankbaar dat jullie ook tijdens de weg naar dit laatste diploma altijd voor me klaar staan. Ik hoop dat we samen nog vele mojito- en wijn avonden gaan beleven! Boston billies: **Casper, Iris, Charles, Hendrina, Suus, Pim, David, Kim en Jeroen**, ik ben blij dat we elkaar na een toffe tijd in Boston nog regelmatig zien als er weer iets te vieren is en met het jaarlijkse Thanksgiving diner. Bedankt voor de gezelligheid! Ook is het altijd weer feest als we naar het zonnige zuiden rijden, **Fabian, Ilse, Freek, Laura, Bart, Nienke, Jochem, Maartje, & co**, ik ben blij dat ik jullie via Bas heb leren kennen. Bedankt voor alle toffe momenten van carnaval, Oktoberfest, Thanksgiving diners en BBQs tot weekendjes weg! Ook kan ik **Jasper, Femke, Niels, Lisa, Mitch, Tim, Lars, Sterre** en **Johanna** zeker niet vergeten, ik vind het super tof dat ik zo’n gezellige vriendengroep hebben overgehouden aan de bachelor studie. Wat begon met een city trip naar Dublin... uhh Cork, escaleerde toen volledig uit de hand tot nog veel meer weekendjes weg naar Krakau, Ljubljana en Arcen, bockbier festivals, carnaval, Snollebollekes, BBQ wedstrijden om de gouden spatula, burgerlijkheidspunten voor de gouden toiletborstel en nog veel meer rariteiten, waardoor ik weer even de stress en frustratie van een PhD-life kon vergeten.

Kees, Marian, Mark en **Jeroen**, bedankt dat ik met open armen in de Castelijns familie ben ontvangen. Ik kijk altijd erg uit naar de gezellige weekendjes weg,

het legendarische sinterklaasspel, lekkere BBQs en borrels tot in de kleine uurtjes! Bedankt dat de deur bij jullie altijd open staat!

Willemijn, Jeffrey, Anouk, Tomas, bedankt voor jullie steun de afgelopen jaren en dat ook bij jullie de deur altijd open staat! Ik hoop dat in dit boek een beetje duidelijk maakt waar ik nu zo druk mee ben geweest de afgelopen 4 jaar. En ja, ik heb nu eindelijk een 'normale' baan. ;)

Lieve **papa** en **mama**, bedankt voor jullie onvoorwaardelijke steun en vertrouwen de afgelopen jaren. Ook als het allemaal even niet goed ging stonden jullie altijd voor me klaar. **Mama**, van stage regelen in Boston tot het reviewen en helpen submitten van mijn manuscript, zowel op carrière als persoonlijk vlak heb je me enorm vooruit geholpen en daar ben ik ontzettend dankbaar voor. Ik ben super trots dat je de academische ladder tot Professor bent beklommen, maar voor mij is het toch tijd om de academische wereld te verlaten...

Voordat ik de laatste woorden op papier heb gezet wil ik nog één iemand in het bijzonder bedanken: Lieve **Bas**, bedankt voor je onvoorwaardelijke liefde en steun de afgelopen jaren. Het begon allemaal op het Hubrecht Instituut, waar ik deze gezellige Brabander leerde kennen. Je bent al ruim 5 jaar mijn beste maatje, we hebben veel lol samen en al heel wat avonturen beleefd. Van toeren in de kever of op de motor en op mooie vakanties tot het kopen van ons eigen huis! Met onze zelfgebouwde Bar Castebleijs, zodat we het behalen van jouw PhD tijdens de pandemie toch nog een beetje kon vieren. Nu kunnen we eindelijk ons Dr. & Dr. naambordje voor naast de voordeur laten maken ;). Ik hou van je en kijk uit naar onze volgende avonturen samen! <3

“Just keep swimming”

Dory

